UNIVERSIDADE FEDERAL DE PERNAMBUCO
DEPARTAMENTO DE FÍSICA – CCEN
PROGRAMA DE PÓS-GRADUAÇÃO EM FÍSICA

PABLO ISAIAS RIQUELME PINCHEIRA

THEORETICAL AND EXPERIMENTAL STUDY OF THE LÉVY STATISTICS AND PHOTONIC SPIN GLASS PHASE IN RANDOM LASERS

Recife
2017

PABLO ISAIAS RIQUELME PINCHEIRA

THEORETICAL AND EXPERIMENTAL STUDY OF THE LÉVY STATISTICS AND PHOTONIC SPIN GLASS PHASE IN RANDOM LASERS

Tese apresentada ao Programa de Pós-Graduação em Física da Universidade Federal de Pernambuco, como requisito parcial para a obtenção do título de Doutor em Física.

Orientador:
Prof. Dr. Anderson Stevens Leônidas Gomes
Universidade Federal de Pernambuco

Recife
2017

Catalogação na fonte
Bibliotecário Jefferson Luiz Alves Nazareno CRB 4-1758

R594t Riquelme Pincheira, Pablo Isaias.
Theoretical and experimental study of the lévy statistics and photonic spin glass phase in random lasers / Pablo Isaias Riquelme Pincheira . – 2017.
103 f.: fig., tab.

Orientador: Anderson Stevens Leônidas Gomes.
Tese (Doutorado) – Universidade Federal de Pernambuco. CCEN. Física, Recife, 2017.
Inclui referências, apêndices e anexo.

1. Laser. 2. Laser Aleatório. 3. Sistemas complexos. 4. Vidro de Spin. I. Gomes, Anderson Stevens Leônidas (Orientador). II. Titulo.

535.5 CDD (22. ed.) UFPE-FQ 2017-37

PABLO ISAIAS RIQUELME PINCHEIRA

THEORETICAL AND EXPERIMENTAL STUDY OF THE LÉVY STATISTICS AND PHOTONIC SPIN GLASS PHASE IN RANDOM LASERS

Tese apresentada ao Programa de Pós-Graduação em Física da Universidade Federal de Pernambuco, como requisito parcial para a obtenção do título de Doutor em Física.

Aprovada em: 18/01/2017.

BANCA EXAMINADORA

_____
Prof. Dr. Anderson Stevens Leônidas Gomes
Orientador
Universidade Federal de Pernambuco

_____
Prof. Dr. Cid Bartolomeu de Araújo
Examinador Interno
Universidade Federal de Pernambuco

_____
Prof. Dr. Ernesto Carneiro Pessoa Raposo
Examinador Interno
Universidade Federal de Pernambuco

_____
Prof. Dr. Christiano José Santiago de Matos
Examinador Externo
Universidade Presbiteriana Mackenzie

_____
Prof. Dr. Felipe Arruda de Araújo Pinheiro
Examinador Externo
Universidade Federal do Rio de Janeiro

Abstract

Since Albert Einstein established the foundations for stimulated emission of radiation in 1916, he paved a long road that culminated in the beginning of the 1960s with the invention of the laser. In a conventional laser avoiding losses by light scattering is very important. However, this paradigm is broken by the theoretical proposal of Letokhov in 1968, which says that in a disordered with gain, the scattering of light plays a positive role increasing the dwell time of light in an active medium, thereby increasing the laser amplification. Due to the disordered nature of the materials used was adopted the name Random Lasers (RLs). Random lasers have taken a new boom because they have recently been exploited as a photonic platform for studies of complex systems. This thesis covers this interdisciplinary approach that opens important new avenues for understanding the behavior of random lasers. We recently studied the intensity fluctuations in the emission of Random lasers, finding the existence of non-Gaussian statistics in these emissions behaving with Lévy-type statistics. On the other hand, in another set of theoretical and experimental work, the glassy behavior of random lasers was studied by other authors, which led to the recent experimental demonstration of symmetry replica breaking phase transition. The investigations mentioned above were taken separately, and in this work shows that these two phenomena are connected. In the first chapter we study the most important concepts of a conventional laser that are necessary to understand the random lasers. In the second chapter, we present the random lasers. We begin with the presentation of the main features of random lasers. Then, we present a connection between the phenomenon of speckle and random lasers where Speckle Contrast is used to demonstrate the multimodal nature of random lasers. This feature is applied to determine the number of modes in a random fiber laser. At the end of this chapter a work is presented where it is demonstrated for the first time Bichromatic random laser in a $NdAl_3(BO_3)_4$ crystalline powder. This observation opens an avenue for random lasers applications, and, as a proof of concept, we demonstrate an optical thermometer owing to the thermal dependence of the RL emissions. The third chapter is dedicated to studying the fundamental concepts of complex systems, to understand the glassy behavior of light in random lasers. In chapter 4 essential rudiments are also given to understand Lévy statistics. In chapter 5 we show a work where we use employ the $NdYBO$ random laser system to show that from a single set of measurement the physical origin of the complex correspondence between the Lévy fluctuation regime and the replica symmetry breaking transition to spin glass phase occurs. In chapter 6 shows the observation of replica symmetry breaking phase transition in a solution of Rhodamine and particles of T_iO_2, where specially designed amorphous T_iO_2 particles were synthesized to obtain identical copies of the system.

Keywords: Random Laser. Lévy statistics. Spin Glass.

Resumo

Desde que Albert Einstein estabeleceu as bases para a emissão estimulada da radiação em 1916, ele pavimentou uma longa estrada que culminou, no começo dos anos 1960, com a invenção do laser. Em um laser convencional, evitar perdas por espalhamento de luz é muito importante. No entanto, este paradigma é quebrado pela proposta teórica de Letokhov em 1968, que diz que em um meio desordenado com ganho, o espalhamento da luz desempenha um papel positivo aumentando a amplificação do laser. Devido à natureza desordenada dos materiais utilizados foi adotado o nome Random Lasers (RLs). Os lasers aleatórios tomaram um novo impulso porque foram explorados recentemente como uma plataforma fotônica para estudos de sistemas complexos. Esta tese estuda esta abordagem interdisciplinar que abre novas e importantes vias para a compreensão do comportamento de lasers aleatórios. Recentemente estudamos as flutuações de intensidade na emissão de lasers aleatórios, encontrando a existência de estatísticas não gaussianas nessas emissões que se comportam como estatísticas tipo Lévy. Por outro lado, em outro conjunto de trabalhos teóricos e experimentais, o comportamento tipo vidro de spin de lasers aleatórios foi estudado por outros autores, o que levou à recente demonstração experimental de transição de fase com quebra de simetria de réplica. As investigações mencionadas acima foram realizadas separadamente, e neste trabalho mostramos que esses dois fenômenos estão conectados. No primeiro capítulo estudamos os conceitos mais importantes de um laser convencional que são necessários para entender os lasers aleatórios. No segundo capítulo, apresentamos os lasers aleatórios. Começamos com a apresentação das principais características de lasers aleatórios. Em seguida, apresentamos uma conexão entre o fenômeno de speckle e lasers aleatórios onde *Speckle Contrast* é usado para demonstrar a natureza multimodal de lasers aleatórios. Esta característica é aplicada para determinar o número de modos de um laser aleatório de fibra. No final deste capítulo é apresentado um trabalho onde é demonstrado pela primeira vez o laser aleatório bicromático em um pó cristalino $NdAl_3\left(BO_3\right)_4$. Esta observação abre caminho para aplicações lasers aleatórios e, como prova deste conceito, demonstramos um termômetro óptico devido à dependência térmica das emissões de RL. O terceiro capítulo é dedicado a estudar os conceitos fundamentais de sistemas complexos, para entender o comportamento tipo vidro de spin da luz em lasers aleatórios. No capítulo quatro, rudimentos essenciais também são descritos para entender as estatísticas de Lévy. No capítulo cinco mostramos um trabalho onde usamos o sistema de laser aleatório $NdYBO$ para mostrar que a partir de um único conjunto de medições ocorre a origem física da correspondência complexa entre o regime de flutuação de Lévy e a transição de simetria de réplicas para a fase de vidro de spin. No capítulo seis, observa-se a transição de fase de ruptura de simetria de réplicas em uma solução de Rhodamine e partículas de T_iO_2, onde se sintetizaram partículas de T_iO_2 amorfas especialmente projetadas para obter cópias idênticas do sistema.

palavras-chave: Laser aleatório. Estatística de Lévy. Vidro de spin.

List of Figures

List of Tables

Contents

1 Laser

The random laser is related to light amplification in a disordered medium. Light amplification by stimulated emission is a fundamental process for generation of the laser-like light. In this sense Random Lasers (RLs) have the same fundamental principles as a conventional lasers. Therefore, in the first part of this chapter we will review the fundamental rudiments necessary to have a general understanding of conventional lasers. Later, we will continue with the discussion of RLs.

1.1 What is a Laser?

The word LASER is the acronym for Light Amplification by Stimulated Emission of Radiation, emphasizing that the laser is an active, amplifying device. In 1917, Einstein proposed the process that makes lasers possible, called stimulated emission. It was Einstein who pointed out that stimulated emission of radiation could occur along with absorption and spontaneous emission. Light interacts with atoms (gain medium) to emit a photon at some random time in a random direction. If stimulated a brief moment of time the atoms emit photons that go in the same direction and have exactly the same frequency as the original photon. The stimulated emission process has several consequences, the most notable of which is the existence of the Laser. Before the LASER there was the MASER, a device a also based on the stimulated emission process. In 1954, Charles Townes and Arthur Schawlow invented the MASER [39] (microwave amplification by stimulated emission of radiation). The technology is very close but does not use a visible light.

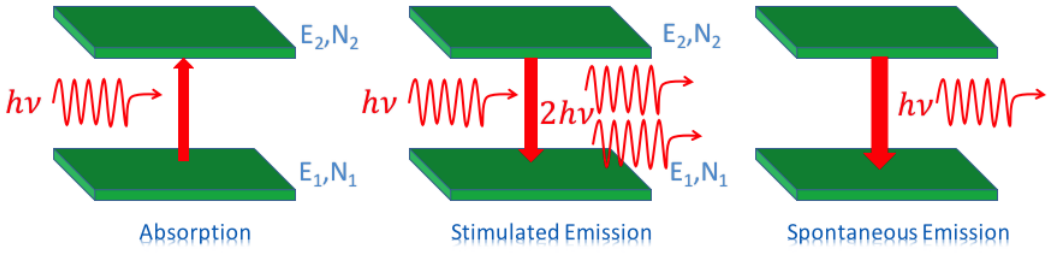

Figure 1.1.1: Schematic representation of the three fundamental interaction between atoms and radiation.

In the figure 1.1.1 shows a simplified two-level system in order to illustrate the interaction processes between atoms and light. N_1 and N_2 are the populations of atoms (or molecules) found in states 1 and 2 respectively. These atoms can be excited at metastable levels of energy through interactions with the environment that provide the energy difference required for the transition, the energy required is $h\nu = \Delta E$, where ΔE is the energy difference between the initial and final states.

In the ***Absorption process***, a photon is absorbed and the atom is promoted to the excited state. More generally, if there are n photons to start with in some resonant mode, then there are $n-1$ photons after the absorption process. The probability of absorption taking place is proportional to the population N_1 of the lowest energy level.

The ***Spontaneus emission*** They take place without external induction. That is, the probability that the electron decays at the lowest energy level through a spontaneous transition is fixed and fundamentally depends on the structure Of the atom. Both the direction of the emitted photon and its phase are random, the overall light obtained will be incoherent and directed in all directions.

In the case of ***Stimulated emission*** the process involves the atom initially being in the excited state, and after the stimulated-emission event, the atom falls to the ground state. The probability of a stimulated emission taking place is proportional to the population N_2 of the highest energy level. In thermal equilibrium the number of atoms excited in the highest energy state is much lower than the number of atoms in the lowest energy state $N_2 \ll N_1$. Therefore, the absorption predominates over the emission.

The absorption and stimulated emission coexist in all moment, they are equiprobables and only depend on the populations N_1 and N_2. For a medium to amplify, it is necessary that the population of N_2 is more abundant than that of N_1, so that, on average, more photons are produced that are lost. This situation, called ***population inversion***, is achieved taking the system out of equilibrium with an external input of energy in the form of, for example, light or electric current excitation.

There are basically three functional parts in a laser see Fig.1.1.2: a ***gain medium*** with energy levels between which are produced radiative transitions which determine the output wavelength, this medium converts the pump energy into the desired light; a resonant cavity called also an ***optical resonator***, which allows to accumulate the radiant energy of frequency corresponding to the stimulated emission. The simplest configuration is constituted by two mirrors where one of them has 100% of reflectivity and the second mirror is partially reflective. It will be this mirror that will allow the emission of the laser emission. With this cavity it is achieved that the emitted radiation passes many times through the gain medium producing a feedback of the stimulated emission process. The separation distance between the mirrors is fundamental in the selection of resonant modes, we will elaborate later on.

Finally, to get the stimulated emission processes to happen we must have a ***pumping***

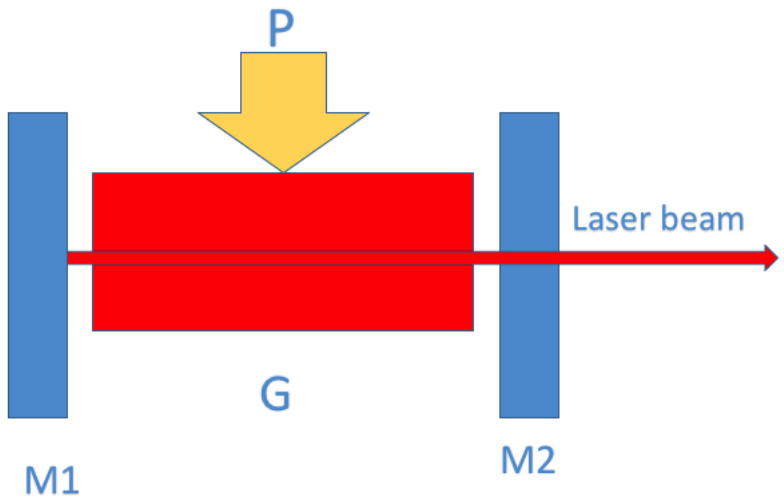

Figure 1.1.2: Schematics of the laser principle. M1 and M2 are the mirrors that make up the cavity, G is the gain medium and P is pumping (excitation)

energy from an external source towards the laser gain medium. The energy will be absorbed by the medium and will produce excited states. The external source of pumping energy depends on the type of medium of gain, we usually find the optical and electric pumping, however, more exotic pumping types such as chemical pumping can be found. It is important to note that the pumping energy must be greater than the lasing threshold of the laser.

1.2 The Laser Threshold

An important feature of a laser is the laser threshold. When the pumping rate is not large enough, the passive losses in the cavity exceed the spontaneous and stimulated emission gain, then no laser emission will occur. Thus, there is a pumping threshold where gain outweigh losses and laser emission occurs. The operating threshold of the laser can be analyzed through the rate equations [89]. To have a simpler vision but without loss of generality consider a system of two levels of energy. Let N_1 and N_2 denote the number density of atoms in ground state and excited state respectively,

$$\frac{dN_2}{dt} = R - nBN_2 - \gamma N_2 \tag{1.2.1}$$

$$\frac{dn}{dt} = -\gamma_c n + nBN_2 + \beta\gamma N_2. \tag{1.2.2}$$

The Eq.(1.2.1) is the rate of variation of atoms in the excited state, where R is the external pumping rate, $\gamma = 1/\tau_2$, τ_2 is the upper-state lifetime and $B = \gamma/p$ is a parameter governing the stimulated emission rate, where p is the number of cavity modes within the gain bandwidth of the medium. The Eq.(1.2.2) is the rate equation for the number of

photons n in the cavity, in this equation $\gamma_c n$ is the cavity decay rate due to losses such as mirror transmission, scattering and absorption and $\beta = 1/p$ is the fraction of spontaneous emission that contributes to lasing. Substituting β in the Eq. (1.2.2), we have

$$\frac{dn}{dt} = -\gamma_c n + BN_2 (n+1). \tag{1.2.3}$$

In the steady state we have $dN_2/dt = 0$ and $dn/dt = 0$, thus hence

$$\begin{aligned} R - nBN_2 - \gamma N_2 &= 0 \\ N_2 &= \frac{R}{nB+\gamma} \end{aligned} \tag{1.2.4}$$

and

$$\begin{aligned} -\gamma_c n + BN_2 (n+1) &= 0 \\ n &= \frac{BN_2}{\gamma_c - BN_2} \\ n &= \frac{N_2}{\frac{\gamma_c}{B} - N_2}. \end{aligned} \tag{1.2.5}$$

Below the threshold we can consider $n = 0$ because there is no generation of photons (actually $n \to 0$), we have

$$N_2 = \frac{R}{\gamma}. \tag{1.2.6}$$

We define the threshold inversion $N_{th} \equiv \gamma_c/B$ as the ratio between losses and the rate of generation per excited particle in the gain medium. With this definition we can obtain $R_{th} = \gamma\gamma_c/B$.

Above the threshold $n >> 1$, the last term in the Eq.(1.2.3) which is the contribution of the spontaneous emission becomes negligible, then

$$\begin{aligned} -\gamma_c n + BN_2 n &= 0 \\ N_2 &= \frac{\gamma_c}{B} \\ N_2 &= N_{th}. \end{aligned} \tag{1.2.7}$$

This result shows that once the threshold of excitation is crossed the population of the excited state becomes constant.

In the case of the generated photons we have to

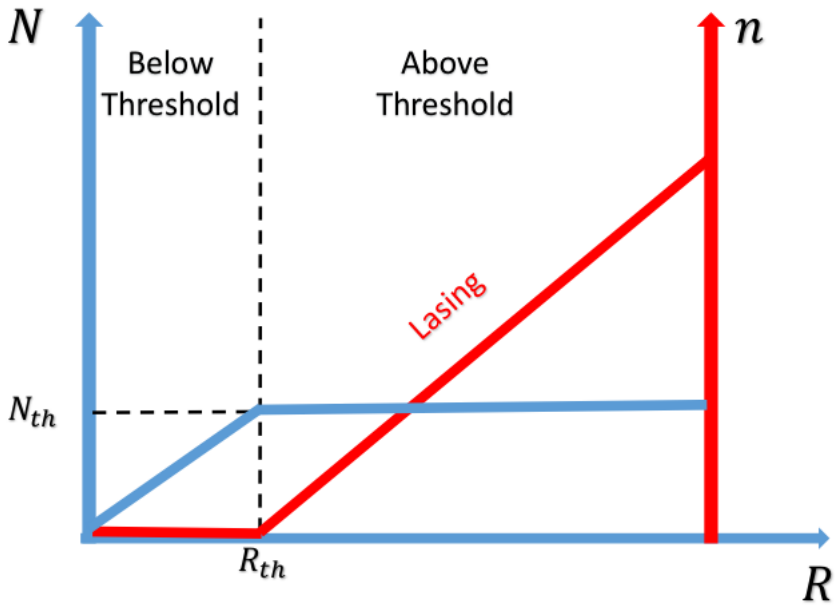

Figure 1.2.1: The figure shows that there is a threshold energy represented by R_{th} in which the system has laser emission. Below the threshold the increase of atoms N towards the excited state is linear with respect to the increase in the energy R, in the case of the emission of photons inside the cavity n is almost zero. Above the threshold the atoms in the excited state are saturated being equal to $N = N_{th}$. On the other hand the number of photons inside the cavity increases dramatically, so the system begins to operate as a laser.

$$\begin{aligned} N_{th} &= \frac{R}{nB+\gamma} \\ nB &= \gamma\left(\frac{R}{N_{th}\gamma}-1\right) \\ n &= \frac{\gamma}{B}\left(\frac{R}{R_{th}}-1\right). \end{aligned} \tag{1.2.8}$$

The number of photons generated above the threshold increases linearly with R. We must consider that R is related to the pumping energy and n is related to the output power. Figure 1.2.1 represents the behaivor described mathematically above.

1.3 Modes in a conventional laser

Previously we reviewed the main parts that make up a laser. In addition we found that for the laser emission to take place the stimulated emission must be amplified over an energy threshold. As already mentioned, the optical resonator is formed by separate mirrors at a distance d. The shape and separation distance between the mirrors determines boundary conditions for the electromagnetic wave. These boundary conditions and the special characteristics of the gain medium generate characteristic modes in the laser emission. Below we will see these characteristics and the necessary conditions for their generation.

Laser modes are the eigen-modes of a laser resonator: only specific distributions of electro-magnetic field can "resonate" in each particular resonator. Due to the Three-dimensional nature of the cavity space, each mode is described by 3 indices, n, m, q; the first two indexes are related to the ***transverse modes*** and the third index indicates the ***longitudinal modes***.

The longitudinal modes are stationary waves along the optical axis of the laser. The essential boundary condition is that the electric field must be zero on the surfaces of the reflecting mirrors, so the laser oscillations occur when the wave inside the cavity is repeated after two reflections in order that the electric fields are summed in phase. The cavity resonates when there is a half-length integer $\lambda/2$ that encompasses the region within the cavity, see Fig. 1.3.1(a)

With the boundary conditions mentioned, we have that the wave inside the cavity is a stationary wave mode, which is a left and right wave overlay

$$\begin{aligned} \vec{E}(\vec{r}) &= E_0 e^{ikz+i\phi_1} + E_0 e^{-ikz-i\phi_2} \\ &= E_0 \left(e^{ikz+i\phi_1} + e^{-ikz-i\phi_2}\right). \end{aligned} \tag{1.3.1}$$

The sum of the waves have the same amplitude because it is assumed that the mirrors are ideal, Multiplying the Eq.1.3.1 by the factor $\left(e^{i\frac{\phi_1}{2}-i\frac{\phi_1}{2}}\right)\left(e^{i\frac{\phi_2}{2}-i\frac{\phi_2}{2}}\right)$ and reorganizing, we have to

$$\vec{E}(\vec{r}) = E_0 \left[e^{ikz} e^{i\left(\frac{\phi_1+\phi_2}{2}\right)} e^{i\left(\frac{\phi_1-\phi_2}{2}\right)} + e^{-ikz} e^{-i\left(\frac{\phi_1+\phi_2}{2}\right)} e^{i\left(\frac{\phi_1-\phi_2}{2}\right)}\right] \tag{1.3.2}$$

$$= E_0 e^{i\left(\frac{\phi_1-\phi_2}{2}\right)} \left[e^{ikz} e^{i\left(\frac{\phi_1+\phi_2}{2}\right)} + e^{-ikz} e^{-i\left(\frac{\phi_1+\phi_2}{2}\right)}\right], \tag{1.3.3}$$

where ϕ_1 and ϕ_2 are the phases of the first and second fields, respectively. We will define the following amounts $\Delta\phi \equiv \phi_1 - \phi_2$ and $\bar{\phi} \equiv (\phi_1 + \phi_2)/2$, and replacing in Eq.1.3.3

$$\begin{aligned}\vec{E}(\vec{r}) &= E_0 e^{i\frac{\Delta\phi}{2}}\left(e^{i\left(kz+\bar{\phi}\right)}+e^{-i\left(kz+\bar{\phi}\right)}\right)\\ &= 2E_0 e^{i\frac{\Delta\phi}{2}} cos\left(kz+\bar{\phi}\right),\end{aligned} \tag{1.3.4}$$

applying the boundary conditions in the above equation we have

$$\vec{E}(z=0)=0 \Rightarrow \bar{\phi}=\frac{\pi}{2} \tag{1.3.5}$$

$$\begin{aligned}\vec{E}(\vec{r}) &= 2E_0 e^{i\frac{\Delta\phi}{2}} cos\left(kz+\frac{\pi}{2}\right)\\ &= 2E_0 e^{i\frac{\Delta\phi}{2}} cos(kz)\, cos\left(\frac{\pi}{2}\right) - sin(kz)\, sin\left(\frac{\pi}{2}\right)\end{aligned}$$

$$\vec{E}(\vec{r}) = 2E_0 e^{i\frac{\Delta\phi}{2}} sin(kz), \tag{1.3.6}$$

applying the condition $\vec{E}(z=d)=0$

$$sin(kd)=0 \Rightarrow kd=q\pi.$$

Thus, the round-trip accumulated phase must be some integer multiple of 2π

$$2kd=2\pi q \qquad (q=0,1,2...)$$

With this resonance condition inside the cavity, we have permitted standing waves, or cavity modes satisfy

$$k_q=\frac{\pi q}{d}. \tag{1.3.7}$$

In terms of frequency this result is equivalent to

$$\nu_q=\frac{qc}{2d}, \tag{1.3.8}$$

the first mode of oscillation available for this optical cavity:

$$\nu_1=\frac{c}{2d}. \tag{1.3.9}$$

This mode is called basic longitudinal mode, and it has the basic frequency of the optical cavity. The frequency of each laser mode is equal to integer (mode number q) times the frequency of the basic longitudinal mode. The frequency spacing is called the ***free spectral range*** (FSR), defined as

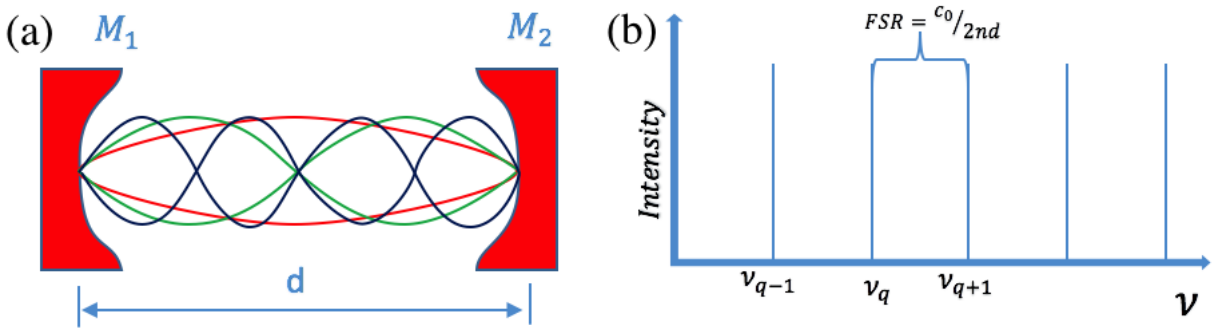

Figure 1.3.1: The allowed frequencies inside an optical cavity are determined by the length of the cavity d and the index of refraction of the active medium. The difference between two resonant frequencies defined the free spectral range (b).

$$FSR = \nu_{q+1} - \nu_q = \frac{c_0}{2nd}, \tag{1.3.10}$$

where n is the refractive index of the active medium, see figure 1.3.1(b).

Real cavities involve some loss of the light on each round trip. If the amplitude of the wave is reduced by a factor of r on each round trip, we can write the ***finesse*** as [93]

$$\mathscr{F} = \frac{\pi\sqrt{r}}{1-r}. \tag{1.3.11}$$

This amount is a parameter that characterizes the natural losses of the cavity. The frequencies are not defined mathematically as single frequencies, but each have a width of frequencies around the possible modes, with the value of the finesse and the free spectral range we can define the characteristic width of the resonance frequencies inside the cavity

$$\delta\nu_{FWHM} = \frac{FSR}{\mathscr{F}}. \tag{1.3.12}$$

We can summarize the characteristics of the Fabry-Perot cavity with these two parameters that completely specify the behavior of the cavity, see figure 1.3.2.

It is often the case that not all of the potential longitudinal modes will actually appear in the laser output and only specific frequencies are possible inside the optical cavity of a laser. In addition we must take into account the gain curve of the active medium, with a pump rate sufficient to overcome the threshold. Any cavity mode falling within this range are candidates for laser operation. From all these possible frequencies, only those that have amplification above certain minimum, will be emitted at the laser output.

1.3.1 *Tranversal modes*

In an optical cavity in addition to generating modes along the optical axis, there are also distributions of intensity in the section perpendicular to the optical axis of the laser. The

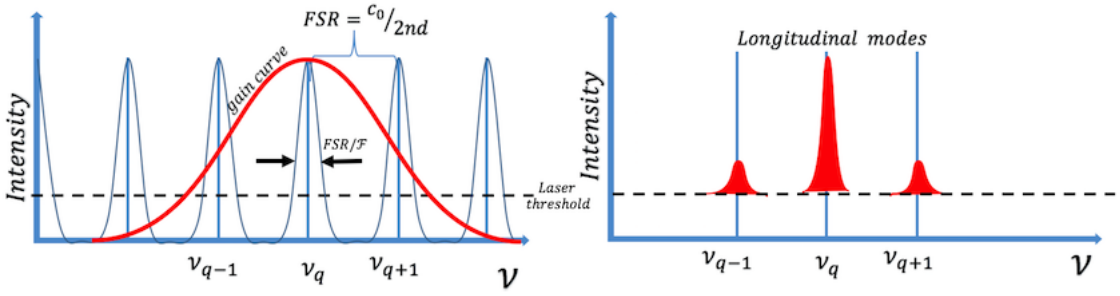

Figure 1.3.2: In the image on the left shows the resonant modes in the cavity with its spectral width given by the division between free spectral range and the finese. The red line represents the gain curve of the amplifier medium. The resulting laser cavity modes are shown on the right side when a gain bandwidth of a laser amplifier is combined with resonances of a two-mirror laser cavity.

beam generated inside the cavity is not perfectly plane wave because both mirrors and the amplifier means have finite dimensions. Considering that the mirrors are flat and of circular form, the tranverse modes can be described mathematically by [90]

$$I_{mn}(x,y) = I_0 \left[H_m\left(\frac{\sqrt{2}x}{\omega}\right) e^{\left(\frac{-x^2}{\omega^2}\right)} \right]^2 \left[H_n\left(\frac{\sqrt{2}y}{\omega}\right) e^{\left(\frac{-y^2}{\omega^2}\right)} \right]^2. \tag{1.3.13}$$

Also known as Transverse Electromagnetic Modes (TEM_{mn}) (see figure 1.3.3), and describe the shape of energy distribution in the beam cross section. In the Eq.(1.3.13) ω is a spatial scale factor and H_m is the Hermite polynomial of degree n:

$$H_n(t) = (-1)^n e^{t^2} \frac{d^n}{dt^n} e^{-t^2}. \tag{1.3.14}$$

The lowest mode is the TEM_{00} mode corresponding to a Gaussian distribution of intensities. Thus, the transverse modes determine the shape of the laser profile at the output. Where m is the number of points of zero illumination (between illuminated regions) along x axis, and n is the number of points of zero illumination (between illuminated regions) along y axis. The output intensity profile of a laser can be reproduced by superimposing all transverse modes allowed, although it is generally desirable for the laser to operate only in the fundamental mode.

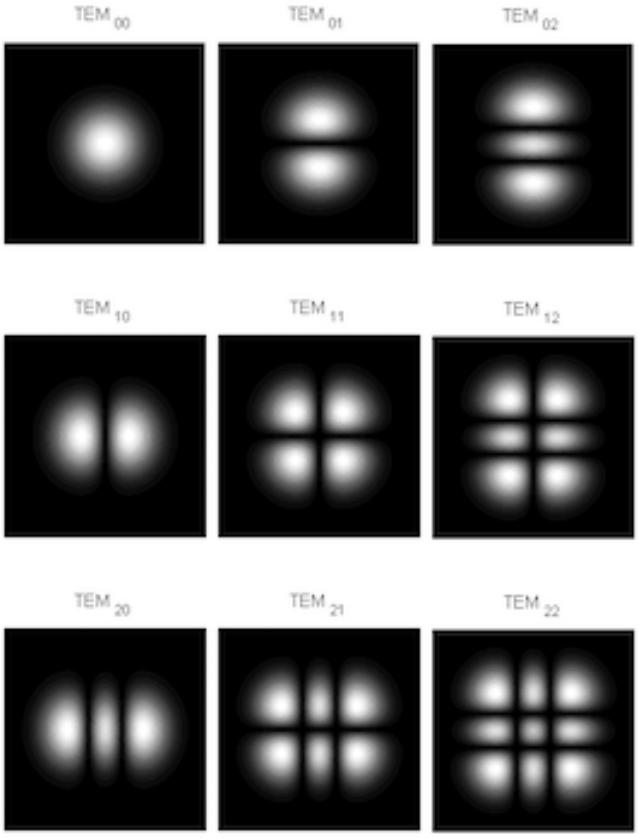

Figure 1.3.3: The figure shows patterns of intensity determined by the different TEM modes of a cavity.

2 Random Laser

Previously we saw that an essential element in a laser is the resonant cavity, and in this element the quality plays a crucial role in the stability of the laser. The disorder in these cavities introduces scattering in light that are considered highly detrimental in the operation of the laser, as they lead to laser. Next we will study a type of laser that takes advantage of the disorder, known as random lasers (RLs).

2.1 Letokhov ideas!

In a laser with a Fabry-Perot cavity and feedback resonance, the stimulated emission is spatially coherent and its frequencies are determined by modes of the resonator. In 1966 [83], in order to have control over the spatial beam coherence of the laser, Ambartsumyan et al. worked on a different type of laser that had a non-resonant feedback. This was achieved by replacing the rear mirror with a scattering surface. With this, they ensured that the light does not return to its original position after a round trip, so that the spatial resonances for the electromagnetic field are absent in the cavity. Central emission frequency of this laser is determined by the resonance frequency of a gain medium instead of eigenmodes of the cavity.

In 1968, Letokhov theoretically proposed the possibility of generating laser radiation in disordered dispersive media with gain [58]. The idea was that radiation with the same characteristics of a conventional laser could be achieved in a dispersive and disordered medium without the need for mirrors or resonant cavities. Figure 2.1.1 shows a scheme comparing a conventional laser with the idea of a random laser. The condition imposed by Letokhov was that the mean free path of the photon is much shorter than the dimension of the scattering medium.

Letokhov solved the diffusion equation for the photon density $W(\vec{r},t)$ in an amplified medium.

$$\frac{\partial W(\vec{r},t)}{\partial t} = D\nabla^2 W(\vec{r},t) + \frac{v}{l_g} W(\vec{r},t), \tag{2.1.1}$$

where v is the transport velocity of light inside the scattering medium, l_g is the gain

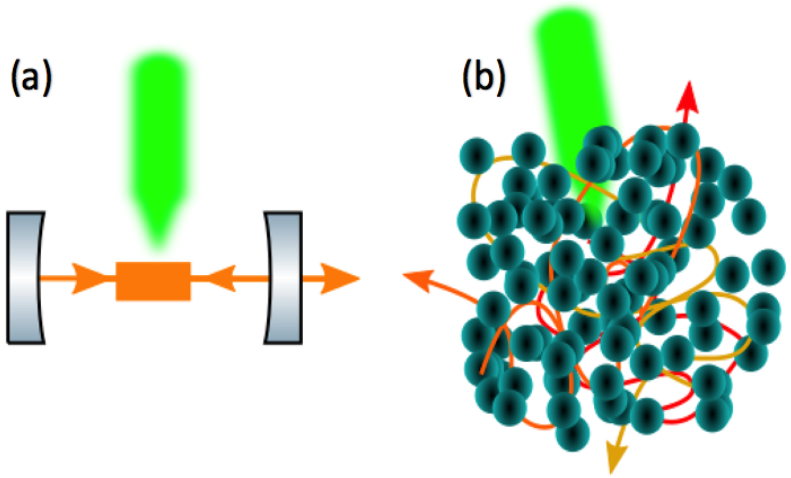

Figure 2.1.1: The figure shows a schematic comparison between a conventional laser and the random laser. (a) Conventional laser usually consists of a gain media embedded in a pair of mirrors which provides positive feedback. When the gain of the system is larger than the loss, lasing start to happen. (b) In the case of a random laser the most important is the scattering and gain media, the trapping of light is not achieved by mirrors, but by multiple scattering between sub-wavelength particles.

length, D is the diffusion constant given by

$$D = \frac{v l_t}{3}, \tag{2.1.2}$$

where l_t is the mean free path. The last term in the Eq.(2.1.1) is the gain term. Later we will make a more detailed development of the characteristic lengths l_g and l_t.

The solution to Eq.(2.1.1) can be written as

$$W(\vec{r}, t) = \sum_n a_n \Psi_n e^{-\left(DB_n^2 - \frac{v}{l_g}\right)t}. \tag{2.1.3}$$

The Eq.(2.1.3) changes from exponential decay to increase in time upon crossing the threshold

$$DB_1^2 - \frac{v}{l_g} = 0, \tag{2.1.4}$$

where B_1 is the lowest eigenvalue of the radial part of solution of the Eq.(2.1.3). If the scattering medium has the shape of sphere of diameter L, the smallest eigenvalue is $B_1 = 2\pi/L$. Substituted into Eq.(2.1.4) the threshold condition predicts a critical volume

$$V_c \simeq L^3 \simeq \left(\frac{l_t l_g}{3}\right)^{3/2}. \tag{2.1.5}$$

This result says that once the volume of the scattering medium exceeds the critical volume V_c increases exponentially with t, establishing a proportional relationship between

the mean free path and the gain length. If we consider a gain length l_g and transport mean free path l_t, once the volume $V$of the scattering medium exceeds the critical volume V_c, $W(\vec{r},t)$ increases exponentially with t. An extension of the calculations can be found in [108].

Many experimental attempts were made in order to demonstrate the theoretical proposal of Letokhov. In the 1970s, Fork et al. observed unusual optical properties in microcrystals of different luminophosphors containing Eu^{2+} [30]. The anomalously efficient and fast emission occurred in single microcrystals, the dimensions of which were on the order of several optical wavelengths, $\lambda = 0.37\mu m$.

In 1971, Varsanyi experimentally observed optically excited stimulated emission ("superradiant emission" as he called it) at the ${}^3P_0 \rightarrow {}^3\ F_2Pr^{3+}$ transition in individual powder particles of $PrCl_3$ and $PrBr_3$ [103]. The stimulated emission, which was not supported by any cavity, occurred in the volumes where linear size exceeded 1μm.

In 1986 Markushev and collegues reported intense stimulated radiation from $Na_5La_1{-}_x\ Nd_x\,(M_0O_4)_4$, found that above a certain pumping energy threshold, the duration of the emission pulse shortened by approximately four orders of magnitude [101]. Later on, was reported similar phenomena in a wide range of Nd^{3+} actived scattering materials.

The unambiguous experimental demonstration of Letokhov's theoretical works took almost 25 years to arrive. In 1994 Lawandy et al. [56] demostrated isotropic laser-like emission from an optically pumped laser dye solution of Rhodamine 640 perchlorate in methanol, the scattered points used were particles of T_iO_2 of mean diameter 250 nm approximately. The authors found that the emission from such systems can exhibit spectral and temporal properties of multimode laser oscillator, even though the systems contain no external cavity. A collapse of the linewidth of emission was observed above the threshold pump power, and was interpreted as the onset of lasing. The explanation for the first observed laser-like behavior of the optically pumped colloidal was not obvious, and generated lots of research this type of non-resonant light was related to the theoretical work of Letokhov. From this work begins to use the term Random Lasers (RLs).

2.1.1 *The regimes of the random laser and its characteristic lengths*

When light propagates through a scattering amplifyng medium performing random trajectories, it is said that light takes a random walk. The multiple scattering increases the length of the path or the residence time of the light in the active medium, thus enhancing the amplification of the light by stimulated emission. As in the case of a conventional laser where the distance between the mirrors of the optical resonator is essential for defining the laser modes, in an RLs there are also relevant length scales describing the scattering process.

2.1.2 *Scattering mean free path l_s*

The scattering mean free path l_s is defined as the average distance that light travels between two consecutive scattering events and defined as

$$l_s = \frac{1}{n_s \sigma_s}, \tag{2.1.6}$$

where n_s is the number density os scatterers and σ_s is the scattering cross-section of the individual scatter and . The σ_s depends on three variables, the size of the scatterer and its refractive index, in addition to the incident wavelength.

2.1.3 *Transport mean free path l_t*

The transport mean free path l_t is defined as the averange distance that the light travels before its direction of propagation is randomized, and defines as

$$l_t = \frac{l_s}{1-g}, \tag{2.1.7}$$

where $g = \langle cos\theta \rangle$ is the anisotropiy parameter, θ is the scattering angle for a single scattering event in the sequence and $\langle ... \rangle$ indicates an ensemble average over all the scattering events of the sequence. For isotropic scattering $g = 0$.

2.1.4 *Gain length l_g and Amplification length l_{amp}*

Light amplification by stimulated emission in random media is described by the gain length l_g and the amplification length l_{amp}. The gain length is defined as the path length in the active medium over which light intensity is amplified by a factor e. The amplification length is defined as the (rms) average distance between the beginning and ending point for paths of length l_g. When the medium is homogeneous without scattering $l_{amp} = l_g$. In the diffusive regime, $l_{amp} = \sqrt{Dt}$, where D is the diffusion coefficient and $t = l_g/v$, v is the transport velocity. In a three-dimensional medium the diffusion is $D = vl_t/3$, thus

$$l_{amp} = \sqrt{\frac{l_t l_g}{3}}. \tag{2.1.8}$$

Similarly we can define the absorption length,

$$l_{abs} = \sqrt{\frac{l_t l_i}{3}}, \tag{2.1.9}$$

where l_i is the inelastic men free path, defined as the path length over wich light intensity is reduced to $1/e$ due to absorption. Hence, the amplification length l_{amp} is analogous to the absorption length l_{abs}.

2.1.5 *Random Lasers with incoherent or non-resonant feedback*

The lasers with non-resonant feedback is a terminology first proposed in the late 1960s [58, 83]. The feedback in such a laser serves to return part of energy of photons to gain medium. The light in the cavity suffers multiple scattering, changing its direction each time it is scattered, thus any spatial resonance is absent.

As already indicated, Letokhov theoretically proposed self-generation of light in a random amplified medium in the ***diffusive regime*** ($L >> l_t >> \lambda$). Letokhov showed that as the volume of the scattering medium exceeds the critical volume, the photon energy density increases exponentially with time. This process is analogous to the multiplication of neutrons in an atomic bomb [95]. In this type of random laser, the phase condition within the scattering medium is ignored because of the non-resonant nature of feedback provided by the scatters. Consequently, the mean frequency of the random laser only depends on the center frequency of the emission band of the gain media. Therefore, this kinds of laser is called a random laser with non-resonant feedback. This terminology is being argued by several authors.

In the references [56, 79] we can find examples of isotropic laser-like emission optically pumped laser dye solution (Rhodamine 640) where a collapse of the linewidth of emission was observed when it was added scattering particles (TiO_2microspheres of mean diameter $< 1\mu m$).

2.1.6 *Random Lasers with coherent or resonant feedback*

When the scattered light is trapped to form a closed loop in the disordered medium, the scattering can provide a coherent feedback. In this case to obtain the closed loops a strong scattering medium and a high optical gain must be obtained. Thus the light returns to a scatter where it was scattered before forming a closed "cavity" analogous to two mirrors. The strong scattering condition is achieved when the mean free path becomes comparable with the emission wavelength (***localization regime,*** $l_t \sim \lambda$). If the amplification along such a loop path exceeds the loss, the oscillation of the laser should occur in the loop which serves as a laser resonator. The requirement that the phase shift along the loop be a multiple of 2π (condition for constructive interference). Random lasing with coherence feedback is characterized by the appearance of a narrow discrete laser peak in the emission spectrum (Spikes) above the pump threshold in addition to a drastic increase in the emission intensity. In references [17, 18] we can find examples of coherent random laser.

2.1.7 *Modes in Random laser*

In conventional lasers, the optical cavity that confines the photons also determines essential characteristics of the lasing modes. Random lasers are disordered media with gain

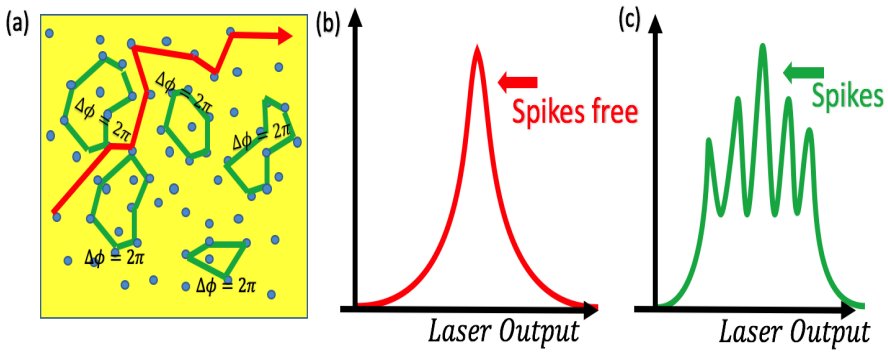

Figure 2.1.2: The random laser regimes are illustrated in (a), the red arrow shows the case of incoherence feedback while the green arrows represent the closed loops for th case of coherent feedback, where the spikes free correspond to incoherent feedback (b), whereas the coherent feedback is recognized by its spiky signature (c).

which do not have mirrors or a well-defined cavity, light is confined in the gain medium by means of multiple scattering. Early random laser experiments showed emission spectra that did not make it clear whether these systems could produce narrow laser lines emission dicrete line (Spikes)[56, 85]. In later studies it was shown that in some random laser systems discrete lasing lines not necessarily located at the center of the gain curve could be found [17, 18] demonstrating that in some cases random lasers behave very much like conventional multimode lasers.

Spikes observations on some types of random lasers led to the proposal of a closed loop model that emulates an optical mirror cavity, figure 2.1.2(a) shows the conceptual idea of loops with a phase shift of 2π (green arrow). These closed loops have the probability of starting at one point and returning to the same point with a phase shift of 2π (**coherent regime**). The modes generated in this regime are also known as strongly localized random laser modes. On the other hand the observation of a continuous emission spectrum with absence of Spikes but with a decrease in the width of the emission spectrum that is characteristic of a laser above the threshold, is known as random laser with weakly localized modes. In this case the resonance occurs with respect to the center frequency line of the gain medium, it is also known as an **incoherent feedback regime**, figure 2.1.2(a) shows the conceptual idea of a random laser with incoherent feedback (red arrow). Figure 2.1.2(b) illustrate the spikes free correspond to incoherence feedback and figure 2.1.2(c) shows typical spikes of the coherence feedback.

Another scenario is the case when we have coexistence of weakly and strongly localized lasing modes that was presented in [28].

Different alternatives scenarios have been proposed to the early model of closed scattering loops. For example another scenario was put forward where spontaneously emitted photons accumulate gain along very long trajectories. This follows the observation of random spikes in the emission spectrum of weakly active scattering systems in single-shot experiments. For a more detailed review of these models see references [8, 9, 71].

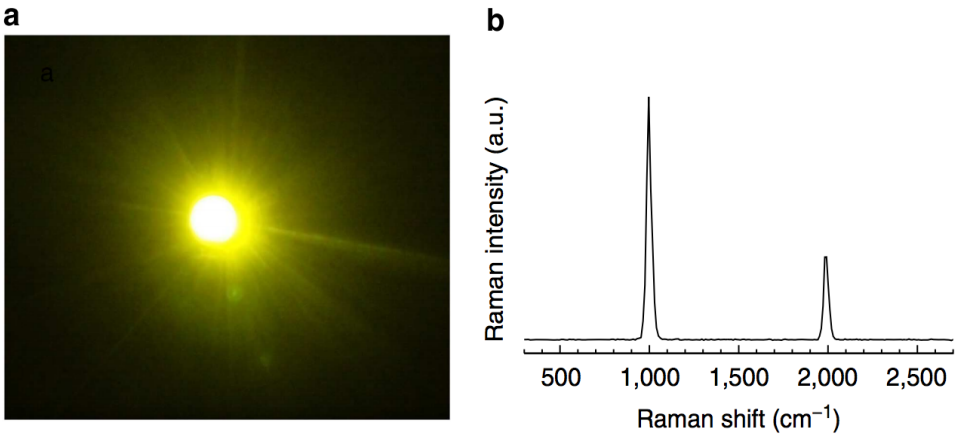

Figure 2.1.3: Bright emission from random Raman lasing. (a) Digital camera photo of random Raman lasing in $BaSO_4$ powder. (b) Spectrum of $BaSO_4$ taken through a 20.3 cm collection optic, 21 m away from the sample. a.u., arbitrary unit.

(figure reprinted from the reference [41])

If we would like to make an analogy with a conventional laser, in any of the cases the generation of the modes is related to the **longitudinal modes**. In the case of closed loops we can say that they are cavity resonators with infinite walls, this completely eliminates the possibility of having **transverse modes** in the random lasers.

2.1.8 *Advances in Random Lasers*

A major advantage of random laser over conventional lasers is that the required technology is relatively simple. This and other advantages have provoked a great interest in this type of lasers. It is the case of **Raman based random lasers**, where stimulated Raman scattering has been used to achieve random lasers. In reference [41] the authors the first experimental evidence of lasing via a Raman interaction in a bulk three-dimensional random medium, with conversion efficiencies on the order of a few percent. The traditional random lasers often have a relatively broad emission spectrum, a random laser that utilizes vibration transitions via Raman scattering allows for an extremely narrow bandwidth, on the order of 10 cm^{-1}. The random Raman laser was made of barium sulphate ($BaSO_4$) powder with particle diameters of $1-5\,\mu m$. $BaSO_4$ has the role of both the Raman gain medium and the scattering centres. The astounding brightness of the random Raman laser is illustrated in Fig. 2.1.3 with a digital photograph and with a spectrum taken from a distance 21 m from the sample using a 20.3 cm off-axis parabolic mirror as a collection optic. The special features of an random Raman laser that can produce a bright, speckle-free, strobe light source with potential application in microscopy, with the most notable application related to non-invasive biomedical imaging [88, 92, 81].

Another case of vanguard are the **Random Fiber Laser** (RFL) that combine features of traditional random lasers with characteristics of conventional fiber lasers, The first work in this direction was reported in [22] where a directional pulsed random lasing was

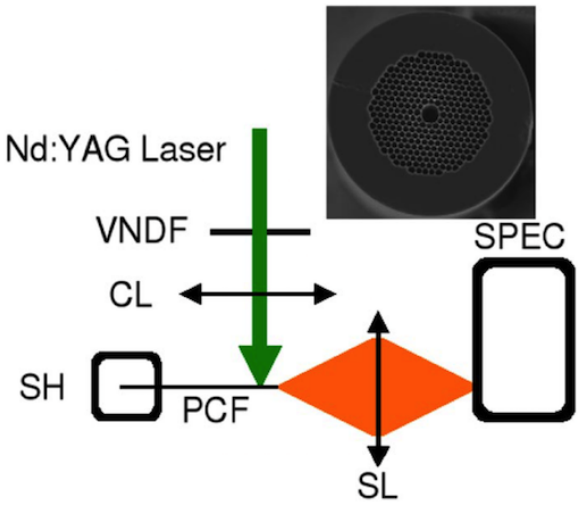

Figure 2.1.4: Side view of the experimental setup. Variable neutral density filter (VNDF); 50 mm focal length cylindrical lens (CL); Sample holder (SH); 50 mm focal length spherical lens (SL); Spectrometer (SPEC); Photonic crystal fiber (PFC) Inset: Scanning electron microscopy of the photonic crystal fiber used in the experiment (provided by Crystal Fibre A/S).
(figure reprinted from the reference [22])

demonstrated in the photonic crystal fibre with the hollow core filled with a suspension of TiO_2 nanoparticles in a Rhodamine 6G dye solution. So the fibre waveguide properties are combined with traditional bulk random material providing one dimensional random lasing. The experimental setup for the optical measurements is shown in Fig. 2.1.4. The work presented in reference [22] as well as being the first demonstration of random fiber laser, makes an important comparison with similar systems in bulk format shows that the random fiber laser presents an efficiency that is at least 2 orders of magnitude higher. The Random Fiber Laser uses also the Raman amplification for telecom applications in quasi-lossless transmission systems [3, 4, 51]

In recent time the applications of the random lasers focused to the applications of biological sensors have increased. The interest for the investigation of biological samples has generated a wealth of different techniques and applications This is the case of two interesting works [45, 33]. In [45] Ignesti and his collaborators take advantage of the fact that the emission characteristics of a random laser are very susceptible to the scattering details, to make active sensors that are used as a diagnostic tool for disordered media such as biological samples. In [33] Ghofranina and his collaborators present a work in the field of biomimetics[1]. They made disordered active materials mimicking the complex structure of paper. The random lasers realized by this material exhibit sharp distinct resonances with broad localization lengths. This is of great interest both in fundamental physics research of random lasers and in research and production of new functional materials advanced miniaturized photonic devices and applications in biomedicine and bioimaging.

In this section we have presented some of the most relevant advances in random

[1]Biomimetic refers to human-made processes, substances, devices, or systems that imitate nature.

lasers. We have made it clear that projections in fundamental physics and applications are immensely large.

2.2 Speckle in Random Laser

Next we will see how the statistical properties of the Speckle can be used to know the number of modes present in a random laser emission. First we will see the static properties of the speckle and then show in counting modes in an Random Fiber Laser that holds a very narrow peak of laser.

2.2.1 *Speckle*

Speckle is the strongly fluctuating, grainy intensity pattern resulting from the interference of a randomly scattered coherent wave.

When a coherent laser is scattered over a rough surface, the signal is decomposed into multiple independent phases and amplitudes. If we project on a screen the different phases and amplitudes after the scattering of the laser, we can treat this as the sum of a set of independent, statistically independent phasors. When these components are added together, they constitute what is know as a "random walk". The resultant of the sum may be large or small, depending on the relative phases of the various components of sum, and in particular whether constructive or destructive interference, as detail in[38].

A random phasor sum may be described mathematically as follows, [38]

$$\mathbf{A} = \frac{1}{\sqrt{N}} \sum_{n=1}^{N} a_n e^{i\phi_n}, \tag{2.2.1}$$

where N represent the number of phasor components in the sum, $\boldsymbol{A}$ represents the resultant phasor. a_n and ϕ_n are the amplitude and phase of the phasor n. It will be convenient to adopt certain assumptions about the statistics of the component phasors:

- The amplitudes and phases a_n and ϕ_n are statistically independent.
- The phases ϕ_n are uniformly distributed on the interval $(-\pi, \pi)$.

With these assumptions we can consider the real and imaginary parts of the resultant phasor

$$\mathcal{R} = Re\left\{\mathbf{A}\right\} = \frac{1}{\sqrt{N}} \sum_{n=1}^{N} a_n cos\phi_n \tag{2.2.2}$$

and

$$\mathcal{I} = Im\left\{\boldsymbol{A}\right\} = \frac{1}{\sqrt{N}} \sum_{n=1}^{N} a_n sin\phi_n. \tag{2.2.3}$$

Calculating the first moment of the real and imaginary part we have

$$\langle \mathcal{R} \rangle = \langle \mathcal{I} \rangle = 0. \tag{2.2.4}$$

Calculating the second moment of the real and imaginary part we have

$$\sigma_{\mathcal{R}}^2 = \sigma_{\mathcal{I}}^2 = \sigma^2 = \frac{1}{N} \sum_{n=1}^{N} \frac{\langle a_n^2 \rangle}{2}. \tag{2.2.5}$$

The variance σ of the real and imaginary parts of the result phasor are identical. Generally the number of elementary phasor contributions is extremely large. From the Central Limit Theorem $N \to \infty$, the joint probability density function for the real and imaginary parts are asymptotically Gaussian,

$$P_{\mathcal{RI}}(\mathcal{R}, \mathcal{I}) = \frac{1}{2\pi\sigma^2} e^{\left\{-\frac{\mathcal{R}^2+\mathcal{I}^2}{2\sigma^2}\right\}}. \tag{2.2.6}$$

Of equal interest are the statistics of the amplitude $\boldsymbol{A}$ and phase θ of the result phasor. considering that:

$$\begin{aligned} \mathbf{A} &= \sqrt{\mathcal{R}^2 + \mathcal{I}^2} && (2.2.7)\\ \theta &= arctan\left\{\frac{\mathcal{I}}{\mathcal{R}}\right\} && (2.2.8)\\ \mathcal{R} &= \boldsymbol{A}cos\theta && (2.2.9)\\ \mathcal{I} &= \boldsymbol{A}sin\theta, && (2.2.10) \end{aligned}$$

the joint probability density function of $\boldsymbol{A}$ and θ are related with $\mathcal{R}$ and $\mathcal{I}$ through

$$P_{\boldsymbol{A}\theta}(\boldsymbol{A}, \theta) = P_{\mathcal{RI}}(\mathcal{R}, \mathcal{I})(\boldsymbol{A}cos\theta, \boldsymbol{A}sin\theta) \|J\|, \tag{2.2.11}$$

where $\|J\|$ represents the Jacobian of the transformation between the two sets of variables. It follows that the joint probability density function of the amplitude and phase of the resultant phasor is given by

$$P_{\boldsymbol{A}\theta}(\boldsymbol{A}, \theta) = \frac{\boldsymbol{A}}{2\pi\sigma^2} e^{\left\{-\frac{\boldsymbol{A}^2}{2\sigma^2}\right\}}, \tag{2.2.12}$$

for $\boldsymbol{A} \geq 0$ and $(-\pi \leq \theta < \theta)$ zero otherwise.

With the joint probability of $\boldsymbol{A}$ and θ, we can find the marginal statistics:

$$\begin{aligned} P(\boldsymbol{A}) &= \int_{-\pi}^{\pi} P_{\boldsymbol{A}\theta}(\boldsymbol{A}, \theta)\, d\theta \\ P(\boldsymbol{A}) &= \frac{\boldsymbol{A}}{\sigma^2} e^{\left\{-\frac{\boldsymbol{A}^2}{2\sigma^2}\right\}} && (2.2.13) \end{aligned}$$

this result is know as the Rayleigth density function. The density function of the phase is

$$P(\theta) = \int_0^\infty P_{\boldsymbol{A}\theta}(\boldsymbol{A},\theta)\, d\boldsymbol{A} \tag{2.2.14}$$

$$P(\theta) = \frac{1}{2\pi}. \tag{2.2.15}$$

The probability of the angle θ of fasor is constant. In the speckle pattern we can measure is the intensity. The amplitude of phasor is related to intensity through to $I = f(\boldsymbol{A}) = \boldsymbol{A}^2$. Let us consider v a random variable that is related to a random variable u through a monotonic transformation $v = f(u)$. A fundamental result of probability theory says that the probability density function $P(v)$ can be found from the probability density function $P(u)$ through

$$P(v) = P(u)\left(f^{-1}(v)\right)\left|\frac{du}{dv}\right|. \tag{2.2.16}$$

Knowing the probability density function $P(\boldsymbol{A})$ we can find the corresponding probability density function $P(I)$, thus

$$P(I) = P\left(\sqrt{I}\right)\left|\frac{d\boldsymbol{A}}{dI}\right|$$

$$P(I) = \frac{1}{2\sqrt{I}}P(\boldsymbol{A}). \tag{2.2.17}$$

When the number of contributing random phasors is large, the probalility density function of the amplitud $P(A)$ is the Eq.(2.2.13), applying the transformation law, the probability density function for the Intensity I is

$$P(I) = \frac{1}{2\sigma^2}e^{\left\{-\frac{I}{2\sigma^2}\right\}} \tag{2.2.18}$$

To find the variance in the Eq.(2.2.18) is convenient to calculate the qth moments of this distribution

$$\langle I^q\rangle = \int_0^\infty I^q P(I)\, dI$$

$$= \int_0^\infty I^q \frac{1}{2\sigma^2}e^{\left\{-\frac{I}{2\sigma^2}\right\}} dI, \tag{2.2.19}$$

after some calculations we have

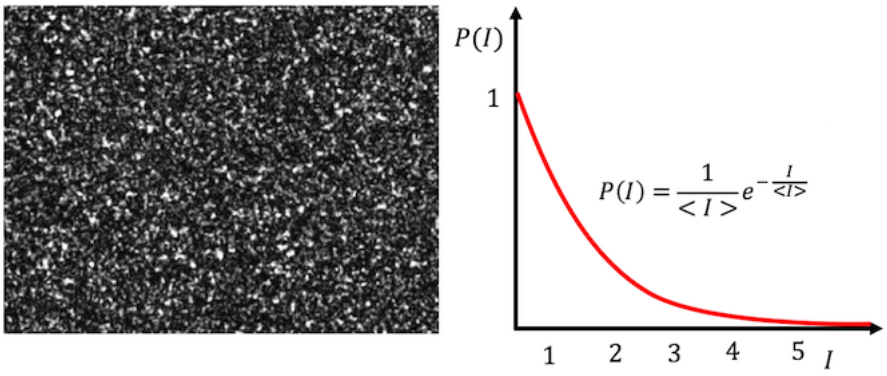

Figure 2.2.1: The figure shows a Speckle pattern produced by a laser CW He-Ne 632,8 nm (Left). The right-hand image shows the distribution for a fully developed speckle.

$$\langle I^q \rangle = \left(2\sigma^2\right)^q q!. \tag{2.2.20}$$

From the first moment we can see that

$$\langle I \rangle = 2\sigma^2. \tag{2.2.21}$$

Inserting Eq.(2.2.21) into Eq.(2.2.18) we have the probability density function can be rewitten

$$P\left(I\right) = \frac{1}{\langle I \rangle} e^{-\frac{1}{\langle I \rangle}}. \tag{2.2.22}$$

Speckle with this intensity distribution is often referred to as fully developed speckle, see fig 2.2.1. Later we will see as a fully developed speckle is related to a monomodal laser.

Of special importance is the ***Speckle Contrast***. Speckle contrast is a measure of how strong are the intensity fluctuations in a speckle pattern compared to the average intensity, given by the ratio of the standard deviation over the mean of the speckle intensity.

$$C = \frac{\sigma_I}{\langle I \rangle}. \tag{2.2.23}$$

It is also necessary to know the characteristic function of the probability density function. It requires the Fourier transform of the Eq.(2.2.22), So then we have to

$$\begin{aligned} M_I\left(\omega\right) &= \int_0^\infty e^{i\omega I} P\left(I\right) dI \\ M_I\left(\omega\right) &= \frac{1}{1 - i\omega \left\langle I \right\rangle}. \end{aligned} \tag{2.2.24}$$

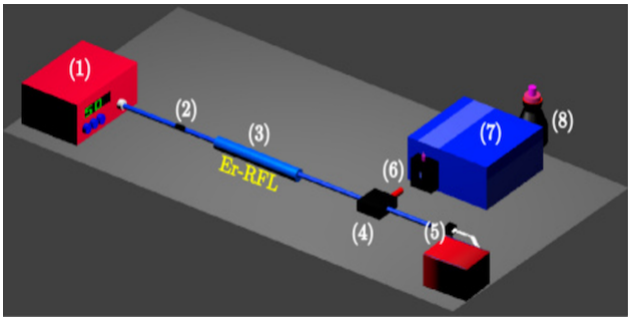

Figure 2.3.1: Experimental setup. (1) Fiber pigtailed semiconductor laser, (2) fiber connector, (3) Er-doped RFL, (4) WDM 1480–1550, (5) power meter to measure the output power, (6) RFL emission out to spectrometer, (7) spectrometer, (8) liquid-N2N2 cooled InGaAs CCD camera.

The results of Eq.(2.2.23) and Eq.(2.2.24) will be used to calculate the number of modes of a random laser emission. We will see this in the next section where we apply the concepts studied to one of our experiments.

2.3 Experiment 1: Speckle contrast to count modes in Random Laser

In the experiment we present below[2], Speckle contrast was used to measure the number of modes present in a laser emission of a random laser and a random fiber laser. A RFL is the one-dimensional fiber waveguide version of random lasers. It was first demonstrated with dye:T_iO_2 colloid in the hollow core of a photonic crystal fiber [22], and was followed by the work of Gagné and Kashyap [31] and Lizarraga et al [60], who exploited an erbium doped fiber with random fiber grating as the scattering elements. The work on RFL has been recently reviewed in the Ref.[19].

In a recent publication [35] we demostrated experimentally the glassy behavior in a one-dimensional continuous-wave erbium-doped random fiber laser (Er-RFL) through the replica symmetry breaking method (RSB). This is a concept inherent to the of spin glass theory. In the next chapter we will make an extensive analysis of this theory, for now it is necessary to know that the experimental demonstration of this theory is closely linked to the multimodal nature of the random laser. Figure 2.3.1 illustrates the experimental setup. The fiber Bragg gratings are used as the scattering medium to obtain random fiber lasers, where the gain is provided by Er ions. The characterization setup is fairly simple: a fiber pigtailed 976 nm, or 1480 nm pump laser is connected to the RFL which in turn is connected to a power meter and the spectrometer.

The important part of the analysis in this section is to notice that the narrowest Er-RFL spectrum measured was limited by the instrument resolution of $0.06\,nm$, and therefore does not show spikes representative of the longitudinal modes, see Figure 2.3.2. Nevertheless, it has been shown in a recent work with Raman RLs [42] that, in spite of a very narrow smooth spectrum with modes averaged out , the emission is actually

[2]The experiment described here is based, and in many parts is similar to the published article [35]

multimode [43].

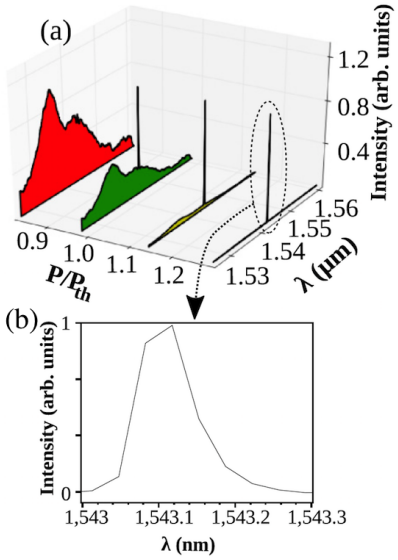

Figure 2.3.2: (a) Spectral evolution as function of the pump power P, normalized by threshold power P_{th}. (b) Resolution limited of lasing spectrum, and therefore does not show spikes representative of the longitudinal modes.

2.3.1 *Speckle Contrast for measuring lasing modes*

In the work of reference [43] the authors were able to measure the number of modes present in an emission considering the Speckle contrast, because the contrast of a Speckle pattern is an important measure of the coherence of the light source.

To address our discussion we will consider a highly coherent laser with a single output mode. A laser with these characteristics is associated with a fully developed speckle, the intensity distribution of the speckle pattern is given by the Eq.(2.2.22) and its characteristic function by the Eq.(2.2.24), also the speckle contrast in this case is $C = 1$. The loss of contrast in a speckle pattern is due to the sum of statistically independent patterns, this fact is related to a multimode laser. Next we will deduce this relation between the loss of contrast and the number of modes.

To be able to add N speckle patterns we will occupy a result from probability theory states that the probability density function of the sum of independent random variables is the convolution of the probability density functions of components of the sum [37]. Equivalently, according to convolution theorem, the characteristic function of the sum is the product of characteristic functions of the components of the sum. Thus, the product of the characteristic function is

$$M_s(\omega) = \prod_{n=1}^{N} M_n(\omega), \tag{2.3.1}$$

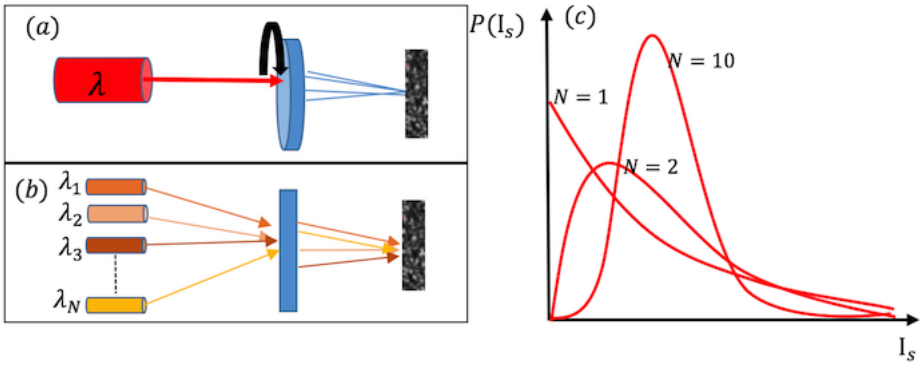

Figure 2.3.3: The figure shows the idea of the model. (a) To obtain a speckle contrast of less than 1, we can add N speckle patterns, for example with a rotating diffuser and a monomodal laser. (b) The analog model is using N monomodal lasers where each mode generates a separate Speckle pattern, leading to a fully summed Speckle pattern. In (c) three curves are shown for the Gamma Density Function of order N. The three curves are for $N = 1, 2$ and 10.

where $M_n(\omega)$ is the characteristic function of I_n, for this case the $M_s(\omega)$ becomes

$$M_s(\omega) = \prod_{n=1}^{N} \frac{1}{1 - i\omega \langle I_n \rangle}, \tag{2.3.2}$$

where $\langle I_n \rangle$ is the mean of the nth component speckle pattern. A Fourier inversion of this characteristic function will yield the probability density function $P(I_s)$ for the total intensity, assuming that all $\langle I_n \rangle$ are identical and equal I_0

$$P(I_s) = \frac{N^N I_s^{N-1}}{\Gamma(N) \langle I \rangle} e^{-N \frac{I_s}{\langle I \rangle}}, \tag{2.3.3}$$

where $\langle I \rangle = N I_0$. Such density function is know as a Gamma density function of order N. This equation is important because we now have a probability distribution to analyze a Speckle pattern that is mixed with the contribution of all Speckles, in our case it contains the contribution of all the laser modes that contributed to the fall of speckle contrast. Eq. (2.3.3) is plotted in the fig. 2.3.3 for different values of N, which also shows how the measurement can be performed.

Finally we will calculate the contrast of the sum of N independent speckle pattern. Let us consider that the total intensity as the sum of the partial intensities

$$I_s = \sum_{n=1}^{N} I_n, \tag{2.3.4}$$

the mean value of the intensity is

$$\langle I_s \rangle = \sum_{n=1}^{N} \langle I_n \rangle . \tag{2.3.5}$$

The second moment of $\langle I_s \rangle$ is

$$\left\langle I_s^2 \right\rangle = \sum_{n=1}^{N} \left\langle I_n^2 \right\rangle + \sum_{n=1}^{N} \sum_{m=1, m\neq n}^{N} \langle I_n \rangle \langle I_m \rangle , \tag{2.3.6}$$

we use the fact that individual component are fully developed speckle, therefore, we use equation (2.2.20), thus

$$\begin{aligned} \left\langle I_s^2 \right\rangle &= \sum_{n=1}^{N} \langle I_n \rangle^2 + \left(\sum_{n}^{N} \langle I_n \rangle \right)^2 \\ \left\langle I_s^2 \right\rangle &= \sum_{n=1}^{N} \langle I_n \rangle^2 + \langle I_s \rangle^2 , \end{aligned} \tag{2.3.7}$$

it follows that the variance of the total intensity is

$$\sigma_s^2 = \left\langle I_s^2 \right\rangle - \langle I_s \rangle^2 \tag{2.3.8}$$

$$\begin{aligned} \sigma_s^2 &= \sum_{n=1}^{N} \langle I_n \rangle^2 + \langle I_s \rangle^2 - \langle I_s \rangle^2 \\ \sigma_s^2 &= \sum_{n=1}^{N} \langle I_n \rangle^2 , \end{aligned} \tag{2.3.9}$$

the speckle contrast is defined as

$$C = \frac{\sigma_s}{\langle I_s \rangle} \tag{2.3.10}$$

$$C = \frac{\sqrt{\sum_{n=1}^{N} \langle I_n \rangle^2}}{\sum_{n=1}^{N} \langle I_n \rangle}. \tag{2.3.11}$$

Under the assumption that the average intensities are equal, i.e. $\langle I_n \rangle = I_0$ all n, this result reduces to the important expresion

$$C = \frac{\sqrt{N \langle I_o \rangle^2}}{N \langle I_0 \rangle} \tag{2.3.12}$$

$$C = \frac{1}{\sqrt{N}} \tag{2.3.13}$$

Where N is the number of independent Speckle patterns. In our case it corresponds to the independent number of random laser modes.

Finally we can see that

$$C = \frac{\sigma_I}{\langle I \rangle} = \frac{1}{\sqrt{N}} \tag{2.3.14}$$

where σ_I and $\langle I \rangle$ are the standard deviation and mean of the speckle intensity, respectively.

2.3.2 *Results*

The problem we addressed was to confirm the multimodal nature of the Er-RFL. As described in [35] to obtain the images of the speckle pattern a Kohler illumination system was employed similar to the reference [81]. To generate light scattering and to obtain speckle patterns a scattering medium with dried T_iO_2 of mean diameter $250\,nm$ in water solution on a microscope slide was used. The speckle pattern was captured by CCD camera operating in the visible $(400 - 900\,nm)$ or in the near infrared $(0.9 - 1.9\,\mu m)$.

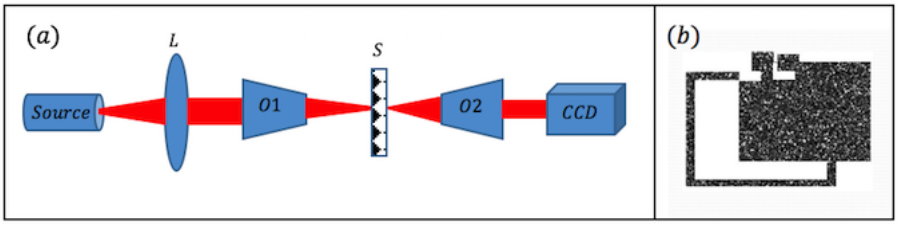

Figure 2.3.4: (a) Schematic of experimental setup. O1 and O2 are objetive lens, S is the scattering surface, the speckle pattern is collected on a CCD camera. (b) It is a scheme where it is shown that the image for Speckle contrast analysis was obtained from the central part of the Speckle pattern and later divided, obtaining the average of the contrasts of these subdivisions.

Once the speckle pattern image was obtained, the central part was selected to avoid aberrations produced by the edges of the sensor. The selected area was 600 x 600 pixeles. This area was divided into subareas of 80 x 80 pixeles, as shown in fig. 2.3.4, obtaining the contrast for each subdivision and avering these result.

The system was tested with comercial laser cw helium-neon of $632.8nm$ yielding a contrast of $C = 0.81$, equivalent to ≈ 2 modes. Furthermore, it was tested a well-characterized RL based on a rhodamine 6G dye and $250nm$ T_iO_2 particles, pumped by the second harmonic $532nm$ of a pulsed $(7ns, 5Hz)$ Nd:YAG laser yielding a contrast $C = 0.058$ equivalent to ≈ 297 modes. These two preliminary results ensure the validity of the method used (see fig. 2.3.5 (a) and (b) and table 2.1).

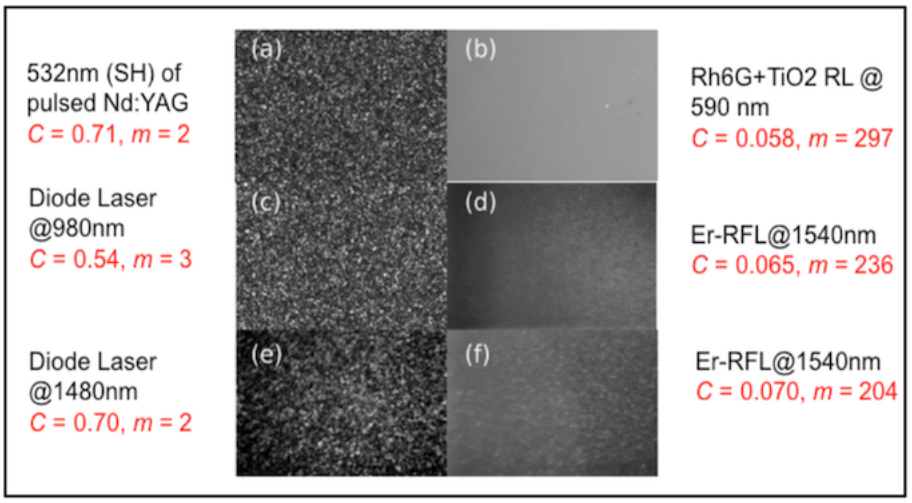

Figure 2.3.5: Speckle images of (a) second harmonic $(532\,nm)$ of a pulsed Nd:YAG laser, (b) Rh6G-T_iO_2 RL $(590\,nm)$, (c) $980\,nm$ semicondutor laser, (d) Er-RFL pumped at $980\,nm$, (e) $1480\,nm$ semiconductor laser, and (f) Er-RFL pumped at $1480\,nm$.

The Er-RFL has been described in detail in [35, 31, 59]. A home- assembled semiconductor laser operating in the continuous- wave (cw) regime at $1480\,nm$ was used as the pump source. The Er-RFL employs a polarization-maintaining erbium-doped fiber from CorActive (peak absorption 28 dB/m at $1530\,nm$, NA 0.25, mode field diameter $5.7\,\mu m$), in which a grating with randomly distributed phase errors was written [31]. Figure 2.4 shown the spectral evolution as a function of pump power for the Er-RFL. As it can be seen in Fig. 2.3.2(b), the resolution limited linewidth ($\sim 0.01\,nm$) does not show any spike, which would characterize a multimode RL.

Using the experimental setup of fig. 2.3.4, we show in figure 2.3.5 the results for the number of modes for all lasers studied, including the pump lasers. The results are summarized in Table 2.1. Therefore, it is clearly shown that the Er-RFL operates in a multimode regime, a requirement for observation of RSB, since it relies on mode interactions.

Laser wavelength	Contrast and number of modes
Pump laser @ $532\,nm$	$C = 0.71$, $m = 2$
Pump laser @ $980\,nm$	$C = 0.54$, $m = 3$
Pump Laser @ $1480\,nm$	$C = 0.70$, $m = 2$
Rh6G+T_iO_2 RL @ $590\,nm$	$C = 0.058$, $m = 297$
1D Er-RFL @ $1540\,nm$	$C = 0.065$, $m = 236$
1D Er-RFL @ $1540\,nm$	$C = 0.070$, $m = 204$

Table 2.1: Contrast ratio C of modes m for pump lasers and RLs. The Er-RFL system pumped 980 and $1480\,nm$ displays, respectively, $m = 236$ and $m = 204$ longitudinal modes.

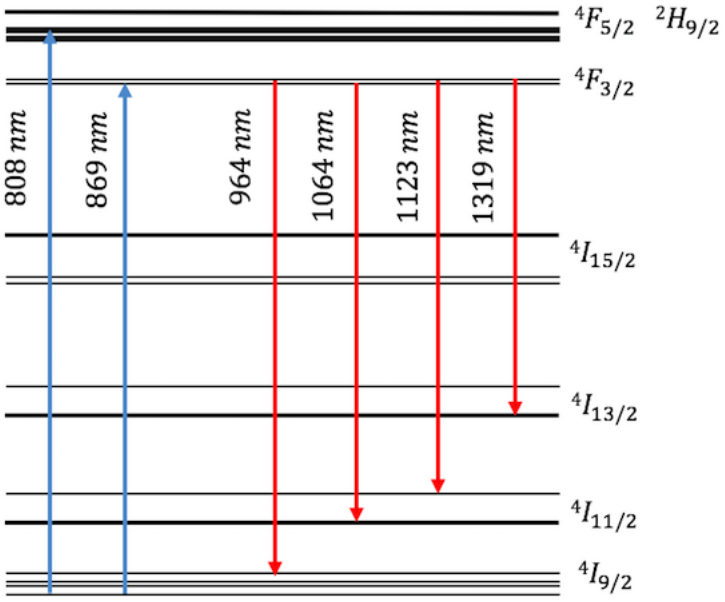

Figure 2.4.1: Energy level structure of the trivalent neodymium ion (with wavelength numbers for Nd:YAG).

2.4 Random Laser application

In the context of the applications of random lasers we present below a work related to a solid state RL system, which shows amazing characteristics[3].

2.4.1 *Experiment 2: Bichromatic Random Laser in a Nd^{3+} powder*

Neodymium (chemical symbol: Nd), is a chemical element belonging to the group of rare earth metals that has had a tremendous impact in laser physics. The Neodymium is widely used in the form of the trivalent ion Nd^{3+} as the laser-active dopant of gain media based on various host materials, including both crystals and glasses.

The Nd-laser operates operates as a four-level system where the energy of the lower laser level is $\approx 2000\,cm^{-1}$ above the Nd^{3+} ground state $^4I_{9/2}$. Usually, the Nd^{3+} is excited from the $^4I_{9/2}$ to the $^4F_{5/2}$, $^4H_{9/2}$ states by light with wavelength around $810\,nm$; afterwards, the electrons in the $^4F_{5/2}$, $^4H_{9/2}$ states decay mainly to the $^4F_{3/2}$ state from where laser action occurs as a transition to the $^4I_{11/2}$. For example, The usual pump for Nd:YAG wavelength is 808 nm (wavelengths for other host materials can somewhat differ), but a higher slope efficiency can be achieved by directly pumping into the upper laser level $4F_{3/2}$ with $869\,nm$ light. The strongest laser transition is that from $^4F_{3/2}$ to $^4I_{11/2}$ for $1064\,nm$, but other transitions are available with longer or shorter wavelengths (see Figure 2.4.1).

[3]The experiment described here is based, and in many parts is similar to the published article [70]

RLs based on the neodymium ion (Nd^{3+}) are among the most studied because the $1.06\,\mu m$ laser emission is interesting for many applications. The RL action accurs when the population inversion between the states $^4F_{3/2}$ and $^4I_{11/2}$ are large enough to provide gain and it is evidenced by narrowing of the emitted spectrum, and abrupt increasing of the emitted intensity, and shortening of the temporal decay from the $^4F_{3/2}$ state as the excitation pulse energy (EPE) is increased beyond certain threshold.

One of the current trends in the RL field is the search for optical effects analogs of the ones observed in conventional lasers (CLs). For example, it was already reported the second-harmonic (SGH) in a mixture of $Nd_{0.5}La_{0.5}Al_3(BO_3)_4$ microcrystal and non-centrosymmetric 2-methyl-4-nitroaniline particles [74], that is analogous to the intra-cavity SHG observed for CLs. More recently, it was demostrated self-frequency conversion of the RL emission at $1062\,nm$ as SHG and sum-frequency generation involving the emission at $1062\,nm$ and the exitation beam at $806\,nm$ in a $Nd_{0.04}Y_{0.96}Al_3(BO_3)_4$ crystalline powder [69].

However, the operation of bichromatic RL based on $Nd3^+$ was not yet reported. Dual-wavelength lasers (DWL) have been reported for CLs based on bulk crystals doped with Nd^{3+}[24, 46, 16] with basis on various mechanisms. The bichromatic emission was due to transitions starting from the Stark levels associated to the $^4F_{3/2}$ state [53]. If the reader had interested in the preparation and characterization Neodymium crystalline powder, you can review Appendix N1.

In this work we report a bichromatic RL based on sub-micrometer grains of crystalline $NdAl_3(BO_3)_4$ labeled as NdAB.

2.4.2 *Experimental methods*

Optical experiments were conducted as in Refs. [10,14] with the powder gently pressed into a sample-holder. The excitation source was an Optical Parametric Oscillator (OPO) pumped by the secondharmonic of a Q-switched Nd:YAG laser ($7\,ns$, $10\,Hz$). The laser repetition rate was low to prevent heating of the grains. The light beam from the OPO (For more information about OPO system see Appendix 2) was focused on the sample by a 10 *cm* focal length lens and the illuminated area was $1.2\,mm^2$. length lens and the illuminated area was tuned around $811\,nm$ to be in resonance with the Nd^{3+} transition $^4I_{9/2} \rightarrow ^4F_{5/2}$. The EPE was controlled by a pair of polarizers and measured with a calibrated photodiode. The angle between the normal to the sample and the incident laser beam was 35^o and the scattered light was collected from the front surface of the sample. Optical filters were used to eliminate the excitation laser residue from the collected signal. To change the powder's temperature, the sample-holder was placed on a hot-plate from where the emitted light was collected with a 5 cm focal length lens, focused inside of an optical fiber and sent to a spectrometer equipped with a cooled CCD (resolution: 0.024 nm). The powder temperature was determined by a thermocouple fitted in the sample

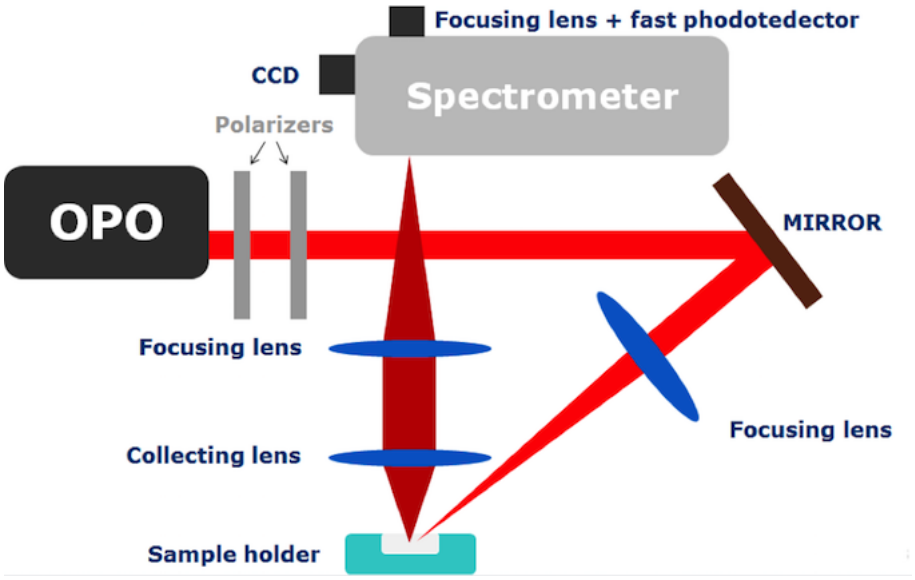

Figure 2.4.2: setup experimental

holder. Unless specified, the measurements were performed at room temperature of 22 °C.

2.4.3 *Result*

The RL emission was characterized by recording the emitted spectra of the Nd^{3+} transition $^4F_{3/2} \rightarrow {}^4I_{11/2}$ and monitoring the emitted light intensity versus the EPE. Fig. 2.4.3(a), (b) and (c) shows the behavior for EPE corresponding to 0.2, 0.3, and 1.6 mJ, respectively. The insets of Fig. 2.4.3(b) and (c) show the Nd^{3+} energy levels diagram with the transitions corresponding to the excitation at $811\,nm$ nm and the emissions around $1.06\,\mu m$. Two narrow emissions at 1063.5 and $1065.1\,nm$ were unveiled as the EPE was increased.

The intensity dependence of the Nd^{3+} emissions versus the EPE is shown in Fig. 3(a) where the RL action is revealed by the change in the slope efficiencies for the emissions at 1063.5 and $1065.1\,nm$. For $0.30\,mJ <$ EPE $< 0.54\,mJ$ only the emission at $1063.5\,nm$ was observed. Another evidence of RL emission is the spectral narrowing that is noticeable by comparing Fig. 2.4.3(a) and (b). The RL emission was also corroborated by the reduction of the lifetime, τ, of the $^4F_{3/2}$ state, e.g. for EPE $< 0.30\,mJ$ we measured $\tau = 50\,\mu s$ while for EPE $> 0.30\,\mu s$ it was measured to be $\tau \approx 10\,ns$. The emissions at 1063.5 and $1065.1\,nm$ are attributed to the Nd^{3+} positioned in two different crystalline sites labeled A and B, indicated in the inset of fig 2.4.3(c). The existence of nonequivalent Nd^{3+} environments in the $NdAl_3(BO_3)_4$ crystal was reported in Ref. [47]. It was demonstrated that the ions in different sites feel different crystalline fields that correspond to different absorption and emission spectra. Depending on the number of sites, it is possible to have multiline laser oscillation, as already reported in conventional lasers [49], and

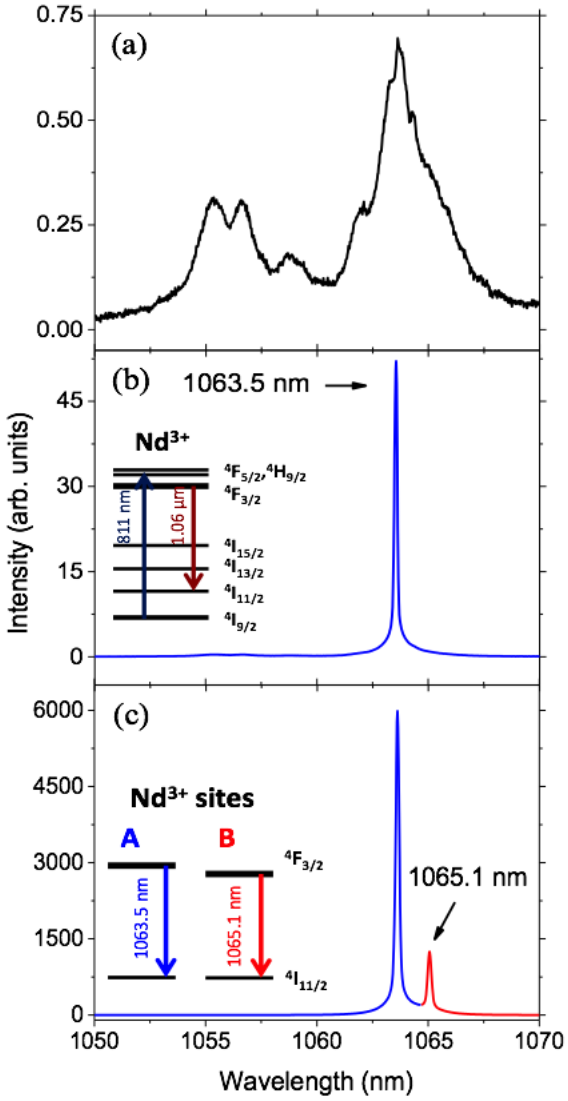

Figure 2.4.3: Spectra of Nd^{3+} transition $^4F_{3/2} \rightarrow ^4I_{11/2}$ for different excitation pulse energies (EPEs). (a), (b) and (c) correspond to EPE=0.2, 0.3 and $1.6mJ$, respectively. The inset in (b) is the Nd^{3+} energy level diagram representing the transitions corresponding to the absorption at $811\,nm$ and random laser (RL) emissions around $1.06\,\mu m$. The inset in (c) illustrates the RL emissions due to Nd^{3+} in two different site-symmetries.

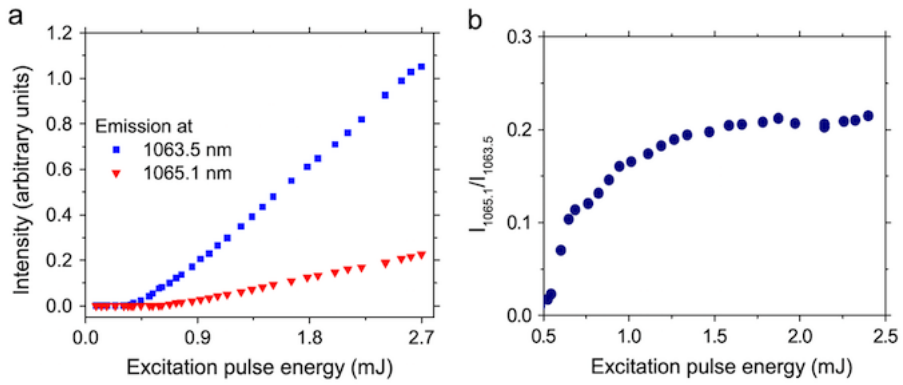

Figure 2.4.4: Intensity dependence of the emissions at 1063.5 and 1065.1 nm versus the excitation pulse energy (EPE). (b) Intensity ratio of the RL emissions at 1065.1 and 1063.5 nm versus the EPE.

the laser spectrum can be strongly dependent on the excitation wavelength due to different absorption spectra of the Nd^{3+} located in the different sites. In a similar manner, the RL spectrum reported in the present manuscript was dependent on the excitation wavelength as follows. For excitation at 810 nm, only the RL emission at 1063.5 nm was observed with the peculiarity that the slope efficiency was larger than that obtained by exciting at 811 nm. For excitation wavelength beyond 811 nm, the intensities of both emissions decreased compared to the intensities when the excitation is tuned to 811 nm. Although $NdAl_3(BO_3)_4$ powders were investigated for RL emissions, the simultaneous RL emissions at 1063.5 and 1065 nm were not observed, probably due to the fact that the excitation wavelength was not scanned around the Nd^{3+} absorption transitions, and this experimental characteristic has not been reported.

The linear growth with the EPE of the two RL emissions and different thresholds in Fig. 2.4.4(a) reinforce that the two RL lines are independent of each other in the sense that the bichromatic emission is not due to energy transfer between the Nd^{3+} in sites A and B. The different thresholds and slope efficiencies are attributed to the different stimulated emission cross section of the two centers. Due to the different EPE thresholds, the intensity ratio of the two emissions is independent of the EPE only for large values of the EPE, as described in Fig. 2.4.4(b). The smaller RL threshold, narrower linewidth, larger efficiency and slope efficiency corresponding to the emission at 1063.5 nm, suggest that the gain for RL emission from site A is larger than from the Nd^{3+} in the B site. This behavior indicates that more Nd^{3+} ions are located in the site A and/or the stimulated emission cross-section of the ions located in the site A is larger than that of the ions located in site B. Regarding the thermal effects observed in a NdAB cavity laser [61], since we used a pulsed laser operating at low repetition rate, the thermal effects are negligible which is evidenced by the linear growth of the RL emissions in Fig. 2.4.4(a) with the absence of deleterious effects.

In RLs, the output spectrum can change from shot-to-shot of the excitation beam due to multimode competition, this change is pronounced around the EPE threshold, and

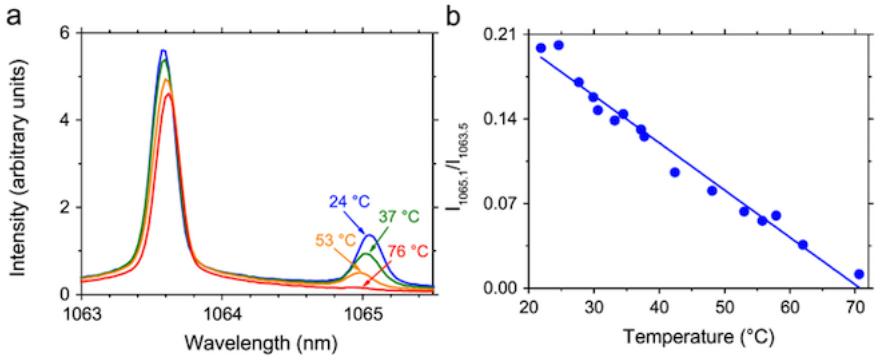

Figure 2.4.5: Emited spectra of the Nd^{3+} transition $^4F_{3/2} \rightarrow ^4I_{11/2}$ for different temperatures. (b) Temperature dependence of the intensities ratio of the signals at 1065.1 ($I_{1065.1}$) and 1063.5 nm ($I_{1063.5}$).

presents a trend of suppression at larger EPE. In the present case, for EPE well-above the RLs thresholds, the RL output spectrum was quite stable in intensity and wavelength.

Fig. 2.4.5(a) shows the RL spectra for different temperatures of the powder. Notice that as the temperature increases, the peak at 1063.5 nm shifts to longer wavelengths while the one at 1065.1 nm shows a blue-shift. The peak intensities of both emissions at 1065.1 nm ($I_{1065.1}$) and 1063.5 nm ($I_{1063.5}$) decrease linearly as the temperature increases, a behavior attributed to the decrease and broadening of the Nd^{3+} stimulated emission crosssection due to the phonon–ion interaction.

Fig. 2.4.5(b) presents the temperature dependence of the intensities ratio, R= $I_{1065.1}/I_{1063.5}$, between the two spectral lines. As above mentioned, the intensities of both emissions decrease linearly with the temperature and the decreasing rate of the emission at 1063.5 nm is smaller than that at 1065.1 nm. Then, R presents a pseudo-linear behavior in the temperature range of the experiments, which explains the linear behavior shown in Fig. 2.4.5(b). Owing to the thermal sensitivity of the RL emissions, we foresee the use of the two-color RL emission as an optical sensor capable to determine the temperature of a medium hosting the NdAB nanocrystals.

2.4.4 *Possible future applications*

By defining the thermal sensitivity $S = \frac{1}{R_0}\frac{dR}{dT}$, as in Refs. [12, 21], with R_0 being the intensity ratio at room temperature, the value of S is $\sim 0.020\,^oC^{-1}$. Notice that the herein demonstrated temperature sensor can be applied for studies of biological systems because the excitation and emission wavelengths are in the first and second biological windows, respectively. It is known as biological windows to the regions of the electromagnetic spectrum in which the absorption of light by the biological tissues is minimized. Biological windows are the spectral ranges in which the tissues have a partial transparency due to the reduction of both absorption and light scattering [55]. The first biological window extends from 700 to 950 nm and corresponds to the spectral space defined between the

visible absorption of hemoglobin[4] and the characteristic absorption band of water at $980\,nm$ [48]. The second biological window extends from 1000 to $1350\,nm$, these limits imposed by the specific absorption of water [91].

Moreover, the emitted wavelengths are close enough to be analyzed using simple detection systems without requiring correction due to the wavelength sensitivity of the equipment. Finally, we emphasize that the proposed optical thermometer can provide excellent results and be an alternative to other thermal sensors based on luminescence such as those shown in the references [50, 14].

[4]Red pigment contained in the blood, whose function is to capture the oxygen and communicate it to the tissues, and to take carbon dioxide from them and transport it back to the lungs to expel it.

3 Random Laser as a complex system

A system is complex if its behavior crucially depends on the details of the system. (G. Parisi)

3.1 Glassy Systems

The idea of a glassy system comes from the behavior of a glass that can be considered as a liquid in which the diffusive movement of the particles is enormously slow and its ability to flow has been suppressed in experimentally accessible time scales. The slowing down is described by a characteristic time, known as relaxation time, over which the slowest measurable processes relax to equilibrium.

In solid-state physics, glassy dynamics designates the extremely slow dynamics observed in disordered systems below and slightly above the glass transition. Generally characterized as "relaxation", it comprises both the aging of quenched systems (relaxation into equilibrium) and fluctuations in a stationary state (relaxation in equilibrium). In a more general sense, the term glassy dynamics designates dynamical processes which are non-stationary on the time scales available to human observers. Such processes are often encountered is systems possessing, for whatever reason, a very large number of metastable configurations.

3.1.1 *Spin glass Theory*

In the 1960ies, certain magnetic alloys such as AuFe or CuMg, were found to have rather anomalous magnetic and thermal properties that seemed to indicate the existence of a new kind of phase transition, clearly distinct from conventional ferromagnetic materials. This type of alloys are systems with localized electronic magnetic moments whose interactions are characterized by *quenched randomness*[1]: a given pair of localized moments (spins) have a roughly equal a priori probability of having a ferromagnetic or an antiferromagnetic interaction. Figure 3.1.1 shows in (a) and (b) a scheme of the spins in the ferromagnetic

[1] In statistical physics, a system is said to present quenched disorder when some parameters defining its behaviour are random variables which do not evolve with time, i.e.: they are quenched or frozen.

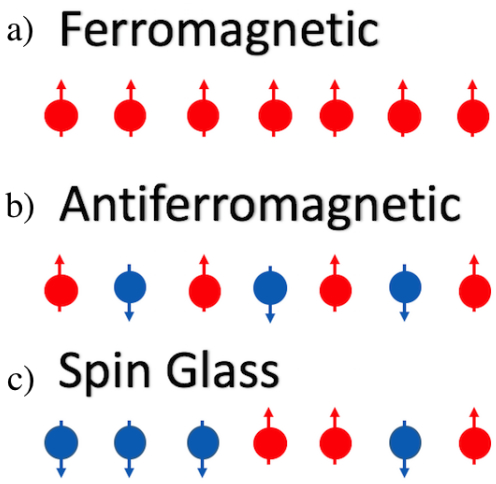

Figure 3.1.1: Schematic representation of the order of the spines in the case (a) Ferromagnetic, consisting of a array of parallel electron spins (nearest neighbor). (b) In materials that exhibit antiferromagnetism the spins of electrons, align in a regular pattern with neighboring spins pointing in opposite directions. (c) In Spin Glass case the magnetic spin are not aligned in a regular pattern. This disorder generates metastable states of energy.

and antiferromagnetic states. In (c) a random mixture of ferro and antiferromagnetic systems that corresponds to a state of Spin Glass is shown.

The term "spin glass" is due to Bryan Coles in the late 1960s. The reason for the name is twofold, first that in the state of the magnetic moments (spins) on the magnetic ions seem to freeze in orientation but without any periodic ordering this reminds of the amorphous freezing of the locations of atoms in a conventional glass, and secondly that the low temperature specific heat is linear in T, again a feature of conventional glasses. In other words, the interactions are characterized by a quenched randomness, a given pair of localized moments have a roughly equal probability of having a ferromagnetic or an antiferromagnetic interaction.

So then a spin glass is constituted by many interacting variables. A major characteristic of these systems resides in the interacting couplings among the variables, if the number of interactions among the modes is high enough, the phase space can decompose in a high number of metastable states.

In a random laser, a similar situation can be expected owing to the large number of random modes that compete for the available gain. This can lead in a random laser to a behaviour similar to that of a glass transition, in which a certain configuration is 'frozen in'. Mode coupling is particularly strong for extended modes that cover a large volume of the sample. Several modes can partially occupy the same volume and therefore compete for the same gain molecules. The mode coupling therefore takes place through the gain mechanism, which means that modes of different wavelengths can still be coupled, even if they are not spectrally overlapping.

3.1.2 *Edwards Anderson model*

The modern theory of spin glasses began with the work of ***Edwards and Anderson*** (EA model) [27], who proposed that the essential physics of spin glasses lie not in the details of their microscopic interactions but rather in the competition between quenched ferromagnetic and antiferromagnetic interactions. It should therefore be sufficient to study the Hamiltonian

$$H_J = -\frac{1}{2}\sum_{i,j} J_{ij}\sigma_i\sigma_j - h\sum_i \sigma_i \tag{3.1.1}$$

where i is a site in a d-dimensional cubic lattice, $\sigma_i = \pm 1$ is the is the Ising spin at site i, h is an external magnetic field, and the first sum is over nearest neighbor sites only. To keep things simple, we take $h = 0$, and the spin couplings J_{ij} to be independent Gaussian random variables whose common distribution has mean zero and variance one. With these simplications, the EA Hamiltonian has global spin inversion symmetry. We denote by J a particular realization of the couplings, corresponding physically to a specific spin glass sample. As already mentioned, each J_{ij} is supposed to be distributed independently according to a probability distribution $P(J_{ij})$. Once often uses the Gaussian model and $\pm J$ model as typical examples of the distribution of $P(J_{ij})$. Their explicit forms are

$$P(J_{ij}) = \frac{1}{\sqrt{2\pi J^2}} e^{\left\{\frac{\left(J_{ij}-J_0\right)^2}{2J^2}\right\}} \tag{3.1.2}$$

$$P(J_{ij}) = p\delta(J_{ij} - J) + (1-p)\,\delta(J_{ij} + J), \tag{3.1.3}$$

respectively. Eq. (3.1.2) is a Gaussian distribution with mean J_0 and variance J^2 while in Eq. (3.1.3) J_{ij} is either $J\,(>0)$ with porbability p, or $-J$ with probability $1-p$. In the EA model the randomness in site positions (site randomness) is considerd less relevant to the macroscopic properties of spin glasses compared to the randomness in interactions (bond randmness). Thus J_{ij} is supposed to be distributed randomly and independently at each (ij) according to a probability like (3.1.2) and (3.1.3).

In this model was necessary to introduce a order parameter to describe magnetic freezing without periodicity. In fact EA model gave two versions: one based explicitly on temporal freezing

$$q(t, t+\tau) = \frac{1}{N}\sum_i \langle \sigma_i(t)\cdot\sigma_i(t+\tau)\rangle, \tag{3.1.4}$$

where $\langle\cdot\,\rangle$ refers to a dynamical average, and the other based on ensemble averaning,

$$q = \frac{1}{N}\sum_i |\langle\sigma_i\rangle|^2, \tag{3.1.5}$$

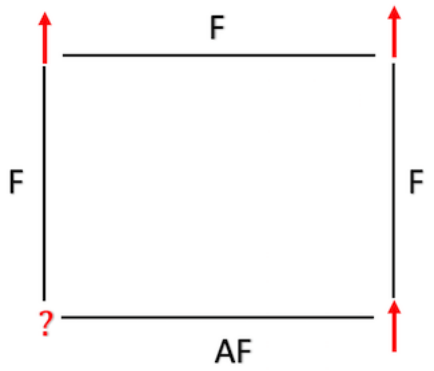

Figure 3.1.2: An example of a 2×2 lattice frustrated. Where F correspond to Ferromagnetic couplings ($J_{ij} > 0$). AF corresponds to an antiferromagnetic coupling ($J_{ij} < 0$). One possible arrangement of spins at the corner sites is shown.

with $\langle \cdot \rangle$ is referring to an ensemble-average restricted to one symmetry breaking macro-state. The phase transition is signalled by q becoming nonzero.

3.1.3 *Sherrington-Kirkpatrick Model*

An important, exactly solvable model of a spin glass was introduced by D. Sherrington and S. Kirkpatrick in 1975. The important feature of Sherrington-Kirkpatrick model is that this model includes ***frustration***. A system is in a frustrated state when there is no single configuration favorable to all spins interactions. In the figure 3.1.2 is shown a schematic representation of the frustration where AF corresponds to an antiferromagnetic coupling, two possible arrangement of spins at the corner sites can satisfy the condition. So then the frustration favors the increase of configurations with the same energy.

The Hamiltonian system in the Sherrington-Kirkpatrick is

$$H\left(J, h, \sigma\right) = -\sum_{i,j} J_{ij}\sigma_i\sigma_j - h\sum_i \sigma_i. \tag{3.1.6}$$

Each i atom is assigned a σ_i corresponding to the magnetic moment, the interaction between these moments is represented by the interchange interaction J_{ij}, which are random and independent values. The Spin Glass systems is related to a ferromagnetic type interaction ($J_{ij} > 0$) when the moments are of equal sign on antiferromagnetic ($J_{ij} < 0$) when the moments are of opposite signs.

The equilibrium solution of the model, after some initial attempts by Sherrington, Kirkpatrick and others, was found by Giorgio Parisi in 1979 within the replica method.

3.1.4 *Replica Symmetry Breaking*

David Sherrington and Scott Kirkpatrick applied the ideas introduced by Edward and Anderson to a model, which allowed an exact mean-field approach. They concluded that

this approach was ill-defined as it led to a solution with negative entropy [87]. In the works [76, 77], Giorgio Parisi introduced the so-called Replica Symmetry Breaking (RSB) scheme for mean-field spin-glass models, which allowed to solve the negative-entropy conundrum and to understand physical properties of the spin glass phase. In this method one considers n non-interacting replicas of the system, which allows for replacing the quenched averages by the $n \to 0$ limit averages. In the year 1984 M. Mezard, G. Parisi and his collaborators [67], proposed a probability distribution for an order parameter for Spin Glasses. In addition they demonstrated that this probability depends on the particular realization of the couplings even in the thermodynamic limit.

The essential idea is that the low-temperature phase consists not of a single spin-reversed pair of states, but rather of "infinitely many pure thermodynamic states" [77], not related by any simple symmetry transformations. In the low temperature phase, and in the limit $N \to \infty$ we can have ergodicity breaking: the system at equilibrium explores only a sub-part of the phase space. When this happens the measure can be split into sub-components, called pure states [73],

The approach to investigate the different phases of a physical system starts with the mean field approximation. In the mean field approximation has been formulated by using the infinite range model [87], where the partition function is given by

$$Z\left(\beta, J, h\right) = \sum_{\{\sigma\}} e^{-\beta H(J,h,\sigma)} \tag{3.1.7}$$

and the Hamiltonian is

$$H\left(J, h, \sigma\right) = -\sum_{i,j} J_{ij}\sigma_i\sigma_j - h\sum_i \sigma_i \tag{3.1.8}$$

where the σ_i $i = 1, ..., N$ are Ising spin, the sum $\sum\limits_{ij}$ runs over all pair of spins, and J_{ij} are random couplings obeying a given probability distribution, which we suppose to be symmetric, with variance $1/\sqrt{N}$. In order to study the Hamiltonian (3.1.8) we used the replica approach.We consider an Ising system, the total nymber of spin (N) being sufficiently large so that we stay near the thermodynamic limit. As usual, the statistical expectation values are given by

$$\langle O\left(\sigma\right)\rangle = \frac{\sum_{\{\sigma\}} O\left(\sigma\right) e^{-\beta H(\sigma)}}{\sum_{\{\sigma\}} e^{-\beta H(\sigma)}}, \tag{3.1.9}$$

$O\left(\sigma\right)$ and $H\left(\sigma\right)$ being an observable and the Hamiltonian, respectively. which can be decomposed as a sum over the pure equilibrium (clustering) states:

$$\langle \cdots \rangle = \sum_{\alpha} P_\alpha \langle \cdots \rangle_\alpha, \quad \sum_{\alpha} P_\alpha = 1 \tag{3.1.10}$$

For each of the pure states (labeled by α) the spontaneous magnetization may be different from zero, while the connected correlation function should go to zero at large distances (clustering). The local moment of a pure state α of a spin glass is $m_i^\alpha = \langle\sigma_i\rangle_\alpha$ at each point i of system. The overlap $q^{\alpha\beta}$ of the two pure states α and β . In terms the Replica Symmetry Breaking α and β are replicas the systems (defined in the importance reference [77])

$$q_{\alpha\beta} = \frac{1}{N}\sum_{i=1}^{N} \langle\sigma_i\rangle_\alpha \langle\sigma_i\rangle_\beta \tag{3.1.11}$$

Note that when $\alpha = \beta$, $q^{\alpha\alpha}$ is the Edwards-Anderson order parameter (Eq. (3.1.5)). Given the infinity of states, quantities referring to individual pure states are of little use, what is really of interest is the distribution of overlaps

$$P_J(q) = \sum_{\alpha,\beta} P_\alpha P_\beta \delta\left(q - q^{\alpha\beta}\right), \tag{3.1.12}$$

when $P_J(q)$ is referred to as the ***Parisi overlap distribution***. Is denoted by $P(q)$ the average of $P_J(q)$ over the coupling distribution:

$$P(q) = \overline{P_J(q)} \tag{3.1.13}$$

This average is needed because the theory predicts that the function P_J changes dramatically from system to system.

If there is a single pure state, such as the paramagnet at $T > T_c$, then $P_J(q)$ is simply a δ-function at $q = 0$. For ferromagnets with free or periodic boundary conditions, there are only two pure states, namely the uniform positive and negative magnetization states. According to the Parisi solution, for fixed J and large N, it has the form qualitatively sketched in fig. (3.1.3)(a). Let is consider $P(q) = lim_{N\to\infty} P_N(q)$, the resulting distribution $P(q)$ will be supported on all values of q in the interval $[-q_{EA}, q_{EA}]$; a sketch is shown in figure 3.1.3(b).

3.1.5 *Glassy behavior of light in random lasers*

Since the 1970s, many authors have outlined that the threshold for lasing can be interpreted as a thermodynamic phase transition and these ideas spread out in the field of photonics [1]. In this reference, the authors shows that when the average energy into each mode increases (i.e., the "temperature" is decreased, in the case of magnetic transitions), the system undergoes a glass transition, meaning that its dynamics slows down and an exponentially large number of states appears. They correspond to "mode-locked" states of a random laser. In this subsection we expand some calculations that are necessary to understand results that will be important for a good understanding of the analyzed

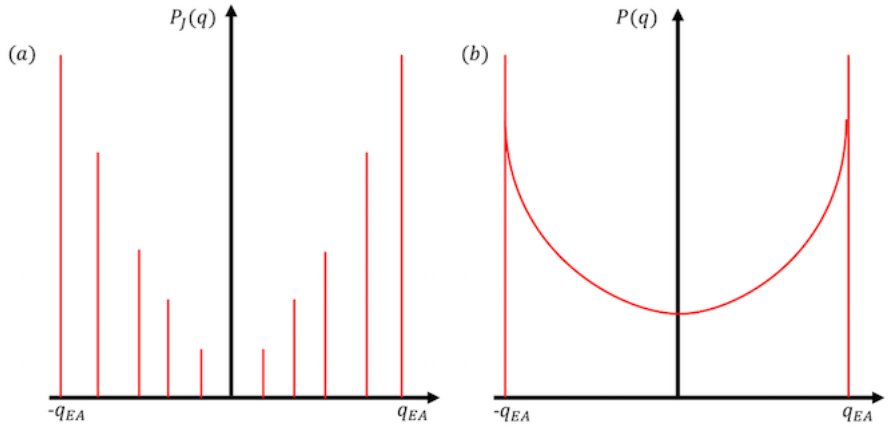

Figure 3.1.3: (a) Overlap distribution of function $P_J(q)$ below T_c. (b) Averagd distribution function $P(q)$ below T_c.

phenomenon.

We considere a dielectric resonator described by refractive index profile $n(\vec{r})$. The Maxwell's equations in the presence of nonlinear polarization $\vec{P}_{NL}$ are

$$\nabla \times \vec{H}(\vec{r},t) = \varepsilon_0 n^2(\vec{r}) \frac{\partial \vec{E}(\vec{r},t)}{\partial t} + \frac{\partial \vec{P}\left(\vec{r},t,\vec{E}\right)}{\partial t} \tag{3.1.14}$$

$$\nabla \times \vec{E}(\vec{r},t) = -\mu_0 \frac{\partial \vec{H}(\vec{r},t)}{\partial t} \tag{3.1.15}$$

In absence of nonlinear polarization $\vec{P}_{NL} = 0$, and multiplying Eq. (3.1.15) by $\nabla\times$, we have

$$\nabla^2 \vec{E}(\vec{r},t) - \varepsilon_0 \mu_0 n^2(r) \frac{\partial^2 \vec{E}(\vec{r},t)}{\partial t^2} = 0 \tag{3.1.16}$$

the solution of equation (3.1.16) decomposed in normal modes is

$$\vec{E}(\vec{r},t) = Re\left[\sum_m \sqrt{\omega_m} a_m \vec{E}(\vec{r})\, e^{-i\omega_m t}\right] \tag{3.1.17}$$

where a_m and ω_m are complex amplitude and angular frequencies respectively. The average electromagnetic energy for each unnormalized mode is given by

$$\mathscr{E} = \int_V \left\{\varepsilon_0 n^2(\vec{r})\,|E(\vec{r})|^2 + \mu_0 |H(\vec{r})|^2\right\} dV \tag{3.1.18}$$

and the total energy stored in the cavity is

$$\mathscr{E} = \sum_m \mathscr{E}_m = \sum_m \omega_m |a_m|^2. \tag{3.1.19}$$

The complex amplitude a_m are the fundamental degree in the statistical mechanical modeling of interacting modes (see [5]). Random lasers present strong non-trivial intensity spectral fluctuation from one excitation pulse of the pumping laser to another one. In reference [2] it found the important result for the variation of a_m

$$\frac{da_m(t)}{dt} = i\frac{\sqrt{\omega_m}}{4}\int_V \vec{E}_m^*(\vec{r})\,\vec{P}_m(\vec{r})\,dV. \tag{3.1.20}$$

It was considered that the case in which many modes are put into oscillations and interact due to the nonlinearity of the amplifying medium. Thus, the component of the nonlinear susceptibility is written as

$$P_m^\alpha = \sum_{\omega_m+\omega_p=\omega_q+\omega_r} \chi_{\alpha\beta\gamma\delta}(\omega_m;\omega_p,\omega_q,-\omega_r,\vec{r})\,E_p^\beta E_q^\gamma E_r^\delta \sqrt{\omega_p\omega_q\omega_r}\,a_p a_q a_r^* \tag{3.1.21}$$

where χ is the third order response suceptibility tensor, which in general depends on the positions in the dielectric resonator. The coupled modes read as

$$\frac{da_m}{dt} = -\frac{1}{2}\sum_{pqr} g_{mpqr}\,a_q a_r a_p^* \tag{3.1.22}$$

while

$$g_{mpqr} = \frac{\sqrt{\omega_m\omega_p\omega_q\omega_r}}{2i}\int_V \chi_{\alpha\beta\gamma\delta}(\omega_m;\omega_p,\omega_q,-\omega_r,\vec{r})\,E_m^\alpha E_p^\beta E_q^\gamma E_r^\delta dV \tag{3.1.23}$$

Eq. (3.1.22) is extended to all the modes combinations satisfying the frequency matching condition $\omega_m = \omega_q + \omega_r - \omega_p$, we recall that the frequencies satisfying this relation can be divided into three categories (In reference [75] the reader will find a good support for multi-mode lasers):

(a) $\omega_m = \omega_q$ and $\omega_r = \omega_p$; (b) $\omega_m = \omega_r$ and $\omega_q = \omega_p$, These two categories determine the energy oscillation values of modes E1, and provide terms such as auto saturation and cross saturation.

(c) $\omega_m = \omega_q + \omega_r - \omega_p$, this relationship is important when the number of competing modes is large. The regime that interests us is when a large number of modes oscillate in a limited spectral range around an oscillation frequency ω_0, which is the resonant frequency of the gain medium, such is the case of a random laser. This opens the way to a "mean field theory" in which all modes are coupled, i.e., the sum in Eq. (3.1.22) is over all possible values of pqr. To summarize, it is assumed that all the lasing modes have frequency $\omega_m \cong \omega_0$, ω_0 being the resonant frequency of a gain medium.

3.1.6 *Langevin equation for the phases*

Let $a_m(t) = A_m(t)\, e^{i\phi_m(t)}$, where A_m as slowly varying with respect to ϕ_m. The fact that the temporal variation of the phases is on a faster time scale than that of the amplitudes, takes place due to the random interference between the modes and not due to the intensity fluctuations of the individual modes. This is established in the theory of mode-locking of standard multimode lasers [40, 25]. The consequence of this is that all dependent phase terms are eliminated in equation (3.1.22), and the resulting equations determine the amplitudes A_m, and therefore the energy of each mode $\mathscr{E}_m$ remains subject to this value after the corresponding mode has been put into oscillation. If the phases can be taken as independent, the output laser signal shows small oscillations around an equilibrium value because the noises in each mode amplitude are independent.

We describe the gain by an amplification coefficient γ_m and the losses by radiation as α_m, these are included in the equation of motion by the complex amplitudes [40]

$$\frac{da_m}{dt} = -\frac{1}{2}\sum_{pqr} g_{mpqr} a_q a_r a_p^* + (\gamma_m - \alpha_m)\, a_m + \eta_m(t)\,, \tag{3.1.24}$$

having introduced, as usual, a complex noise term, mainly due to spontaneous emission. The tensor g is a quantity symmetric with respect to the exhange of $m \leftrightarrow p$, $q \leftrightarrow r$, while under $\{m,p\} \leftrightarrow \{q,r\}$ one has $g_{mpqr} = g^*_{qrmp}$, see reference [75, 13]. Introducing the real-value potential function

$$\begin{aligned} H &= \frac{1}{4} Re\left[\sum_{mpqr} g_{mpqr} a_q a_r a_p^* a_m^*\right] \\ &= \frac{1}{4}\sum_{mpqr} g^R_{mpqr} a_q a_r a_p^* a_m^* - \frac{1}{4i}\sum_{mpqr} g^I_{mpqr} a_q a_r a_p^* a_m^* \end{aligned} \tag{3.1.25}$$

let

$$\mathcal{H} = \sum_m (\alpha_m - \gamma_m)\, |a_m|^2 + H, \tag{3.1.26}$$

the equation (3.1.24) is rewritten as

$$\frac{da_m}{dt} = -\frac{\partial \mathcal{H}}{\partial a_m^*} + \eta_m(t) \tag{3.1.27}$$

where

$$\frac{\partial}{\partial a^*} = \frac{1}{2}\left[\frac{\partial}{\partial a^R} + i\frac{\partial}{\partial a^I}\right] \tag{3.1.28}$$

The previous equation is a standard Langevin model for a system of N particles moving in 2N dimensions, represented by $\left\{a_m^R, a_m^I\right\}_{m=1,\ldots,N}$. Finally, the phases ϕ_m can be taken as the relevant dynamic variables, due to the quenched approximation for the amplitudes

A_m (For a more extensive calculations suggest see Appendix A of the reference [2]),

$$\mathcal{H} = \sum_{\{k_1 k_2\}'} g^{(2)}_{k_1 k_2} a_{k_1} a^*_{k_2} + \frac{1}{2} \sum_{\{k_1 k_2 k_3 k_4\}'} g^{(4)}_{k_1 k_2 k_3 k_4} a_{k_1} a^*_{k_2} a_{k_3} a^*_{k_4}, \tag{3.1.29}$$

where $\{...\}'$ implies the frequency matching condition $|\omega_{k_1} - \omega_{k_2}| \lesssim \gamma$ and $|\omega_{k_1} - \omega_{k_1} + \omega_{k_3} - \omega_{k_4} \lesssim \gamma$ in the quadratic and quartic terms, respectively, with γ denoting the finite linewidth of the modes.

3.1.7 *RSB in Random Lasers*

In the year 2015 was published the article of reference [7]. In this article the authors (Antenucci,F et al.) present new concepts that relate the traditional Spin Glass phenomena to random lasers. This section of the chapter we review this work and summarize the main ideas.

Recall that the frustration is given when in a magnetic system there are multiple metastable states. In a random laser, a similar situation can be expected due to the large number of random modes competing for the available gain. This glassy light regime is associated to an effective thermodynamic phase where the tendency of the modes to oscillate coherently in intensity is frustrated. The experimental validation between of the random-glassy laser connection, and, particularly, of the RSB predicted by the theory, has, nevertheless, recently been put forward in ref. [32], measuring the overlap between intensity fluctuations of the spectral emission.

Consider that the behavior of the gain in the medium has an overall optical power $\mathscr{E} = \sum_k |a_k|^2$ that remains constant. To determine a spin-glass phase transition in random lasers, the replicate method can be used. This method consists of considering identical copies of the system that act as probes by exploring the multi-state phase space of the system. An order parameter is introduced [77], resulting from the overlap between the amplitudes of the replica α and the replica β.

$$Q_{\alpha\beta} = \frac{1}{N\epsilon} \sum_{k=1}^{N} a^{\alpha}_k \left(a^{\beta}_k\right)^* \tag{3.1.30}$$

where $\epsilon = \varepsilon/N$. If the overlap is of the Parisi type then it is identified as the beginning of the random laser regime for a given energy. Note that equation (3.1.30) is analogous to equation (3.1.11), where the complex amplitude corresponds to a magnetization of a pure state. Experimentally phase correlation measurements necessary for the assessment of the complex amplitudes are not available (at least at this stage). In an experiment we have access to the fluctuations of intensities of two real replicas through $I_\alpha(k) = |a^\alpha_k|^2$, where α is the label of the replica ($\alpha = 1, ..., n$).

Having the intensities as the only degree of freedom available experimentally as the

intensities, a suitable overlap is defined based on its acquisition in different shots

- The average emission spectrum

$$\bar{I}(k) \equiv \frac{1}{n}\sum_{\alpha=1}^{n} I_{\alpha}(k) \tag{3.1.31}$$

- the intensity fluctuation of shot a around the average profile

$$\Delta_{\alpha}(k) \equiv I_{\alpha}(k) - \bar{I}(k) \tag{3.1.32}$$

It defines the overlap between the normalized intensity fluctuation of shots α and β as [7]

$$C_{\alpha\beta} = \frac{\sum_{k=1}^{n} \Delta_{\alpha}(k)\,\Delta_{\beta}(k)}{\sqrt{\sum_{k=1}^{n} \Delta_{\alpha}^{2}(k)}\sqrt{\sum_{k=1}^{n} \Delta_{\beta}^{2}(k)}}, \tag{3.1.33}$$

where k denotes the frequency. From n measured spectra one can calculate the $n(n-1)/2$ values of the $C_{\alpha\beta}$ and the distribution $P(C_{\alpha\beta})$, and the probability distribution can be calculated to have the information of the phase transition.

So far we have reviewed generalities about spin glass systems. We will then review the progress in fluctuations in random lasers, with special attention to the conditions that lead to a Lévy statistics. These ideas may seem unconnected, but in Chapter 5 we will make the link between these two different areas.

4 Fluctuations in RLs

Random lasers are complex systems with many internal elements that interact with each other. The dynamics of these systems are difficult to understand due to the complexity of such interactions and the number of factors that influence them. One can try to understand the laws that govern random lasers from studies of observable variables. The fluctuations in intensity spectrum of a random laser emission is an easily accessible measure where a single measurement instrument (spectrometer) is needed. Fluctuations in emission spectra can be modeled in a first approach by a Gaussian stochastic process (Brownian motion). This model is natural if we consider that the fluctuation in intensity is the result of many independent parameters, and using the Central Limit Theorem leads to a Gaussian distribution. However, empirical studies of intensity fluctuations show that under some given conditions, the associated probability density has a kurtosis larger than that given by the Gaussian distribution.

The idea then of this chapter is to show that the Brownian motion under certain conditions that we will detail later does not adjust adequately to the fluctuations of emission in a random laser. The distributions of Lévy are presented. This distribution is able to model the strong fluctuations. In addition we present the α-parameter that indicates in which statistical regimen we are. Finally it is concluded that this parameter is associated with the pumping energy, and that under certain conditions it can indicate the emission threshold in a random laser.

4.1 Lévy statistics

In the last decades the economic and financial phenomena have begun to be studied through rigorous mathematical models, standing out the models for breaks and financial collapses or "crashes". The empirical characterization of stochastic processes usually requires the determination of asymptotic probability densities functions (PDF). The simplest model proposed to describe the evolution of these processes is known as Brownian motion. However, the empirical study of the real series of prices of some of the most important indexes showed that at short time scales, such as those used to study the evolution of stock indexes near a financial collapse, the PDFs of these series have greater

kurtosis than that of a Gaussian distribution [64]. The first attempt to explain this behavior was made in 1963 by Mandelbrot [62], who proposed to model the increase of the cotton price with a stable stochastic process of non-Gaussian Lévy. Simultaneously there was the birth of a new discipline called "Econophysics" [82]. Physicists have broadened the scope of their interest, including research on animal foraging, [105] fluid dynamics [104], and photons [11], just to name a few.

4.1.1 *Random Walk*

A random walk is defined as a path composed of many independent random steps. Allegorically, it compares to the completely erratic movements of drunks wandering from one pole of light to another. Brownian motion, which describes the completely erratic movement of very small particles that collide with the surrounding particles, which strike them from all sides, is the simplest of random walks. Dynamic processes, atomic and molecular diffusion on surfaces, and movement of microorganisms are some examples have been described in terms of Brownian motion.

Einstein showed that the mean square displacement of a particle with Brownian motion increases linearly with time, ($\langle x^2(t)\rangle \sim t$), which implies that the mean square displacement of the Brownian particle from its starting point increases with the square root of time ($\sqrt{t}$), and not linearly. The probability that a Brownian particle is at a distance d from its starting point after time t is represented by a Gaussian distribution centered on the origin that falls very quickly to zero. The width is proportional to $\sqrt{t}$ and is a measure of the distance beyond which there is little probability of finding the particle, that is, when the particle moves away from the mean value, the probability rapidly to zero.

4.1.2 *Central Limit Theorem (CLT)*

The theorem states that the distribution of the mean of a random sample of N independent, identically distributed random variable with finite variance has an approximately Gaussian distribution when the sample size is large regardless of the shape of the population distribution.

Let $x_1, x_2, x_3, x_4..., x_N$ be N independent, identically distributed random variable, with their sum

$$X_N = \sum_{i=1}^{N} x_i = x_1 + x_2 + ... + x_N \;\; with\, N \to \infty. \tag{4.1.1}$$

The mean of each of the independent, identically distributed random variable is $\langle x\rangle$ and variance be σ^2, then CLT states that the probability density function of X_N is given as:

$$p\left(X_N\right) = \frac{1}{\sqrt{2\pi\sigma_N^2}} e^{\frac{-(x-\langle x\rangle)^2}{2\sigma_N^2}}. \tag{4.1.2}$$

The CLT is valid under very general conditions. Irrespective of the law of probability followed by x_i. The Gaussian law predicted by the CLT for this problem is almost always observed experimentally. The CLT, however, fails when the second moment of the distribution of random variable $\langle x^2 \rangle$ is infinite.

4.1.3 *Lévy flights*

There are physical phenomena that can exhibit properties that are beyond the Central Limit Theorem. CLT is violated and a non-Gaussian distribution is obtained, where the mean may or may not exist but the variance always diverges. These random walks termed as Lévy flights arise from rare or atypical events that are so large in magnitude that many small events dominate [68]. This results in a finite probability of observing improbable events giving the distribution a "Fat or Heavy tail" in the asymptotic limit. Further, the Lévy sums are exceptional in that they are rigorously hierarchy. A very small number of terms dominate all other and the contribution of the latter to the sum X_N is negligible. Thus, in the Lévy distributions, the determining event is the rare event and the sum mainly reflects the value of the larger terms.

In particular, the probability density $f\left(x\right)$ of a random variable x with power-laws tails

$$f\left(x\right) \approx \frac{1}{x^{1+\alpha}} \quad when\, x \to \infty \tag{4.1.3}$$

if

- $\alpha \geq 2$ the variace $\langle x^2 \rangle$ is finite and the classical CLT applies.
- $\alpha < 2$ The probability of obtaining a given value of x decreases less rapidly than $1/x^3$ for the large x.The usual CLT does not apply.

Paul Lévy, in the 1930s, generalized the Central Limit Theorem to take into account the possibility of the existence of infinite moments, in particular divergent variance. He showed that for such cases, the sum X_N increases faster than the square root of the number of terms it contains, and the distribution obtained is no longer a Gaussian, but obeys a law which is now called the stable or Lévy law.

The Generalized Central Limit Theorem (GCLT) states that the sum X_N of large number of independent, identically distributed random variable $x_1, x_{2,}..., x_3$ converges to a Lévy-stable law. Thus, GCLT shows that if the assumption of finite variance is dropped, the only possible resulting non-trivial limits are Lévy-stable distribution.

4.1.4 *Stable Distribution*

We have already mentioned that in some natural phenomena the Central Limit Theorem is not a good modeling for heavy tail events. In response to the empirical evidence Mandelbrot and Fama [29] proposed the stable distribution as an alternative model. The stable distributions are supported by the generalized Central Limit Theorem, which states that stable laws are the only possible limit distributions for properly normalized and centered sums of independent, identically distributed random variables.

Stable Distribution also called α-stable or Lévy stable distribution, were introduced by Lévy in 1925 During their investigations of the behavior of sums of independent random variables.

The α-stable distribution requieres four parameters for complete description:

- $\alpha \in (0, 2]$ is the index of stability, also called the tail index or characteristic exponent.
- $\beta \in [-1, 1]$ is the skewness parameter, is a measure of asymmetry. If $\beta = 0$, the distribution is symmetric, if $\beta > 0$ it is skewed toward the right, if $\beta < 0$ it is skewed toward the left.

The parameters α and β determine the shape of the distribution.

- $\gamma > 0$ is a scale parameter.
- $\delta \in \mathbb{R}$. is a location parameter. It shifts the distribution right if $\delta > 0$, and left if $\delta < 0$.

4.1.5 *Characteristic function*

Due to the lack of closed form formulas for densities for all but three distributions, the α-stable law can be most conveniently described by its characteristic function $\phi(t)$ that is the inverse Fourier transform of the probability density function.

$$ln\phi(t) = \begin{cases} -\gamma^{\alpha}|t|^{\alpha}\left\{1 - i\beta sign(t)\, tan\frac{\pi\alpha}{2}\right\} + i\gamma t, & \alpha \neq 1 \\ -\gamma|t|\left\{1 + i\beta sign(t)\,\frac{2}{\pi} ln|t|\right\} + i\gamma t, & \alpha = 1 \end{cases} \tag{4.1.4}$$

Gaussian distribution is realized when $\alpha = 2$. When $\alpha < 2$, the tails behave asymptotically as power-laws with exponent α.

4.1.6 *Estimation of $\alpha, \beta, \gamma, \delta$ parameters*

There are many ways to estimate characteristic parameters. We use the methods mentioned in [26, 66] to get the four parameters. Then the adjustment was improved by calculating the inverse Fourier transform of the characteristic function from the parameters calculated with the quantiles method. This is performed as follows.

Under the definition of the characteritic function (Eq. (4.1.4)), define

$$\nu_\alpha = \frac{x_{.95} - x_{.025}}{x_{.75} - x_{.25}}$$

$$\nu_\beta = \frac{x_{.95} + x_{.05} - 2x_{.5}}{x_{.95} - x_{.05}}$$

Here, x_p represent the p-th population quantile. Since, ν_α and ν_β are function of α and β, the relation can be inverted to estimate the parameters using the values found in the tables of the article by McCulloch [66]. The relationship with the tables is:

$$\begin{aligned} \alpha &= \psi_1(\nu_\alpha, \nu_\beta) \\ \beta &= \psi_2(\nu_\alpha, \nu_\beta) \end{aligned}$$

where ψ_1 and ψ_2 are the table as function of ν_α and ν_β. A similar procedure is used to estimate δ and γ.

4.1.7 *Fluctuations in the emission intensity from a RLs*

The first theoretical approach, that was proposed by Letokhov [58], was based on a process of diffusion in an environment with optical gain. Optical transport was described as a multiple scattering process in which light waves are dispersed by a large number of randomly spaced elements. In such materials light is multiplied, dispersed, and also amplified. Under this model, the best way to think of the dispersive movement within the medium was a Brownian motion model. When the number of photons that describe random walks is very large and summoning the Central Limit Theorem (CLT) should be expected that the fluctuation in the intensity spectrum describe a Gaussian distribution. This is partially true.

In the reference work [86], the authors studied the emissions of a dye scattering system. They found that emissions exhibited non-Gaussian emission intensity statistics in the system of random realizations, where the amplification was dominated by certain improbable events that were "larger than rare", which gave a statistic of Lévy with a tunable exponent. In this paper the authors further claim that, to their knowledge, the first experimental realization of the Lévy statistic is provided in the optics of a random amplifier medium.

In a simulation work based on a feedback model [57], it was shown that fluctuations change under a control parameter, from a regime Gaussian to Lévy statistical regimes. In this paper the authors say that the origin of the Lévy statistic can be understood from the following reasoning: the spontaneously emitted photons are amplified in the active medium due to the stimulated emission. Their emission energy is exponentially large in

the path length l,

$$I(l) = I_0 e^{(l/l_G)}, \tag{4.1.5}$$

where we have introduced the gain length l_G. On the other hand, the path length in a diffusing medium is a random variable with exponential probability distribution

$$p(l) = \frac{e^{(-l/\langle l \rangle)}}{\langle l \rangle}, \tag{4.1.6}$$

where and $\langle l \rangle$ is the average length of the photon path within the sample. The combination of Eqs. 4.1.5 and 4.1.6 provides that the probability distribution of the emitted intensity follows a power law

$$P(I) = \frac{l_g}{\langle l \rangle} I^{-(1+\alpha)},\ \alpha = \frac{l_g}{\langle l \rangle} \tag{4.1.7}$$

where l_g is the gain length The most striking one is that for $0 < \alpha \leq 2$ the average $\langle I \rangle$ exists but the variance (and all higher-order moments) diverges. The gain length l_g is controlled by population inversion of the active medium. Increasing the latter, l_g and the exponent α decrease thus enhancing the fluctuations. Actually, the Lévy regime is limited to a specific range of gain length, while Gaussian statistics occur with both low and high pumping energy. Three different statistical regimes are then possible, depending on the gain.

In the reference [44] the authors clarify the landscape with a theoretical and experimental study aimed at characterizing statistical regimes in a random laser. Both the theoretical simulations and the experimental results showed the possibility of three regions of fluctuations when increasing the pumping energy. An initial Gaussian regime is followed by Lévy statistics, and Gaussian statistics is recovered again for high pump pulse energy. These different statistical regimes are possible in a weakly diffusive active medium, while the region of Lévy statistics disappears when the medium is strongly diffusive presenting always a Gaussian regime with smooth emission spectrum. In this paper, the authors propose to establish the Gaussian regime $1.8 \leq \alpha \leq 2$, due to the finite number of measurements it is in general rather difficult to reliably resolve the tail of the distributions. Also performed experiments with different l_t (mean free path) concluding that in a medium strongly diffusive medium displays a Gaussian intensity distribution at any value of the pump pulse. In the case of weaker diffusive media three different statistical regimes are possible, increasing the pumping energy: The intensity distribution is Gaussian at low pump energies, becomes a Lévy-type distribution at increasing pumping energy and then becomes Gaussian again for higher pumping energies. Figure 4.1.1 shows the scheme of the behavior of the α-parameter with respect to the Energy Pump where the three regions can be seen.

In the works [100, 98, 99] critical excitation in random lasers under picosecond and

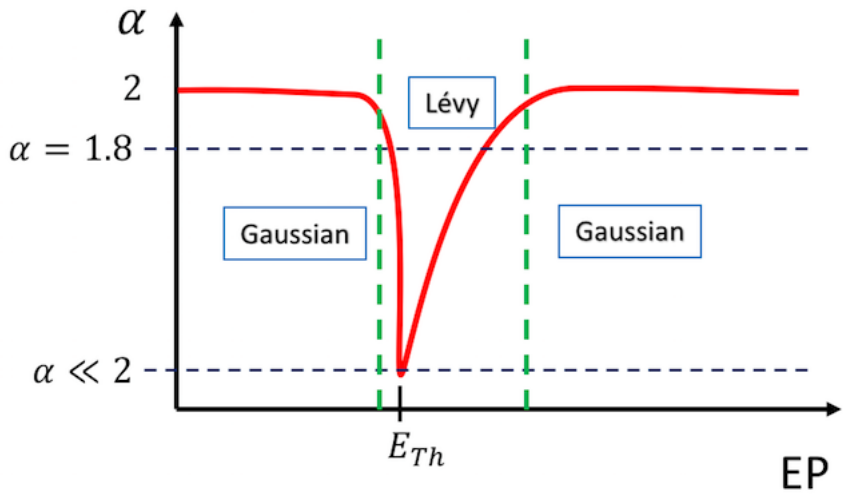

Figure 4.1.1: The figure shows the scheme of the behavior of the α-parameter with respect to the Energy Pump where the three regions can be seen. Below the threshold where the behavior of the fluctuations follows a Gaussian regime. Close to threshold the fluctuations become strong, in the lower part of the red curve you see the energy of the threshold. Finally for greater energies, the behavior returns to be a Gaussian regime. Also emphasizes the region between $1.8 \leq \alpha \leq 2$ which is where it is considered that the statistic of the fluctuations is Gaussian.

nanosecond pumping was experimentally studied. The resulting emission intensity statistics were analyzed using fits to α-stable distributions. It was found that the transition value of α, the tail exponent of the stable distribution, is a clear indicator of the threshold of random lasing. They proposed this exponent as an identifier of the threshold. Comparing it with the conventional definitions for the threshold, namely, the probability of random lasing in the case of coherent random lasers and the intensity enhancement and bandwidth collapse for diffusive random lasing emission. This proposal is based on that random lasers are inherently statistical systems, so any relevant parameter needs to take the fluctuations into account. This criterion is satisfied by the α exponent. Using parameter α as a statistically consistent identifier precludes the subjectivity associated with threshold identification, such as that in the case of the probability of random lasing.

4.1.8 *Results*

In this section we present results, obtained from a random laser system consisting of Crystalline powders of Nd^{3+} doped YBO_3 (Nd^{3+} 4.0% concentration). We show the strong fluctuations near the threshold that are typical of the presence of Lévy statistics. We also show a curve that relates the pumping energy to the α-parameter. In these preliminary results the comparison of the $\alpha-$parameter with the traditional methods to identify the threshold of the laser emission is not made. That will be shown in the next chapter, as we will show even deeper conclusions.

Figure 4.1.2 shows the fluctuations in the intensity. Figures 4.1.2(a) and (b) show

the intensity fluctuations produced shot to shot, the energies are $1.4\,mJ$ and $2.1\,mJ$ respectively. Note that in these figures the approximation symbol ($\sim$) for the intensity fluctuations is used, that is because a drift with respect to the emission wavelength of about $\Delta\lambda \sim 0.5\,nm$ from one shot to another is perceived. This fluctuation is centered on $\lambda = 1056\,nm$.

Figures 4.1.2(c) and (d) are the intensity fluctuations centered on $\lambda = 1056\,nm$. The pumping energy used in the fluctuation of Figure 4.1.2(c) is very close to the threshold of the laser action, the strong fluctuations can be appreciated. In this same figure two yellow boxes help us to see the difference between fluctuations, where it is noticed that the fluctuation can quickly change from almost zero to a maximum fluctuation.

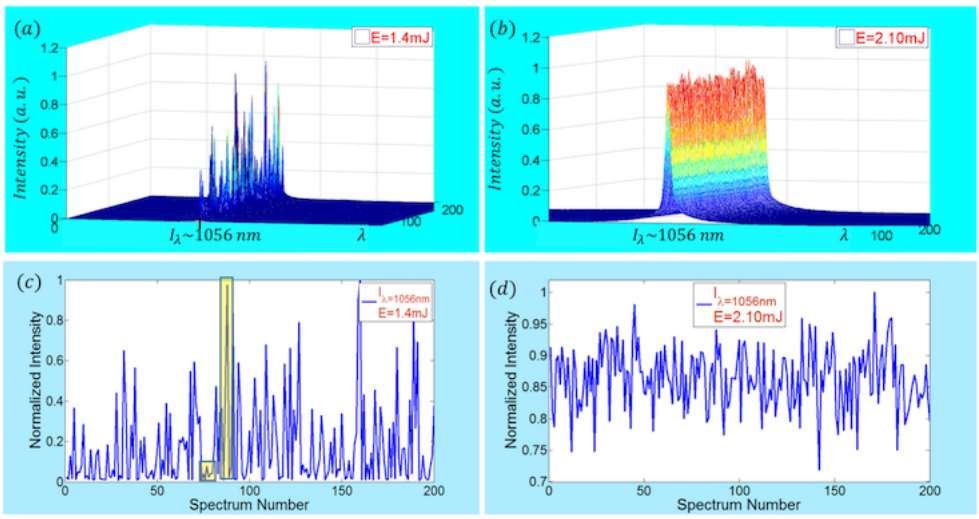

Figure 4.1.2: The figure shows the intensity fluctuations around the emission wavelength ($1056\,nm$). (a) and (b) show the intensity fluctuations in a three-dimensional perspective, The pumping energies are $1.4\,mJ$ (close to threshold) and $2.10\,mJ$ (above the threshold) respectively. (c) and (d) they are the fluctuations for one the emission wavelength ($I_\lambda = 1056\,nm$).

Here we should be in the presence of a fluctuation of the Lévy type. The oscillation shown in Figure 4.1.2(d) is clearly softer, this should be an indicator of a Gaussian regime.

In Figures 4.1.3(a), (b) and (c) histograms of intensity fluctuations for energies $1\,mJ$, $1.4\,mJ$ and $2.1\,mJ$ respectively shown. Figures 4.1.3(d), (e) and (f) are representations of the probability density function corresponding to the frequency histograms of Figures 4.1.3(a), (b) and (c) respectively. These figures are generated after using the quantiles method to obtain the parameters α, β, γ and δ. Subsequently, the inverse Fourier transform of the characteristic function Eq.(4.1.4) is calculated using numerical methods.

Figure 4.1.3 shows the calculated values for parameter α, showing that for an energy of $1.4\,mJ$ $\alpha = 0.28$, being clearly in a Lévy regime. Below and above the threshold $\alpha = 2$, which indicates that for these energies the regime is Gaussian. Although the comparison of parameter α with the traditional methods of calculating the threshold will be done in the next chapter, we inform for clarity of the reader that the threshold was calculated in

$E_{th} = 1.4\,mJ.$

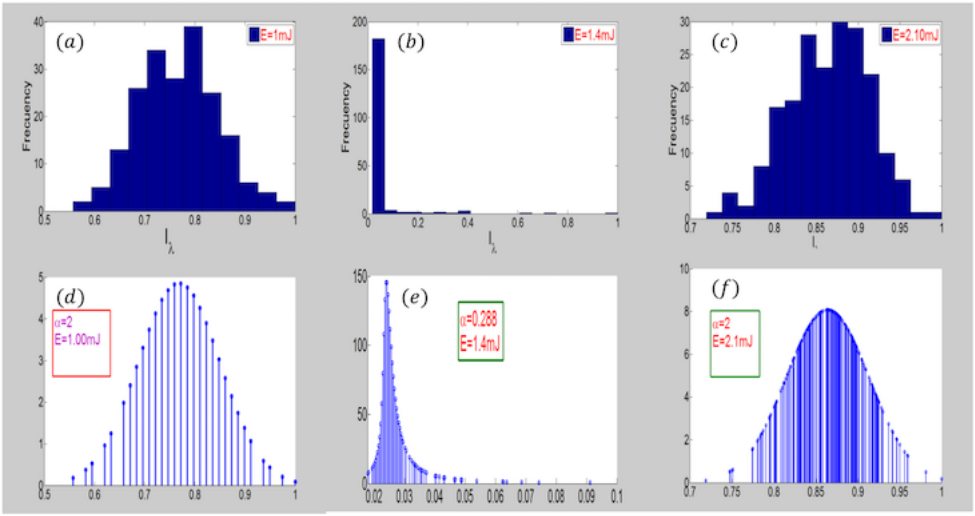

Figure 4.1.3: Figures 4.1.3(a), (b) and (c) show the frequency histograms of the intensity fluctuations for energies $1\,mJ$, $1.4\,mJ$ and $2.1\,mJ$ respectively. Figures 4.1.3(d), (e) and (f) show the probability density functions calculated from the inverse Fourier transform.

5 Experiment 3: Observation of Lévy distribution and RSB in RLs from a single set of measurements

Among the most unique aspects of random lasers is that, for systems composed of a large number of modes, if these modes do not respond to a specific frequency that dominates the others, the narrow emission peaks in the spectra can change the frequency from one excitation pulse to another with emission spectra that appear completely uncorrelated from shot to shot [102]. Even in the case that the experimental conditions of the system remain perfectly constant, strong fluctuations in intensity can be seen due to the "fight" for the gain. In these conditions it is observed that the intensity distribution is not Gaussian, but rather of the Lévy type. This is true close to the lasing threshold, where the mentioned spectra fluctuations are expected, whereas far below and far above the threshold the statistics remains Gaussian [106].

On the other hand, random lasers have been exploited as a platform to study complex systems benefiting from the great progress that has occurred in recent decades in complex systems theory. The value of complex systems theory for random lasers was realized very soon. It was shown that using the replica method in a random laser where a large number of random modes compete for the available gain can lead to a behavior similar to that of a glass transition [32].

The arguments and works presented in chapters 3 and 4 have been separate investigations considered so far two different areas of physics.

In this work, we employ the Nd:YBO random laser system to obtain, from a single set of measurements, the physical origin of the complex correspondence between the Lévy fluctuations regime and the replica-symmetry breaking transition to the spin-glass phase.

In the photonic context, the term spin glass (SG) means that intensity spectra emitted under identical experimental conditions keep a complex pattern of correlations, as quantified below. Moreover, the Lévy statistics implies strong fluctuations in the emission intensity, with non-Gaussian heavy-tailed distribution.

In ref. [32] a replica-symmetry-breaking (RSB) transition to the spin glass phase was experimentally reported for the first time in RLs employing a functionalized thiophene-based oligomer (T_5OC_x) in amorphous solid state with planar geometry. RL emission

was obtained by pumping with a frequency doubled pulsed Nd:YAG laser (10 Hz, 6 ns, 1.06 μm). The RL spectrum with several spikes could be interpreted as depicting the modes riding on a broad pedestal around 610 nm, as observed when high resolution spectral measurements were employed. When a lower spectral resolution was employed, a somewhat smooth spectrum was measured. The authors analyzed the shot-to-shot intensity fluctuations in order to obtain the RSB signature and clearly demonstrated the photonic paramagnetic to SG phase transition. Regarding this point we must highlight that a random laser is always multimodal, despite having a smooth spectrum and no spikes. Even in the case of presenting such an extremely fine spectrum that exceeds the spectral resolution of the measuring equipment. This was demonstrated in an RFL system where the emission spectrum is extremely thin. (See reference [35]).

Here, we advance on the understanding and characterization of the photonic behaviors of RLs by reporting on a remarkable match between the Lévy regime of intensity emission and the critical region of the RSB glassy transition. The experimental results were obtained from a single spectral set of data on the Nd:YBO RL system[1].

5.1 Theoretical Framework

The complex correspondence between the RSB transition to the photonic SG phase and the changes in the statistics of intensity fluctuations in RLs can be explained within the same framework.

A phase diagram for lasers in random amplifying media has been recently built based on the Langevin equations for the complex slow-amplitude modes $a_k(t)$,

$$\frac{da_k}{dt} = -\frac{\partial \mathcal{H}}{\partial a_k^*} + F_k \tag{5.1.1}$$

where F_k is a Gaussian (white) uncorrelated noise term and the general complex-valued functional $\mathcal{H}$ reads [6]

$$\mathcal{H} = \sum_{\{k_1 k_2\}'} g^{(2)}_{k_1 k_2} a_{k_1} a^*_{k_2} + \frac{1}{2} \sum_{\{k_1 k_2 k_3 k_4\}'} g^{(4)}_{k_1 k_2 k_3 k_4} a_{k_1} a^*_{k_2} a_{k_3} a^*_{k_4} \tag{5.1.2}$$

The symbol $\{...\}'$ implies the frequency-matching condition $|\omega_{k_1} - \omega_{k_2}| \lesssim \gamma$ and $|\omega_{k_1} - \omega_{k_1} + \omega_{k_3} - \omega_{k_4}| \lesssim \gamma$ in the quadratic and quartic terms, respectively, with γ denoting the finite linewidth of the modes. The physical origin of the quadratic coupling $g^{(2)}_{k_1 k_2}$ lies in the spatially inhomogeneous refractive index, as well as in a nonuniform distribution of the gain and an effective damping contribution due to the "cavity" leakage. In systems with null or weak leakage in which the off- diagonal contribution is negligible, the real part of the diagonal coupling accounts for the coefficient rates of the amplifica-

[1]The experiment described here is based, and in many parts is similar to the published article [36]

tion (gain) (γ_k) and radiation loss (α_k) through $g_{kk}^{(2)R} = \mathrm{Re}\left\{g_{kk}^{(2)}\right\} = \alpha_k - \gamma_k$. On the other hand, the quartic coupling $g_{k_1k_2k_3k_4}^{(4)}$ is related to a modulation of the nonlinear χ^3 susceptibility with a random spatial profile [1, 5, 2, 7, 32, 6].

The spatial disorder generally makes the explicit calculation of the quadratic and quartic couplings in equation (5.1.2) rather difficult. In fact, in refs. [1, 5, 2, 7, 32, 6] these couplings have been considered as quenched Gaussian variables, with probability distributions independent of the mode combinations $\{k_1, k_2\}'$ and $\{k_1, k_2, k_3, k_4\}'$, respectively. In a mean-field approach, all modes are coupled and the frequency-matching restrictions are relaxed. In addition, by considering the total optical intensity, $I = \sum_k c_k|a_k|^2$, as a constant, with time-independent prefactors c_k, the real part $\mathcal{H}^{\mathrm{R}}$ of the functional (5.1.2) becomes analogue to the Hamiltonian of the p-spin model with spherical constraint [20], which is given by a sum of quadratic ($p = 2$) and quartic ($p = 4$) terms with Gaussian-distributed couplings. It is important to notice that in the photonic-to-magnetic analogy the excitation (pump) energy plays the role of the inverse temperature. An equilibrium statistical physics approach, with the replica trick applied to $\mathcal{H}^{\mathrm{R}}$ in terms of the slow-amplitude modes a_k, then led [7, 6] to a phase diagram for the pumping rate as a function of the disorder strength. Photonic paramagnetic, ferromagnetic, phase-locking-wave and RSB spin-glass phases have been characterized [7, 6], depending on the trend of the disorder to hamper the synchronous oscillation of the modes. A photonic order parameter q_{max}, analogue to the Parisi parameter in SG theory, was suitably defined (see below), so that $q_{max} = 0$ in the prelasing replica-symmetric paramagnetic regime and $q_{max} \neq 0$ in the random lasing RSB glassy phase. As a consequence, the RL threshold became identified with the RSB phase transition to the photonic SG phase.

We now turn to the discussion on the statistical regimes of intensity fluctuations of RL systems in disordered nonlinear media. Noteworthy, the set of Langevin equations, given by equation (5.1.1), also provides the underlying theoretical basis for such analysis. Indeed, by writing $I_k = c_k|a_k|^2$, manipulation of equation (5.1.1) leads to

$$\frac{1}{c_{k_2}}\frac{dI_{k_2}}{dt} = -2\mathrm{Re}\left\{\sum_{\{k_1\}'} g_{k_1k_2}^{(2)} a_{k_1} a_{k_2}^* + \frac{1}{2}\left[g_{k_1k_2k_3k_4}^{(4)} + g_{k_1k_4k_3k_2}^{(4)}\right] a_{k_1} a_{k_2}^* a_{k_3} a_{k_4}^* + a_{k_2}^* F_{k_2}\right\} \tag{5.1.3}$$

The restricted sum in the quartic coupling generally involves three classes of mode combinations [2, 75] $\omega_{k_1} = \omega_{k_2}$ and $\omega_{k_3} = \omega_{k_4}$, $\omega_{k_1} = \omega_{k_4}$ and $\omega_{k_2} = \omega_{k_3}$, and the remaining possibilities satisfying the frequency-matching condition, which have been usually disregarded [2, 75]. We consider the diagonal contribution in the quadratic coupling to dominate over the off-diagonal part. By expressing the optical noise as the sum of additive and multiplicative statistically independent stochastic processes [84] so that $F_k(t) = F_k^{(0)}(t) + a_k(t) F_k^{(1)}(t)$, and considering slow-amplitude modes $a_k(t)$ (if compared

to the rapidly evolving phase dynamics), we obtain the Fokker-Planck equation [84, 80] for the probability density function (PDF) of emission intensity

$$\frac{\partial P}{\partial t} = -\frac{\partial}{\partial I_k}\left[\left(-d_k I_k - b_k I_k^2 + 2QI_k\right)P\right] + 2Q\frac{\partial^2}{\partial I_k^2}\left(I_k^2 P\right), \tag{5.1.4}$$

where the parameter Q controls the magnitude of the multiplicative fluctuations through $\left\langle F_k^{(1)\mathrm{R}}(t)\, F_n^{(1)\mathrm{R}}(t')\right\rangle = 2Q\delta_{k,n}\delta(t-t')$, $b_k = 2g_{kkkk}^{(4)\mathrm{R}}/c_k$, and

$$d_k = \sum_{n\neq k}\left(g_{kknn}^{(4)\mathrm{R}} + g_{knnk}^{(4)\mathrm{R}} + g_{nkkn}^{(4)\mathrm{R}} + g_{nnkk}^{(4)\mathrm{R}}\right)\frac{I_n}{c_n} - 2\left(\gamma_k - \alpha_k\right).$$

We notice that, by averaging out the rapidly evolving phases to obtain Eq. (5.1.4), the so-called free running approximation has been employed in which the dynamics of the phases and amplitudes are considered as eventually decoupled [2]. In this context, some features of the original model are removed, such as the phase-locking regime. Also, in a statistical physics approach we observe that integrating out irrelevant degrees of freedom should be properly done in the partition function, rather than in the Hamiltonian level, though the technical difficulties involved are rather challenging. The steady-state solution of equation (5.1.4) is [84, 80]

$$P(I_k) = A_k I_k^{-\mu_k} e^{-\left(\frac{b_k I_k}{2Q}\right)}, \tag{5.1.5}$$

with $I_k > 0$, A_k as the normalization constant, and the power-law exponent $\mu_k = 1 + d_k/2Q$. At this point we remark that, as the statistics of the sum of N independent random variables x with power-law distribution $P(x) = Ax^{-\mu}$, $1 < \mu < 3$, is described [63] by the α-stable Lévy distribution with $\alpha = \mu - 1$, the PDF (5.1.5) thus identifies an exponentially truncated Lévy-like distribution of intensities for $1 < \mu_k < 3$ and $0 < \alpha < 2$. In this case, strong fluctuations in I_k emerge and the ultraslow convergence to the $\alpha = 2$ Gaussian behavior due to the presence of the exponential factor in equation (5.1.5) is achieved only for a remarkably large N. In contrast, for $\mu_k \leq 1$ or $\mu_k \geq 3$ the central limit theorem assures fast convergence to the $\alpha = 2$ Gaussian statistics of weakly-fluctuating intensities. Therefore, for a given disorder strength, an increasing pumping rate (or excitation pulse energy) raises [80] the value of μ_k and the statistics of emission intensities shifts progressively from an initial Gaussian ($\mu_k \leq 1$, $\alpha = 2$), to the Lévy-like ($1 < \mu_k < 3$, $\alpha = \mu_k - 1$), and to a subsequent Gaussian ($\mu \geq 3$, $\alpha = 2$) regime.

The correspondence with the RSB glassy transition relies foremost in the recent proposals [57, 99] that assign the Lévy index α as an identifier of the RL threshold, which, as discussed, can be also determined by the order parameter q_{max}. Indeed, the above description matches accordingly with recent results on RL systems which report on [100, 98, 99, 97]: (i) a prelasing weakly-fluctuating Gaussian regime at low pump en-

ergies, corresponding in refs. [1, 5, 2, 7, 32, 6] to the photonic paramagnetic (or even the phase-locking-wave) phase with $q_{max} = 0$; followed by (ii) an abrupt change in α at the RL threshold to the strongly-fluctuating Lévy-like regime at intermediate pump energies, signaled in [1, 5, 2, 7, 32, 6] by the RSB transition to the glassy regime with $q_{max} \neq 0$; and (iii) a subsequent crossover at high pump energies to the so-called self-averaged RL regime, with $q_{max} \neq 0$ and Gaussian statistics of emitted intensities. Noticeably, this latter Gaussian regime taking place deep in the glassy RL phase has not been anticipated in refs. [1, 5, 2, 7, 32, 6], since the scope of these works did not include the analysis of the statistics of intensity fluctuations.

5.2 Experimental Results and Discussion

The experimental investigation on the correspondence between the Lévy fluctuation regime and the replica symmetry breaking transition to the spin-glass phase is possible through the measurements in actual RLs systems of the order parameter q_{max}, whose behavior identifies the boundary between the prelasing paramagnetic and RLs glassy phases, and the Lévy index α, that defines the statistics of the intensity fluctuations as being Gaussian or Lévy type.

The RLs system investigated in this work consisted of crystalline powders of Nd^{3+} doped YBO_3(Nd:YBO) (For more details see appendix 1). A feature of our system is that dispersers nanoparticles also serve as the gain medium. An advantage of working with this solid-state material is assumed, because replica symmetry theory works on systems in identical experimental conditions. In the present case the positions of the scatterers do not change from shot to shot, thus allowing fairly identical experimental conditions to hold over subsequent excitation pulses.

Figure 5.2.1(a) displays the spectral emission of the Nd:YBO system for excitation pulse energies below ($1.2\,mJ$) and above ($1.75\,mJ$). The emission intensity and bandwidth narrowing are shown in Fig. 5.2.1(b). With basis on the input-output measurement the estimated RL threshold is $1.36\,mJ$, which closely agrees with the value $1.4\,mJ$ determined from the full width half maximum (FWHM) of the emitted spectrum. The error bar in the energy measurements is less than 7%.

The characterization of the photonic RSB glassy transition requires the definition of an overlap parameter $q_{\alpha\beta}$ analogue to the Parisi overlap parameter in SG theory (Eq. 3.1.33). Two point correlations can be calculated either among mode amplitudes a_k, phases or intensities $I_k \propto |a_k|^2$, though the latter are the only ones accessible experimentally. In particular, by measuring fluctuations in the spectral intensity averaged over N_s system replicas. Recalling Chapter 3, we know that the order parameter can be calculated as:

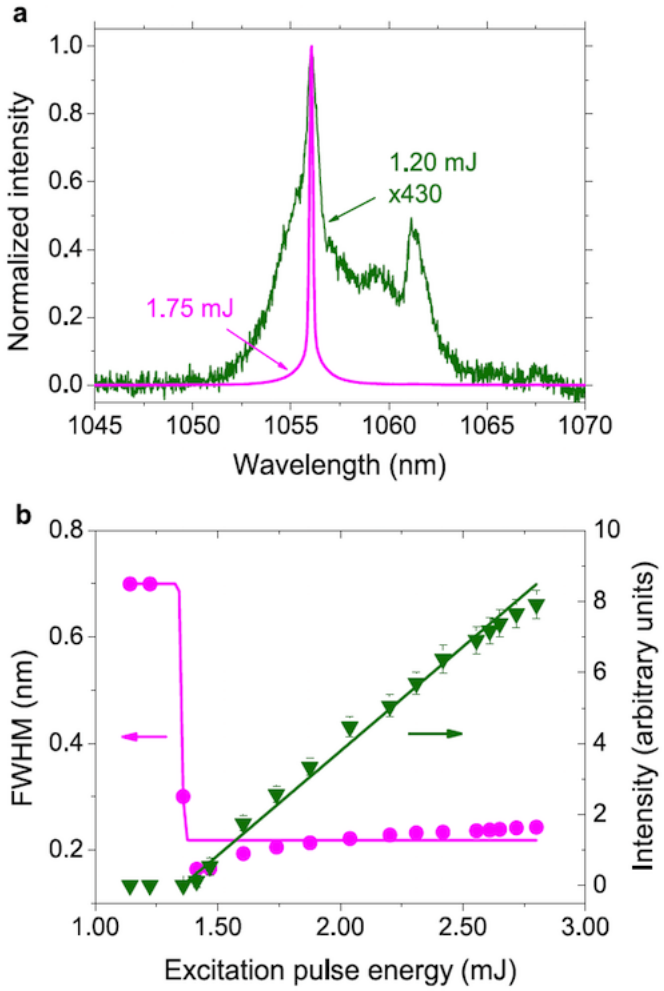

Figure 5.2.1: **Intensity spectra and the RL threshold**. (a) Spectral emission of the Nd:YBO system for two excitation pulse energies: below (green, $1.2\,mJ$ and above (magneta, $1.75\,mJ$) the RL threshold. (b) Emitted intensity (green) and bandwidth narrowing (FWHM, magenta) versus the excitation pulse energy. The intensity measure of the RL threshold implies $1.36\,mJ$, in close agreement with the FWHM value ($1.4\,mJ$).

$$q_{\alpha\beta} = \frac{\sum_{k=1}^{N_s} \Delta_\alpha(k)\,\Delta_\beta(k)}{\sqrt{\sum_{k=1}^{N_s} \Delta_\alpha^2(k)}\sqrt{\sum_{k=1}^{N_s} \Delta_\beta^2(k)}} \tag{5.2.1}$$

where α and $\beta = 1, 2, ..., N_s$, with $N_s = 200$, denote the replica labels. The average intensity at the wavelength $\bar{I}(k)$ and the Intensity fluctuation given by $\Delta_\alpha(k)$ Are defined by equations (3.1.31) and (3.1.32) respectively. Each excitation pulse (shot) of the pumping laser defines a replica, i.e. a copy of the RL system under identical experimental conditions. The PDF $P(q)$ describes the distribution of replica overlaps $q_{\alpha\beta}$, signaling a photonic uncorrelated paramagnetic or a SG phase if it peaks exclusively at $q = 0$ (no RSB) or also at values $|q| \neq 0$ (RSB), respectively.

In Figs. 5.2.2a-f the pulse-to-pulse intensity fluctuations in the Nd:YBO system can be appreciated, as it evolves from the prelasing (Fig. 5.2.2a) to the RL regime (Figs. 5.2.2b-f). The corresponding plots of the PDFs $P(q)$, shown in Figs. 5.2.2g-l, reveal a rich phase structure, emerging from the photonic paramagnetic (Fig. 5.2.2g) to the glassy RL behavior above the threshold. For excitation pulse energies below and just above the threshold (Figs. 5.2.2g-i) the photonic behavior is similar to that described in [32].

For excitation pulse energies well above the RL threshold, the PDF $P(q)$ starts to broaden (Figs. 5.2.2j-l). This is the first report of such behavior, which is related to the deep entry into the Gaussian statistical regime of intensity emission, as discussed below.

The value $|q| = q_{max}$ at which the distribution $P(q)$ assumes the maximum value defines the equivalent to the Parisi order parameter in SG theory. Its behavior for the Nd:YBO system is displayed in Fig. 5.2.3a, indicating the low-energy prelasing paramagnetic ($q_{max} \approx 0$), saturated RL SG ($q_{max} \approx 1$), and high-energy unsaturated RL SG ($q_{max} \approx 0.9$) regimes. Differently from the results reported in [32], however, the behavior of q_{max} does not remain nearly constant at the saturation value $q_{max} \approx 1$, but starts to roll over at high energies, consistently with Fig. 5.2.2. Indeed, as seen in Figs. 5.2.2e-f, well above the threshold the fluctuations of intensities decline considerably, leading to a decrease in the deviations from the pulse-to-pulse average. Correlations among intensity fluctuations also reduce, causing q_{max} to decay.

The above results on the photonic behavior of the Nd:YBO system find an interrelated counterpart in the statistical properties of intensity fluctuations. By analyzing the data in Figs. 5.2.2a-f, the PDFs of intensities were identified with the family of α-stable Lévy distributions, with Lévy index $\alpha \in (0, 2]$ and boundary value $\alpha = 2$ corresponding to the Gaussian behavior, according to the preceding discussion in the chapter 4. By comparing Figs.5.2.3a and 5.2.3b, it is a remarkable fact that, after shifting from the prelasing Gaussian ($\alpha = 2$) regime corresponds to the narrow critical region of the RSB transition from the photonic paramagnetic ($q_{max} \approx 0$) to the satured SG RL ($q_{max} \approx 1$) behaivor. Actually, due to the sharp bandwidth narrowing around the threshold, the variation in α near the transition is also very acute. Moreover, as the excitation pulse

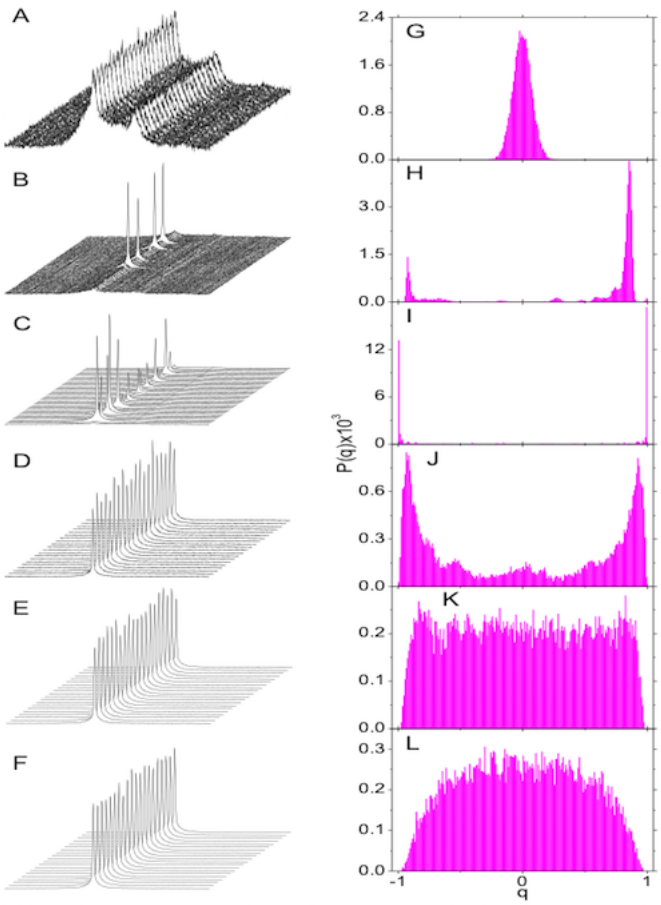

Figure 5.2.2: **Pulse-to pulse intensity fluctuations and corresponding overlap distributions signalizing the photonic RSB glassy transition**. (a)-(f) Intensity spectra showing the fluctuations from shot to shot of the Nd:YBO system for excitation pulse energies (a) $1.2\,mJ$ (below the RL threshold), (b) $1.36\,mJ$, (c) $1.41\,mJ$ (both around the threshold), (d) $1.6\,mJ$, (e) $2.20\,mJ$ and (f) $2.8\,mJ$ (above the threshold). (g)-(l) PDF distributions of the overlap parameter corresponding to the data in Figs. 5.2.2a-f. Fluctuations are stronger (Lévy-type) close to the threshold, in the critical region of the RSB transition from the prelasing paramagnetic to the saturated RL glassy behavior. As the excitation pulse energy increases well above the threshold, fluctuations decline considerably (Gaussian regime) and the SG behavior tends to be suppressed.

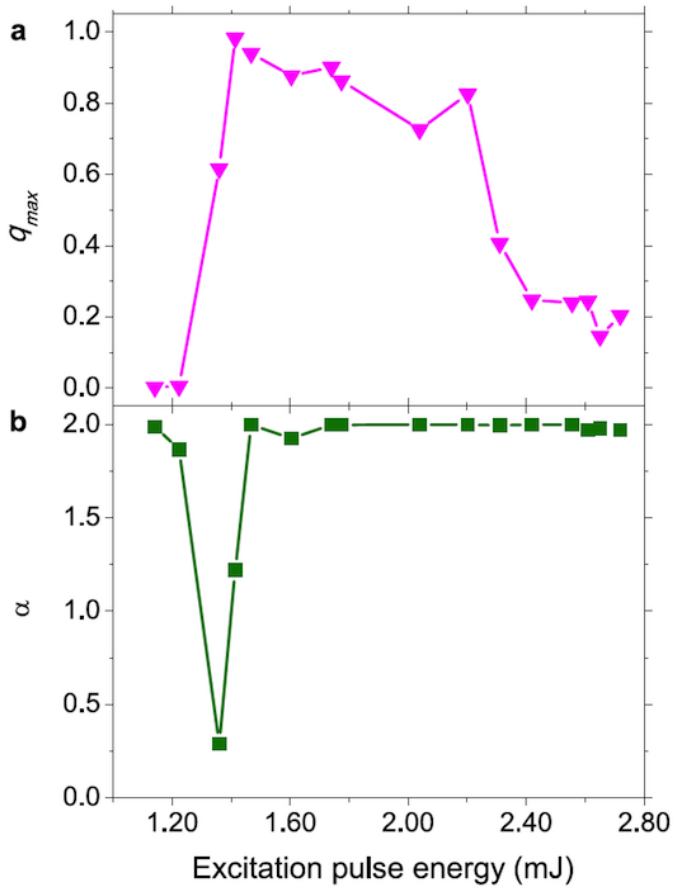

Figure 5.2.3: **Lévy statistics of intensity emission and the RSB glassy transition**. Dependence on the excitation pulse energy of (a) the Parisi overlap order parameter q_{max} and (b) the Lévy index calculated from the data in Fig.5.2.2 of the Nd:YBO system. The regime of Lévy statistics ($0 < \alpha \leq 2$) coincides with the critical region of the RSB transition to the RL glassy behavior. The value $= 2$ identifies the Gaussian regimes below and above the transition. Notice that well above the threshold the SG behavior tends to be suppressed as q_{max} decreases.

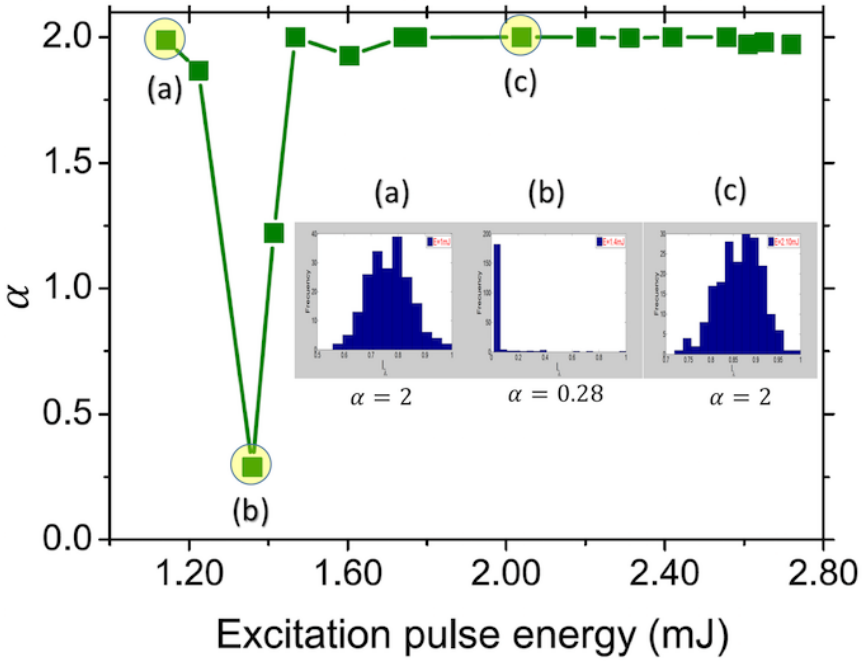

Figure 5.2.4: **α-parameter dependent on the excitation energy**. The figure shows three yellow balls that indicate the values of the α-parameter dependent on the excitation energy, in the insert the three frequency distributions corresponding to the yellow balls are shown.

energy increases further a subsequent $\alpha = 2$ Gaussian RL regime sets in, with a trend to suppress the photonic SG phase. Indeed, in this deep Gaussian regime the system presents a considerable weakening of the intensity fluctuations, which also become less correlated as indicated by the decrease in q_{max}.

Overall, we remark that the experimental findings on the Nd:YBO system, displayed in Figs. 5.2.2 and 5.2.3, corroborate the preceding theoretical discussion on the correspondence between the photonic RSB glassy transition and the statistics of intensity fluctuations in RLs.

From Figure 5.2.4 and 5.2.1b we can make a comparison with the traditional methods of calculating the laser threshold. We can clearly see that the transition from the Gaussian regime to a Lévy regime coincides with the threshold of the laser. This is in agreement with the article, nevertheless we must be careful with the assertion of the authors of [99] that propose to the α-parameter as a universal identifier of the of the threshold of the random laser. In the article [44] they demonstrate that the manifestation of the Lévy statistic depends on the concentration of the medium, that is, the mean free path of the random laser system. On the other hand we have that the beginning of the transition phase to spin glass, also coincides with the laser threshold, which leads us to think of the q-parameter as an indicator of the laser threshold. At this point we will leave an open question that we will answer in the following chapter: does the absence of a Lévy regime imply absence of laser emission?

Finally, we have analyzed both theoretically and experimentally the physical origin

of the complex correspondence between the Lévy flight statistics of intensity emission and the photonic RSB glassy transition in RLs. The experimental demonstration from a single set of spectral measurements on the Nd:YBO RL system indicated a remarkable connection between the behaviors of the Lévy index and the equivalent of the Parisi order parameter as a function of the excitation pulse energy. In particular, the Lévy statistical regime of intensities sets in at the RL threshold concurrently with the RSB transition from the photonic paramagnetic to SG behavior. Our results opens up new possibilities to characterize other RLs such as random fiber lasers. Moreover, the statistical nature of the emission provided by RLs can also have impact on their use as sources for speckle-free laser imaging, which is one of the most promising RL applications that can benefit even cancer research. Ultimately, these practical aspects are much strengthened by the recent account [96] showing that the directionality degree of RLs raises to its peak value precisely within the Lévy statistical regime.

6 Experiment 4: Observation of photonic paramagnetic to spin-glass transition in dye-colloidal RLs

A central concept in replica theory is that identical systems under identical conditions can reach different states. This effect is known as a replica symmetry breaking and is revealed by the form of the probability distribution function of an order parameter called Parisi overlap. This was first demonstrated in the excellent work of Reference [32]. The random laser system used in this reference mentioned was a amorphous solid state, this system ensures the required replica condition. In this same work [32] was studied the behavior of $P(q)$ generated by an analysis of a liquid random laser system, where the dispersers were particles of titanium dioxide in solution of rhodamine B-ethylene glycol. There were no obvious signs of RSB above the lasing threshold.

In the present work[1], specially-designed amorphous TiO_2 nanoparticles were synthesized by a sol-gel method. As a consequence, this modified colloidal RL presents a clear replica-symmetrybreaking phase transition from the paramagnetic fluorescence to spin-glass RL behavior, which has not been observed in the system with non-functionalized TiO_2 particles. We remark that transition coincides with the RL excitation threshold, providing evidence of its role as an identifier of RL emission and threshold.

6.1 Need to specially-designed TiO_2 particles

As we mentioned above, the demonstration of a transition from the photonic paramagnetic phase to a glassy phase of light was performed in solid state RLs, our attempts to display RSB in colloidal RLs were unsuccessful. This was an intriguing negative result, because RLs based in colloidal systems have been well studied before. Possibly, the demonstration of RSB failed because the positions of the scatterers changed considerably during the experiment, so that system replicas, a concept central to the theory, could not establish, and/or the excitation energy was not large enough.

Colloidal dye-based RLs are highly efficient and have been used as a platform for the demonstration of optical effects, such as the bichromatic emission due to monomers

[1]The experiment described here is based, and in many parts is similar to the published article [78]

and dimers in rhodamines [10], multi-photon excitation [34], and low spatial coherence [81]. In spite of the promising characteristics of dye-based RLs, the dye photodegradation enhanced due to the presence of scatterers is a drawback for basic investigations and practical applications [15, 52]. The most used scatterers are TiO_2 particles in the rutile phase, due to its high refractive index ($\sim$ 2.6 at $638\,nm$) which implies a large index contrast with the dye solution. However, the energy bandgap of rutile is $\sim 3.2\,eV$, which allows, by exciting with visible light, two-photon excitation of electrons from the valence to the conduction band. As a consequence, a photocatalytic process occurs, leading to fast dye degradation [107]. Nevertheless, two important points neglected in most works are the particle precipitation and the chemical bonding with the cuvette walls. A relevant consequence is the impossibility of making long-time observations of RL properties that require the prevalence of disorder configurations over a large number of laser shots, in contrast with the RL behavior observed in solid-state samples with quenched disorder [32, 36].

The system studied here consists of amorphous TiO_2 particles suspended in an ethanol solution containing Rhodamine 6G. The particles were functionalized to minimize precipitation in the timescale of the experiments, and do not make chemical bonds with silica at the cuvette walls.

6.2 Experimental Results and Discussion

The excitation source was the second harmonic at $532\,nm$ of a Nd-YAG laser operating at $5\,Hz$, a $7\,ns$ pulse width, with a beam area of $0.7\,mm^2$, an incidence angle of 30° with respect to the normal to the surface, and an excitation pulse energy (EPE) up to $4.6\,mJ$, mounting a scheme that can be seen in Figure 2.4.2. The shot-to-shot intensity fluctuations of the pump laser were less than 5% and, since it was always operating well above threshold, they caused no impact on the statistics of the RL intensity fluctuations, as shown in [32]. For each excitation pulse, a single spectrum was recorded.

A dye-based colloid with commercial T_iO_2 particles, acquired from Dupont Inc., displaying the crystalline structure of rutile (the average diameter of $250\,nm$), was initially studied. These particles present fast precipitation and attach to the cuvette walls. As reported below, such features prevent both the existence of stable RL properties and the RSB phase transition to the glassy behavior.

To compensate for these deleterious effects, amorphous TiO_2 particles with an average diameter of $168\,nm$ were synthesized by the sol-gel method, as described in [94].

The optimized samples consisted of an ethanol solution of Rhodamine 6G and TiO_2 particles at concentrations of $10^{-4}M$ and $6.7 \times 10^{11}\,cm^3$, respectively, placed in a quartz cuvette with the dimensions $10\,mm \times 10\,mm \times 50\,mm$. Using the Mie scattering theory, we estimate the mean free path of photons in the system to be $\sim 57\mu m$, consistent with the

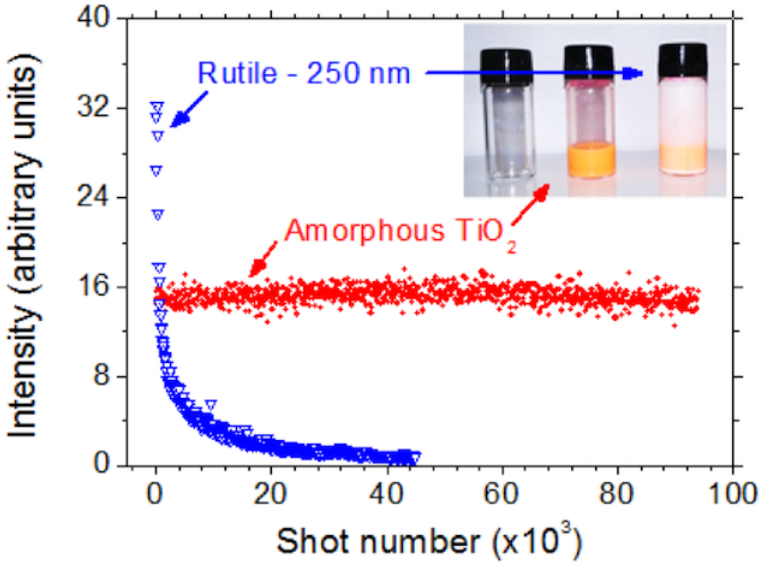

Figure 6.2.1: Evaluation of dye photodegradation and precipitation of T_iO_2 particles in both nonfunctionalized (rutile T_iO_2) and functionalized (amorphous T_iO_2) samples. RL peak intensity as a function of the number of shots, with measurements performed at $5\,Hz$ and EPE $4.00\,mJ$ (above threshold). The inset shows, from right to left, solutions with rutile and amorphous T_iO_2 particles, and an empty flask.

results described in [54] for $250\,nm$ size T_iO_2 particles. The x-ray diffraction pattern and the measurement of the size distribution indicated that 100% of the in-house synthesized T_iO_2 particles are actually amorphous.

The functionalized amorphous T_iO_2 particles do not precipitate in the ethanol solution during a time equivalent to hundreds of thousands of shots. This occurs because they have hydroxyl groups on their surfaces that make hydrogen bonds with the ethanol molecules. Also, due to this hydrogen bonding, the T_iO_2 particles do not make chemical bonds with silica at the cuvette walls. A visual comparison of samples with commercial nonfunctionalized and in-house synthesized T_iO_2 particles at the same concentration can be appreciated in the inset of Fig. 6.2.1. The color of the solutions looks different because, after some time, only the commercial rutile particles attach to the cuvette walls, preventing light transmission. Moreover, precipitation of the commercial T_iO_2 particles is clearly noticed by the accumulation of powder at the bottom of the cuvette. Dye photodegradation analysis was inferred in both nonfunctionalized and functionalized samples by measuring the RL peak intensity with EPE $4.00\,mJ$ (above the threshold), as a function of the number of shots, as also shown in Fig. 6.2.1. Unlike the dye solution with commercial T_iO_2, which displays considerable decay of the intensity already in the first 100 shots, the functionalized solution with in-house synthesized T_iO_2 does not present any relevant indication of photodegradation for at least $\sim 10^5$ shots, being therefore useful for RL studies and applications that require long exposure to the incident optical pulses.

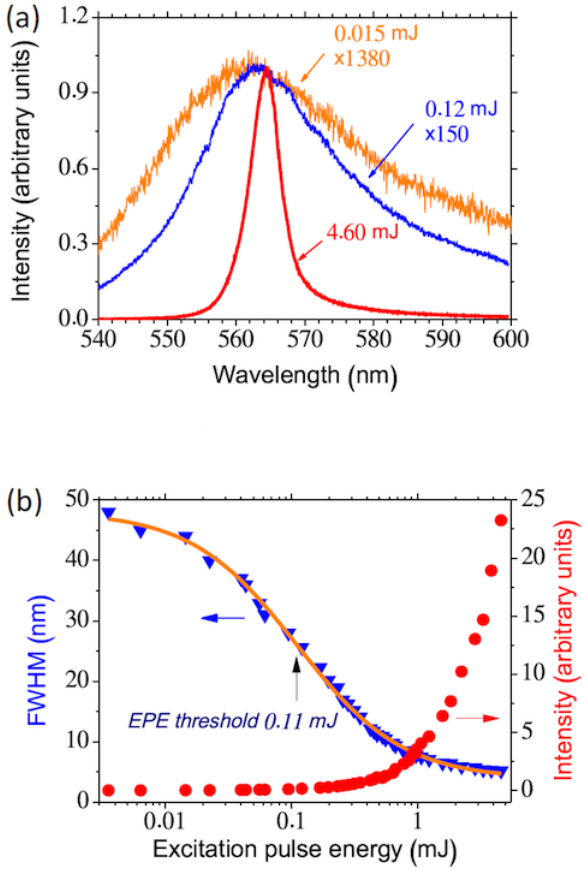

Figure 6.2.2: RL characterization of the functionalized sample with amorphous T_iO_2 particles. (a) Emitted spectra for EPE of 0.015, 0.12, and 4.60 mJ, respectively, smaller, around, and larger than the RL threshold of 0.11 mJ. (b) FWHM and peak intensity of the emitted spectra as a function of the EPE. The solid line is a sigmoidal fit to the FWHM data.

6.2.1 *Characterization of RL*

The characterization of the RL emission of the functionalized solution is shown in Fig. 6.2.2. The emitted spectra for EPE smaller (0.015 mJ), around (0.12 mJ), and larger (4.60 mJ) than the RL threshold of 0.11 mJ (see below) are displayed in Fig. 6.2.2(a), from which the bandwidth narrowing and redshift of the spectra are evident. Figure 6.2.2(b) presents the bandwidth narrowing, characterized by the full width at half maximum (FWHM), and the peak intensity as a function of the EPE. The indicated threshold separates the fluorescent and RL regimes. The smooth RL spectrum (without spikes) and the spectral narrowing are typical of dye-based RLs, and it has been clearly shown that it is not due to amplified spontaneous emission[56, 54, 23]

The RL threshold can be determined either from the input-output curve or from the EPE corresponding to the median value of FWHM. As shown below, the threshold value for the present RL system is determined by the FWHM narrowing median. The solid line in Fig. 6.2.2(b) shows a sigmoidal fit to the FWHM data for better determination of the EPE threshold, inferred to be at 0.11 mJ. This value is in close agreement with the one determined by the input-output curve, 0.18 mJ.

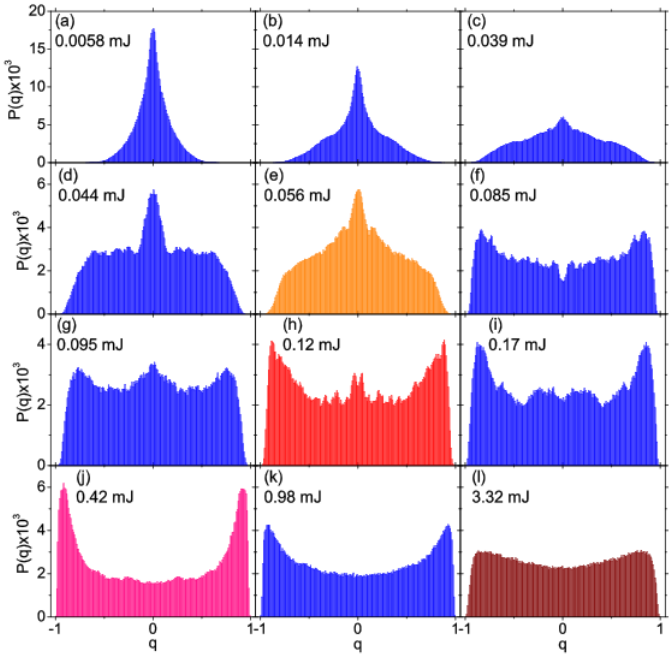

Figure 6.2.3: (a)–(l) Overlap distribution for $N_s = 1000$ shots in the functionalized system. (m)–(p) Pulse-to-pulse fluctuations for 20 emitted spectra of the functionalized system. EPE values are as indicated. (The RL threshold is $0.11\,mJ$.)

6.2.2 *RSB with specially designed TiO_2 particles*

As an interdisciplinary application and motivation for this article, we now demonstrate that the photonic analogue of the spin-glass behavior in a colloidal RL is actually feasible, as reported in [32, 36] for solid-state RLs, but not previously observed with conventional TiO_2 particles and dye [32]. The characterization of the transition from the fluorescent paramagnetic to the RL glassy behavior can be made by evaluating the two-point correlation function that measures pulse-to-pulse fluctuations in the spectral intensity averaged over N_s laser shots at each EPE, using the equation (5.2.1) defined in the previous chapter.

The concept of replica is central to the theory. In the present context, each laser shot gives rise to a replica, i.e., a copy of the RL system under fairly identical experimental conditions, if the disorder configuration set by the random positions of the scatterer particles does not change sensitively during the N_s laser shots. Thus, a careful analysis about the establishment or not of system replicas during the experiment is in order. We start with the nonfunctionalized sample containing commercial rutile particles. As discussed above, the fast precipitation of these particles prevents a stable RL emission. Therefore, no RSB glassy transition can be established in the nonfunctionalized dye-based system with commercial rutile TiO2 particles, a conclusion similarly reached in [32].

On the other hand, the existence of hydrogen bonds between amorphous TiO_2 particles and ethanol molecules presents non appreciable precipitation over hundreds of thousands of shots, so that $L_p \ll L_s$. This fact can be also read in terms of a much larger effective

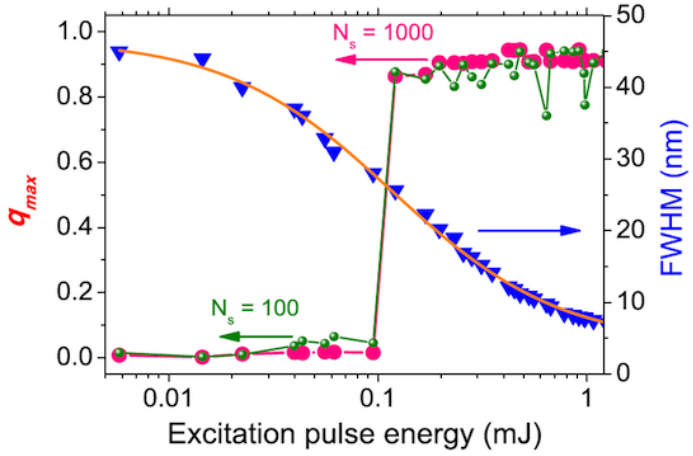

Figure 6.2.4: Agreement between photonic paramagnetic to spin-glass phase transition and the RL threshold of $0.11\,mJ$. Parisi overlap parameter at which $P(q)$ is maximum and bandwidth dependence as a function of the EPE (in log scale) for $N_s = 100$ and $N_s = 1000$ shots in the functionalized system.

viscosity, which also reduces L_B considerably, yielding $L_B \ll L_s$. Thus, the conditions for the existence of replicas are set in the functionalized system, and we analyze below its behavior as a function of the EPE.

Figures 6.2.3(a)–6.2.3(l) display the PDF $P(q)$ of the functionalized system for $N_s = 1000$ shots at the EPE values indicated. In addition, the pulse-to-pulse intensity fluctuations over 20 spectra are presented in Figs. 6.2.3(m)–6.2.3(p). We recall that the pulse-to-pulse fluctuations are not correlated with the excitation source fluctuations, as described in [109]. We also remind that in the RL framework the EPE plays the role of the inverse temperature in spin-glass theory. The parameter q_{max} of the functionalized system is presented in Fig. 6.2.4 for $N_s = 100$ and $N_s = 1000$ shots, together with the FWHM of the emission bandwidth, as a function of the EPE. Although the FWHM changes smoothly as the EPE increases, a RSB phase transition from the paramagnetic fluorescent to the spin-glass RL phase is clearly observed for both N_s by the abrupt change of q_{max} around the EPE value of $0.11\,mJ$, coinciding with the EPE threshold determined from the FWHM variation.

Looking at the behavior of q_{max}, the conclusion is that for values of EPE smaller than the RL threshold the system is still in the photonic paramagnetic regime ($q_{max} = 0$), with the modes (analogue to the spins) uncorrelated. On the other hand, just above the threshold, while the spectral narrowing is taking place, the system is already in the photonic RSB spin-glass regime ($q_{max} \sim 1$). Interestingly, by investigating the RSB behavior in a solid-state Nd^{3+} based RL, we have also identified [36] a broadening of the $P(q)$ distribution similar to that found in Figs. 6.2.3(k)–6.2.3(l).

In conclusion, in this chapter, we exploited specially synthesized amorphous TiO_2 particles as random scatterers for RL characterization and application. Owing to hydroxyl groups on the TiO_2 surface, these particles do not precipitate in ethanol solution and do

not make chemical bonds at the cuvette walls, providing a nonphotodegraded and efficient RL system. We used this functionalized system as a platform for the first demonstration of RSB in a colloidal-based RL. A phase transition from the paramagnetic fluorescent to the spin glass RL phase, evaluated by the Parisi parameter at which the overlap distribution is maximum, was observed, suggesting this parameter as an indicator of RL threshold. Finally, the herein presented results also demonstrate that the intensity fluctuation behavior and the RSB glassy transition of specially designed colloidal-based RLs can be similar to the ones previously reported for solid-state RLs.

7 General conclusions

The first thing I must say is that random lasers are an important research subject over the lasts 20 years and novel investigations highlight their importance in the area of optics. Throughout this thesis we review different works. After a general introduction in Chapter 1, Chapter 2 describes conventional and random lasers, and how the speckle phenomenon was used to determine the number of modes in a random laser. This fact has major implications because it was shown that a random laser is multimodal even in the absence of pronounced spikes or with a very fine spectrum. In this same chapter and in the context of the applications, a bichromatic random laser that has thermal sensitivity was reported, showing that random lasers are systems with applicability in many areas. Deep research into random lasers directed the attention of some research groups to analyzing laser emission fluctuations. Those groups concluded that there is a transition between statistical regime, from a Gaussian regime to a Lévy regime at the threshold of the random laser, and for energies above the threshold the fluctuations return to the Gaussian type. These conclusions led to the proposal that the Lévy parameter could be used as a universal indicator of the threshold of the random laser. However, as shown in this thesis, Lévy regimen can sometimes not be present in the particular random laser system studied. On the other hand, investigations was dedicated to understand random lasers as a photonic platform to observe phase transition similar to spin glass. In the reported works and in this thesis, it was also conclusive that the phase change coincides with the threshold of the random laser. In chapters 3 and 4 we give a brief theoretical description of Lévy fluctuations and spin glass phenomena and theirs relation to random lasers. In chapter 5 we described a work where we unified these two areas, showing that the nature of these two phenomena have a common origin. In this same work, the coincidence between the phase change and the laser threshold results cearly demonstrated the understanding the Parisi Overlap parameter as an indicator of the laser threshold. In Chapter 6 a work was presented that I consider revolutionary because it was possible to observe the paramagnetic photonic transition to spin glass in colloidal RL. Here the fundamental condition of the replicate method is "Bypassed". This fact is drawing a lot of attention from research groups because of the physical implications of applying the replicate method

to a dynamic system. What are the limits to be able to occupy system of replicas in a dynamic system ?. This question is valid since in the first investigations with this type of system, namely a coloidal based RL, the authors were not able to observe the phase change. Finally, it is necessary to know the robustness of the parameter of order of Parisi in terms of universal indicator of the laser threshold, and to consider α -parameter as an indicator of the weak or strong regime of the random laser. These aspects deserve further studies.

References

[1] L. Angelani, C. Conti, G. Ruocco, and F. Zamponi. Glassy behavior of light. *Physical Review Letters*, 96(6):065702–, 02 2006.

[2] L. Angelani, C. Conti, G. Ruocco, and F. Zamponi. Glassy behavior of light in random lasers. *Physical Review B*, 74(10):104207–, 09 2006.

[3] J. D. Ania-Castañón, V. Karalekas, P. Harper, and S. K. Turitsyn. Simultaneous spatial and spectral transparency in ultralong fiber lasers. *Physical Review Letters*, 101(12):123903–, 09 2008.

[4] Juan Diego Ania-Castañón. Quasi-lossless transmission using second-order raman amplification and fibre bragg gratings. *Optics Express*, 12(19):4372–4377, 2004.

[5] F. Antenucci, C. Conti, A. Crisanti, and L. Leuzzi. General phase diagram of multimodal ordered and disordered lasers in closed and open cavities. *Physical Review Letters*, 114(4):043901–, 01 2015.

[6] F. Antenucci, A. Crisanti, and L. Leuzzi. Complex spherical 2 + 4 spin glass: A model for nonlinear optics in random media. *Physical Review A*, 91(5):053816–, 05 2015.

[7] Fabrizio Antenucci, Andrea Crisanti, and Luca Leuzzi. The glassy random laser: replica symmetry breaking in the intensity fluctuations of emission spectra. *Scientific Reports*, 5:16792 EP –, 11 2015.

[8] V. M. Apalkov, M. E. Raikh, and B. Shapiro. Random resonators and prelocalized modes in disordered dielectric films. *Physical Review Letters*, 89(1):016802–, 06 2002.

[9] V. M. Apalkov, M. E. Raikh, and B. Shapiro. Almost localized photon modes in continuous and discrete models of disordered media. *Journal of the Optical Society of America B*, 21(1):132–140, 2004.

[10] Renato Barbosa-Silva, Andrea F. Silva, Antonio M. Brito-Silva, and Cid B. de Araújo. Bichromatic random laser from a powder of rhodamine-doped submicrometer silica particles. *Journal of Applied Physics*, 115(4):043515, 2014.

[11] Pierre Barthelemy, Jacopo Bertolotti, and Diederik S. Wiersma. A levy flight for light. *Nature*, 453(7194):495–498, 05 2008.

[12] Antonio Benayas, Blanca del Rosal, Alberto Pérez-Delgado, Karla Santacruz-Gómez, Daniel Jaque, Gustavo Alonso Hirata, and Fiorenzo Vetrone. Nd:yag near-infrared luminescent nanothermometers. *Advanced Optical Materials*, 3(5):687–694, 2015.

[13] R. W. Boyd. *Nonlinear Optics*. Academic Press, New York, 2nd ed edition, 2002.

[14] Carlos D. S. Brites, Patricia P. Lima, Nuno J. O. Silva, Angel Millan, Vitor S. Amaral, Fernando Palacio, and Luis D. Carlos. Thermometry at the nanoscale. *Nanoscale*, 4(16):4799–4829, 2012.

[15] A. M. Brito-Silva, André Galembeck, Anderson S. L. Gomes, Alcenisio J. Jesus-Silva, and Cid B. de Araújo. Random laser action in dye solutions containing stöber silica nanoparticles. *Journal of Applied Physics*, 108(3):033508, 2010.

[16] Hong Cai, Jun Zhou, Tao Feng, Gang Yao, Yunfeng Qi, Qihong Lou, Jingxing Dong, and Yunrong Wei. Dual-wavelength competitive output in nd:y3sc1.5al3.5o12 ceramic disk laser. *Optics Communications*, 281(17):4401–4405, 9 2008.

[17] H. Cao, Y. G. Zhao, S. T. Ho, E. W. Seelig, Q. H. Wang, and R. P. H. Chang. Random laser action in semiconductor powder. *Phys. Rev. Lett.*, 82:2278–2281, Mar 1999.

[18] H. Cao, Y. G. Zhao, H. C. Ong, S. T. Ho, J. Y. Dai, J. Y. Wu, and R. P. H. Chang. Ultraviolet lasing in resonators formed by scattering in semiconductor polycrystalline films. *Applied Physics Letters*, 73(25):3656–3658, 2016/12/20 1998.

[19] Dmitry V. Churkin, Srikanth Sugavanam, Ilya D. Vatnik, Zinan Wang, Evgenii V. Podivilov, Sergey A. Babin, Yunjiang Rao, and Sergei K. Turitsyn. Recent advances in fundamentals and applications of random fiber lasers. *Advances in Optics and Photonics*, 7(3):516–569, 2015.

[20] H-J Crisanti, A. Sommers. The spherical p-spin interaction spin glass model: the statics. *Z. Phys. B*, 87:341–354, 1992.

[21] Menezes Leonardo Cid B. de Araujo J.Braz. Optically Detected Thermal Effects in Rare-Earth Doped Materials for Host Characterization, Thermometric Devices, Nanothermometry and Biothermometry. *Journal of the Brazilian Chemical Society*, 26:2405 – 2417, 12 2015.

[22] Christiano J. S. de Matos, Leonardo de S. Menezes, Antônio M. Brito-Silva, M. A. Martinez Gámez, Anderson S. L. Gomes, and Cid B. de Araújo. Random fiber laser. *Physical Review Letters*, 99(15):153903–, 10 2007.

[23] Molíria V. dos Santos, Christian T. Dominguez, João V. Schiavon, Hernane S. Barud, Luciana S. A. de Melo, Sidney J. L. Ribeiro, Anderson S. L. Gomes, and Cid B. de Araújo. Random laser action from flexible biocellulose-based device. *Journal of Applied Physics*, 115(8):083108, 2017/01/09 2014.

[24] Yanmin Duan, Haiyong Zhu, Changwen Xu, Hao Yang, Dewei Luo, Hui Lin, Jian Zhang, and Dingyuan Tang. Comparison of the 1319 and 1338 nm dual-wavelength emission of neodymium-doped yttrium aluminum garnet ceramic and crystal lasers. *Applied Physics Express*, 6(1):012701, 2013.

[25] J. Ducuing and N. Bloembergen. Statistical fluctuations in nonlinear optical processes. *Physical Review*, 133(6A):A1493–A1502, 03 1964.

[26] R. Roll E. F. Fama. Parameter estimates for symmetric stable distribution. *Journal of the American Statistical Association*, 66(334):331–338, 1971.

[27] S F Edwards and P W Anderson. Theory of spin glasses. *Journal of Physics F: Metal Physics*, 5(5):965, 1975.

[28] Johannes Fallert, Roman J. B. Dietz, Janos Sartor, Daniel Schneider, Claus Klingshirn, and Heinz Kalt. Co-existence of strongly and weakly localized random laser modes. *Nat Photon*, 3(5):279–282, 05 2009.

[29] Eugene F. Fama. Mandelbrot and the stable paretian hypothesis. *The Journal of Business*, 36(4):420–429, 1963.

[30] R. L. Fork, D. W. Taylor, K. R. German, A. Kiel, and E. Buehler. Unusual luminescence from crystals containing eu^{2+}. *Physical Review Letters*, 32(14):781–783, 04 1974.

[31] Mathieu Gagné and Raman Kashyap. Demonstration of a 3 mw threshold er-doped random fiber laser based on a unique fiber bragg grating. *Optics Express*, 17(21):19067–19074, 2009.

[32] N. Ghofraniha, I. Viola, F. Di Maria, G. Barbarella, G. Gigli, L. Leuzzi, and C. Conti. Experimental evidence of replica symmetry breaking in random lasers. *Nature Communications*, 6:6058 EP –, 01 2015.

[33] Neda Ghofraniha, Luca La Volpe, Daniel Van Opdenbosch, Cordt Zollfrank, and Claudio Conti. Biomimetic random lasers with tunable spatial and temporal coherence. *Advanced Optical Materials*, 4(12):1998–2003, 2016.

[34] Anderson S. L. Gomes, Mariana T. Carvalho, Christian T. Dominguez, Cid B. de Araújo, and Paras N. Prasad. Direct three-photon excitation of upconversion random laser emission in a weakly scattering organic colloidal system. *Optics Express*, 22(12):14305–14310, 2014.

[35] Anderson S. L. Gomes, Bismarck C. Lima, Pablo I. R. Pincheira, AndréL. Moura, Mathieu Gagné, Ernesto P. Raposo, Cid B. de Araújo, and Raman Kashyap. Glassy behavior in a one-dimensional continuous-wave erbium-doped random fiber laser. *Physical Review A*, 94(1):011801–, 07 2016.

[36] Anderson S. L. Gomes, Ernesto P. Raposo, AndréL. Moura, Serge I. Fewo, Pablo I. R. Pincheira, Vladimir Jerez, Lauro J. Q. Maia, and Cid B. de Araújo. Observation of lévy distribution and replica symmetry breaking in random lasers from a single set of measurements. *Scientific Reports*, 6:27987 EP –, 06 2016.

[37] Joseph W. Goodman. *Statistical Optics*. Wiley -Interscience, 1985.

[38] Joseph W. Goodman. *Speckle Phenomena in Optics: Theory and Applications*. Roberts and Company, 2007.

[39] J. P. Gordon, H. J. Zeiger, and C. H. Townes. Molecular microwave oscillator and new hyperfine structure in the microwave spectrum of nh_3. *Phys. Rev.*, 95:282–284, Jul 1954.

[40] Hermann A Haus. *Waves and fields in optoelectronics*. Prentice-Hall, 1984.

[41] Brett H. Hokr, Joel N. Bixler, Michael T. Cone, John D. Mason, Hope T. Beier, Gary D. Noojin, Georgi I. Petrov, Leonid A. Golovan, Robert J. Thomas, Benjamin A. Rockwell, and Vladislav V. Yakovlev. Bright emission from a random raman laser. *Nature Communications*, 5:4356 EP –, 07 2014.

[42] Brett H. Hokr, Joel N. Bixler, Michael T. Cone, John D. Mason, Hope T. Beier, Gary D. Noojin, Georgi I. Petrov, Leonid A. Golovan, Robert J. Thomas, Benjamin A. Rockwell, and Vladislav V. Yakovlev. Bright emission from a random raman laser. *Nature Communications*, 5:4356 EP –, 07 2014.

[43] Brett H. Hokr, Alexander Cerjan, Jonathan V. Thompson, Luqi Yuan, Seng Fatt Liew, Joel N. Bixler, Gary D. Noojin, Robert J. Thomas, Hui Cao, A. Douglas Stone, Benjamin A. Rockwell, Marlan O. Scully, and Vladislav V. Yakovlev. Evidence of anderson localization effects in random raman lasing. volume 9731, pages 973110–973110–6, 2016.

[44] Emilio Ignesti, Federico Tommasi, Lorenzo Fini, Stefano Lepri, Vivekananthan Radhalakshmi, Diederik Wiersma, and Stefano Cavalieri. Experimental and theoretical

investigation of statistical regimes in random laser emission. *Physical Review A*, 88(3):033820–, 09 2013.

[45] Emilio Ignesti, Federico Tommasi, Lorenzo Fini, Fabrizio Martelli, Niccolò Azzali, and Stefano Cavalieri. A new class of optical sensors: a random laser based device. *Scientific Reports*, 6:35225 EP –, 10 2016.

[46] Lionel Jaffres, Alexis Labruyère, Vincent Couderc, Julie Carreaud, Alexandre Maître, Rémi Boulesteix, Alain Brenier, Georges Boulon, Yannick Guyot, Yoël Rabinovitch, and Christian Sallé. Gain structuration in dual-wavelength nd:ysag ceramic lasers. *Optics Express*, 20(23):25596–25602, 2012.

[47] D. Jaque, O. Enguita, U. Caldino G., M. O. Ramirez, J. Garcia Sole, C. Zaldo, J. E. Munoz Santiuste, A. D. Jiang, and Z. D. Luo. Optical characterization and laser gain modeling of a ndal3(bo3)4 (nab) microchip laser crystal. *Journal of Applied Physics*, 90(2):561–569, 2001.

[48] D. Jaque, L. Martinez Maestro, B. del Rosal, P. Haro-Gonzalez, A. Benayas, J. L. Plaza, E. Martin Rodriguez, and J. Garcia Sole. Nanoparticles for photothermal therapies. *Nanoscale*, 6(16):9494–9530, 2014.

[49] D. Jaque and J. García Solé. Tunable Nd^{3+} : $Ca_3Ga_2Ge_3O_{12}$ site-selective laser operating around 1.33 μm,. *Physical Review B*, 70(15):155116–, 10 2004.

[50] Daniel Jaque and Fiorenzo Vetrone. Luminescence nanothermometry. *Nanoscale*, 4(15):4301–4326, 2012.

[51] Xin-Hong Jia, Yun-Jiang Rao, Zi-Nan Wang, Wei-Li Zhang, Zeng-Ling Ran, Kun Deng, and Zi-Xin Yang. Detailed theoretical investigation on improved quasi-lossless transmission using third-order raman amplification based on ultralong fiber lasers. *Journal of the Optical Society of America B*, 29(4):847–854, 2012.

[52] Ernesto Jimenez-Villar, Valdeci Mestre, Paulo C. de Oliveira, Wagner M. Faustino, D. S. Silva, and Gilberto F. de Sá. Tio2@silica nanoparticles in a random laser: Strong relationship of silica shell thickness on scattering medium properties and random laser performance. *Applied Physics Letters*, 104(8):081909, 2017/01/09 2014.

[53] A. A. Kaminskii, S. N. Bagaev, K. Ueda, A. Shirakawa, T. Tokurakawa, H. Yagi, T. Yanagitany, and J. Dong. Stimulated-emission spectroscopy of fine-grained "garnet"ceramics nd3+:y3al5o12 in a wide temperature range between 77 and 650 k. *Laser Physics Letters*, 6(9):682–687, 2009.

[54] J Kitur, G Zhu, M Bahoura, and M A Noginov. Dependence of the random laser behavior on the concentrations of dye and scatterers. *Journal of Optics*, 12(2):024009, 2010.

[55] K. König. Multiphoton microscopy in life sciences. *Journal of Microscopy*, 200(2):83–104, 2000.

[56] N. M. Lawandy, R. M. Balachandran, A. S. L. Gomes, and E. Sauvain. Laser action in strongly scattering media. *Nature*, 368(6470):436–438, 03 1994.

[57] Stefano Lepri, Stefano Cavalieri, Gian-Luca Oppo, and Diederik S. Wiersma. Statistical regimes of random laser fluctuations. *Physical Review A*, 75(6):063820–, 06 2007.

[58] V.S. Letokhov. Generation of light by a scattering medium with negative resonance absorption. *JETP*, 26, 1968.

[59] Bismarck C. Lima, Anderson S. L. Gomes, Pablo I. R. Pincheira, AndréL. Moura, Mathieu Gagné, Ernesto P. Raposo, Cid B. de Araújo, and Raman Kashyap. Observation of lévy statistics in one-dimensional erbium-based random fiber laser. *Journal of the Optical Society of America B*, 34(2):293–299, 2017.

[60] N. Lizárraga, N. P. Puente, E. I. Chaikina, T. A. Leskova, and E. R. Méndez. Single-mode er-doped fiber random laser with distributed bragg grating feedback. *Optics Express*, 17(2):395–404, 2009.

[61] Z. D. Luo, Y. D. Huang, M. Montes, and D. Jaque. Improving the performance of a neodymium aluminium borate microchip laser crystal by resonant pumping. *Applied Physics Letters*, 85(5):715–717, 2004.

[62] Benoit Mandelbrot. The variation of certain speculative prices. *The Journal of Business*, 36(4):394–419, 1963.

[63] Rosario N. Mantegna and H. Eugene Stanley. Stochastic process with ultraslow convergence to a gaussian: The truncated l\'evy flight. *Physical Review Letters*, 73(22):2946–2949, 11 1994.

[64] Rosario N. Mantegna and H. Eugene Stanley. Scaling behaviour in the dynamics of an economic index. *Nature*, 376(6535):46–49, 07 1995.

[65] E. Mariana and F. Zuliani. Numerical simulations of the four-dimensional edwards-anderson spin glass with binary couplings. *J PHYS A*, 32(43):7447–7461, 1999.

[66] J. Huston McCulloch. Simple consistent estimators of stable distribution parameters. *Communications in Statistics - Simulation and Computation*, 15(4):1109–1136, 01 1986.

[67] Marc Mézard, Giorgio Parisi, Nicolas Sourlas, Gérard Toulouse, and Miguel Virasoro. Replica symmetry breaking and the nature of the spin glass phase. *Journal de Physique*, 45(5):843–854, 1984.

[68] Uriel Frisch Micheal F. Shlesinger, George M. Zaslavsky. *Lévy Flights and Related Topics in Physics*, volume 450. Springer Velarg Berlin, 1995.

[69] AndréL Moura, Vladimir Jerez, Lauro J Q Maia, Anderson S L Gomes, and Cid B de Araújo. Multi-wavelength emission through self-induced second-order wave-mixing processes from a nd(3+) doped crystalline powder random laser. *Scientific Reports*, 5:13816, 2015.

[70] AndréL. Moura, Pablo I. R. Pincheira, Lauro J. Q. Maia, Anderson S. L. Gomes, and Cid B. de Araújo. Two-color random laser based on a nd3+ doped crystalline powder. *Journal of Luminescence*, 181:44–48, 1 2017.

[71] Sushil Mujumdar, Marilena Ricci, Renato Torre, and Diederik S. Wiersma. Amplified extended modes in random lasers. *Physical Review Letters*, 93(5):053903–, 07 2004.

[72] Ali H. Nayfeh. *Introduction to Perturbation Techniques*. Wiley Interscience, NY, Jan 1993.

[73] C. M. Newman and D. L. Stein. The state(s) of replica symmetry breaking: Mean field theories vs. short-ranged spin glasses. *Journal of Statistical Physics*, 106(1):213–244, 2002.

[74] M. A. Noginov, S. U. Egarievwe, N. Noginova, J. C. Wang, and H. J. Caulfield. Demonstration of a second-harmonic powder laser. *Journal of the Optical Society of America B*, 15(12):2854–2860, 1998.

[75] C. L. O'Bryan and M. Sargent. Theory of multimode laser operation. *Physical Review A*, 8(6):3071–3092, 12 1973.

[76] G Parisi. The order parameter for spin glasses: a function on the interval 0-1. *Journal of Physics A: Mathematical and General*, 13(3):1101, 1980.

[77] Giorgio Parisi. Order parameter for spin-glasses. *Physical Review Letters*, 50(24):1946–1948, 06 1983.

[78] Pablo I. R. Pincheira, Andréa F. Silva, Serge I. Fewo, Sandra J. M. Carreño, AndréL. Moura, Ernesto P. Raposo, Anderson S. L. Gomes, and Cid B. de Araújo. Observation of photonic paramagnetic to spin-glass transition in a specially designed tio2 particle-based dye-colloidal random laser. *Optics Letters*, 41(15):3459–3462, 2016.

[79] B. Raghavendra Prasad, Hema Ramachandran, Ajay Kumar Sood, C. K. Subramanian, and Narendra Kumar. Lasing in active, sub-mean-free path-sized systems with dense, random, weak scatterers. *Applied Optics*, 36(30):7718–7724, 1997.

[80] E. P. Raposo and A. S. L. Gomes. Analytical solution for the l\'evy-like steady-state distribution of intensities in random lasers. *Physical Review A*, 91(4):043827–, 04 2015.

[81] Brandon Redding, Michael A. Choma, and Hui Cao. Speckle-free laser imaging using random laser illumination. *Nat Photon*, 6(6):355–359, 06 2012.

[82] H.E Stanley R.N. Mantegna. *An Introduction to Econophysics: Correlations and Complexity in Finance*. Cambridge University Press, 1999.

[83] P.G. Kryukov V.S. Letokhov R.V. Ambartsumyan N.G. Basov. A laser with a nonresonant feedback. *IEEE J. Quantum Electronics*, Qe-2(9), September 1966.

[84] A. Schenzle and H. Brand. Multiplicative stochastic processes in statistical physics. *Physical Review A*, 20(4):1628–1647, 10 1979.

[85] W. L. Sha, C. H. Liu, and R. R. Alfano. Spectral and temporal measurements of laser action of rhodamine 640 dye in strongly scattering media. *Optics Letters*, 19(23):1922–1924, 1994.

[86] DIVYA SHARMA, HEMA RAMACHANDRAN, and N. KUMAR. Lévy statistical fluctuations from a random amplifying medium. *Fluctuation and Noise Letters*, 06(01):L95–L101, 2006.

[87] David Sherrington and Scott Kirkpatrick. Solvable model of a spin-glass. *Physical Review Letters*, 35(26):1792–1796, 12 1975.

[88] Masood Siddique, Li. Yang, Q. Z. Wang, and R. R. Alfano. Mirrorless laser action from optically pumped dye-treated animal tissues. *Optics Communications*, 117(5):475–479, 1995.

[89] A. E. Siegman. *Lasers*. University Science Books, Mill Valley, 1986.

[90] W. Silfvast. *Laser Fundamentals*. Cambridge University Press, 2004.

[91] Andrew M Smith, Michael C Mancini, and Shuming Nie. Second window for in vivo imaging. *Nature nanotechnology*, 4(11):710–711, 11 2009.

[92] Qinghai Song, Shumin Xiao, Zhengbin Xu, Jingjing Liu, Xuanhao Sun, Vladimir Drachev, Vladimir M. Shalaev, Ozan Akkus, and Young L. Kim. Random lasing in bone tissue. *Optics Letters*, 35(9):1425–1427, 2010.

[93] Danien A. Steck. *Classical and Modern Optics*. University of Oregon, 2010.

[94] Tadao Sugimoto and Takashi Kojima. Formation mechanism of amorphous tio2 spheres in organic solvents. 1. roles of ammonia. *The Journal of Physical Chemistry C*, 112(48):18760–18771, 12 2008.

[95] B. Davison J.B. Sykes. *Neutron Transport Theory*. Oxford University Press, 1957.

[96] Federico Tommasi, Emilio Ignesti, Lorenzo Fini, and Stefano Cavalieri. Controlling directionality and the statistical regime of the random laser emission. *Physical Review A*, 91(3):033820–, 03 2015.

[97] Ravitej Uppu and Sushil Mujumdar. On the coherent modes of ultranarrowband random lasers with nonresonant feedback. *Applied Optics*, 50(25):E13–E19, 2011.

[98] Ravitej Uppu and Sushil Mujumdar. Dependence of the gaussian-*Lévy* transition on the disorder strength in random lasers. *Physical Review A*, 87(1):013822–, 01 2013.

[99] Ravitej Uppu and Sushil Mujumdar. Lévy exponents as universal identifiers of threshold and criticality in random lasers. *Physical Review A*, 90(2):025801–, 08 2014.

[100] Ravitej Uppu, Anjani Kumar Tiwari, and Sushil Mujumdar. Identification of statistical regimes and crossovers in coherent random laser emission. *Optics Letters*, 37(4):662–664, 2012.

[101] V M Markusev V F Zolin, Ch M Briskina. Luminescence and stimulated emission of neodymium in sodium lanthanum molygdate powders. *SOV J QUANTUM ELECTRON*, 16(2):281–283, 1986.

[102] Karen L. van der Molen, Allard P. Mosk, and Ad Lagendijk. Intrinsic intensity fluctuations in random lasers. *Physical Review A*, 74(5):053808–, 11 2006.

[103] F. Varsanyi. Surface lasers. *Applied Physics Letters*, 19(6):169–171, 1971.

[104] Shankar C. Venkataramani, Thomas M. Antonsen, Jr., and Edward Ott. L\'evy flights in fluid flows with no kolmogorov-arnold-moser surfaces. *Physical Review Letters*, 78(20):3864–3867, 05 1997.

[105] G. M. Viswanathan, Sergey V. Buldyrev, Shlomo Havlin, M. G. E. da Luz, E. P. Raposo, and H. Eugene Stanley. Optimizing the success of random searches. *Nature*, 401(6756):911–914, 10 1999.

[106] Diederik S. Wiersma. The physics and applications of random lasers. *Nat Phys*, 4(5):359–367, 05 2008.

[107] Aaron Wold. Photocatalytic properties of titanium dioxide (tio2). *Chemistry of Materials*, 5(3):280–283, 03 1993.

[108] Emil Wolf. *Progress in Optics*, volume 45. Advisory Board, 2003.

[109] G. Zhu, Lei Gu, and M. A. Noginov. Experimental study of instability in a random laser with immobile scatterers. *Physical Review A*, 85(4):043801–, 04 2012.

Appendix

Appendix 1: Neodymium crystalline powder, preparation and characterization

The NdAB powder was synthesized by the polymeric precursor method using aluminum nitrate nonahydrate ($Al(NO_3)_3.9H_2O$), neodymium hexahydrate ($Nd(NO_3.6H_2O$), boric acid (H_3BO_3), citric acid ($C_5O_7H_8$) as a complexing agent, and d-sorbitol ($C_6O_6H_{14}$) as polymerizing agent. The synthesis was achieved by dissolving the aluminum and neodymium nitrates in an aqueous solution of citric acid at room temperature. This solution was added to another solution of d-sorbitol and boric acid previously dissolved in water. The obtained solution was annealed at 150 ^{o}C in an oven to prompt the polymerization process and to form a dried resin. The molar ratio of citric acid to metals plus boron was 3:1. The citric acid/d-sorbitol mass ratio was set to 3:2. The dried resin was calcinated at 400 °C during 24 h, heat-treated at 700 °C during 24 h and finally annealed at 1150 °C for 5 min under richoxygen atmosphere. The powder was characterized using a JEOL JEM 2010 high-resolution transmission electron microscope (HRTEM) operating at 200 keV.

Images of the particles are presented in Fig. 7.0.1(a) and (b) and the particles' size histogram, shown in Fig. 7.0.1(c), was obtained by measuring 110 particles with most particles having dimension of 55 nm. The crystalline NdAl3(BO3)4 particles present well defined structural planes, and Fig. 1(b) shows that the powder is composed of non-spherical particles of irregular forms.

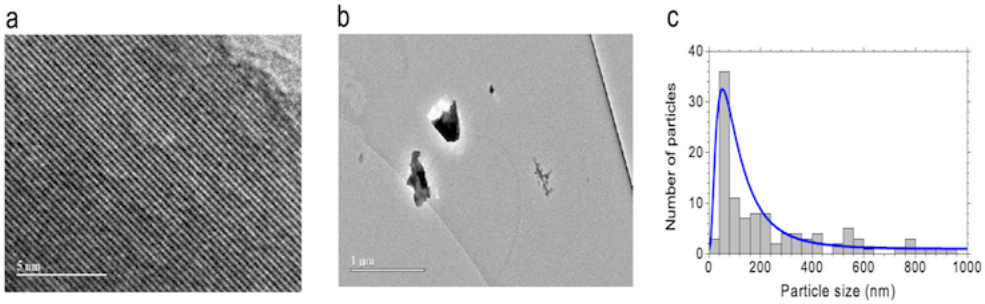

Figure 7.0.1: (a) TEM, (b) HRTEM images and (c) particle size histogram of the $NdAl_3(BO_3)_4$ powder.

Appendix 2: Optical parametric oscillators

Optical parametric oscillators (OPOs) are convenient sources of coherent light that suit numerous scientific applications, including various types of spectroscopy, multiphoton excitation, and light detection and ranging.

In contrast to a laser, which relies on stimulated emission from a gain medium, OPOs use a nonlinear crystal to convert a pump beam into an idler beam and a signal beam. By placing the nonlinear crystal in a cavity, an oscillator is formed and operation commences when the pump power is above a certain threshold value. Figure 7.0.2(a) show a Opolette 532 tunelable laser system used in our experiments. Figure 7.0.2(b) show a scheme of a OPO system, in a suitable nonlinear crystal, a high frequency and high intensity pump beam λ_{pump} amplifies a lower frequency, lower intensity beam (the signal beam λ_{signal}); in addition a third beam (the idler beam λ_{idler}) is generated.

A unique feature of OPOs is that the output wavelengths of the idler and signal beams can be tuned by changing the phase-matching properties of the nonlinear crystal. This is often accomplished by altering the temperature or orientation of the crystal, or by using a crystal that contains a grating.

An important benefit of OPOs is that their wide wavelength tunability allows them to produce wavelengths that are inaccessible to conventional lasers. Emission can typically be tuned over hundreds of nanometres, giving researchers selectable access to all wavelengths spanning from the ultraviolet to the near-infrared — and all from a single source.

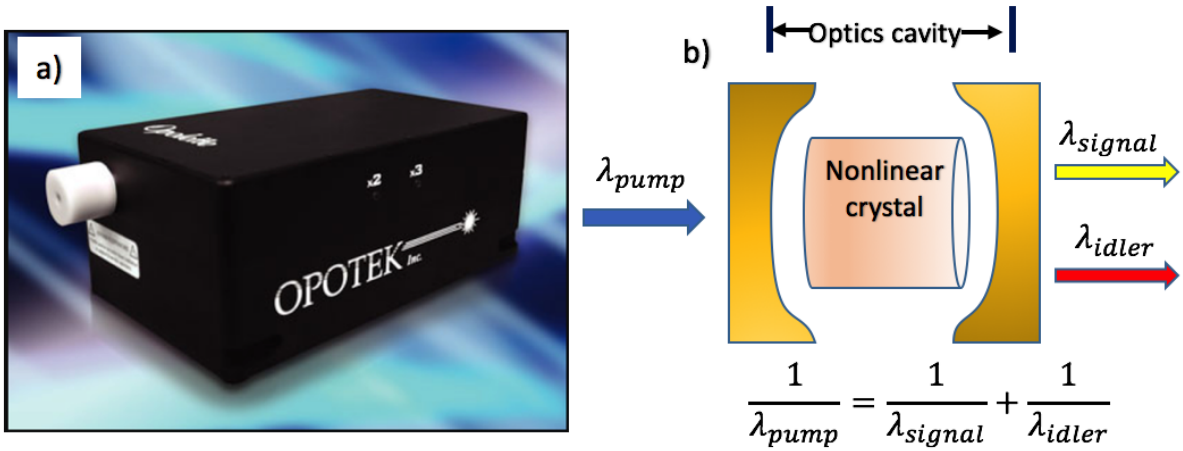

Figure 7.0.2: (a) The Opolette 532 tunable laser system utilizes patented optical parametric oscillator (OPO) technology to generate wavelengths over a broad range in the NIR. (b) An scheme of a typical optical parametric oscillator is shown, when a nonlinear crystal is placed inside a optics cavity an optical parametric oscillator is established.

Annex

List of publications basic of this thesis

- **Observation of Lévy distribution and replica symmetry breaking in random lasers from a single set of measurements** Anderson S. L. Gomes, Ernesto P. Raposo, André L. Moura, Serge I. Fewo, **Pablo I. R. Pincheira**, Vladimir Jerez, Lauro J. Q. Maia, and Cid B. de Araújo Sci. Rep. 6, 27987 (8pp); doi: 10.1038/srep27987 (2016).

- **Observation of photonic paramagnetic to spin-glass transition in specially-designed TiO2 particles-based dye-colloidal random laser *Pablo I. R. Pincheira***, Andréa F. Silva, Sandra J. M. Carreño, Serge I. Fewo, André L. Moura, Ernesto P. Raposo, Anderson S. L. Gomes and Cid B. de Araújo Opt. Lett. 41(15), 3459-3462 (2016)

- **Glassy behavior in a one-dimensional continuous-wave erbium-doped random fiber laser** Anderson S. L. Gomes, Bismarck C. Lima, **Pablo I. R. Pincheira**, André L. Moura, Mathieu Gagné, Ernesto P. Raposo, Cid B. de Araújo, and Raman Kashyap Phys. Rev. A 94, 011801-5(R) (2016)

- **Two-color random laser based on a nd3+ doped crystalline powder** André L. Moura, **Pablo I. R. Pincheira**, Lauro J. Q. Maia, Anderson S. L. Gomes, and Cid B. de Araújo. Journal of Luminescence, 181:44–48, 1 2017.

Work not featuring in the thesis

- Tunable ultraviolet and blue light generation from Nd:YAB random laser bolstered by second-order nonlinear processes. André L. Moura, Sandra J. M. Carreño, **Pablo I. R. Pincheira**, Zanine V. Fabris, Lauro J. Q. Maia, Anderson S. L. Gomes, and Cid B. de Araújo Sci. Rep. 6, 27107 (6pp); doi: 10.1038/srep27107 (2016)

- **Interplay between random laser performance and self-frequency conversions $\mathbf{Nd}_x\mathbf{Y}_{1.00-x}\mathbf{Al}_3\mathbf{(BO}_3\mathbf{)}_4$ in nanocrystals powders.** Sandra J. M. Carreño, André L. Moura, **Pablo I. R. Pincheira**, Zanine V. Fabris, Lauro J. Q. Maia, Anderson S. L. Gomes and Cid B. de Araújo Optical Materials 54 (2016) 262–268

- **Observation of Lévy statistics in one-dimensional erbium-based random fiber laser** Bismarck C. Lima, Anderson S. L. Gomes, **Pablo I. R. Pincheira**, André L. Moura, Mathieu Gagné, Ernesto P. Raposo, Cid B. De Araújo, Raman Kashyap J. Opt. Soc. Am. B 34(2), 293-299 (2017)\